


5-2011

# Exfoliated Graphite Nanoplatelet-Filled Impact Modified Polypropylene Nanocomposites

Alex Duguay

Follow this and additional works at: <http://digitalcommons.library.umaine.edu/etd>

 Part of the [Civil Engineering Commons](#), [Organic Chemistry Commons](#), and the [Polymer Chemistry Commons](#)

---

## Recommended Citation

Duguay, Alex, "Exfoliated Graphite Nanoplatelet-Filled Impact Modified Polypropylene Nanocomposites" (2011). *Electronic Theses and Dissertations*. 1574.

<http://digitalcommons.library.umaine.edu/etd/1574>

This Open-Access Thesis is brought to you for free and open access by DigitalCommons@UMaine. It has been accepted for inclusion in Electronic Theses and Dissertations by an authorized administrator of DigitalCommons@UMaine.

**EXFOLIATED GRAPHITE NANOPATELET-FILLED  
IMPACT MODIFIED POLYPROPYLENE  
NANOCOMPOSITES**

By

Alex Duguay

B.S. University of Maine, 2009

A THESIS

Submitted in Partial Fulfillment of the

Requirements for the Degree of

Master of Science

(in Civil Engineering)

The Graduate School

The University of Maine

May, 2011

Advisory Committee:

Habib J. Dagher, Professor of Civil Engineering, Co-Advisor

Douglas J. Gardner, Professor of Wood Science and Technology, Co-Advisor

Eric N. Landis, Professor of Civil Engineering

Roberto Lopez-Anido, Professor of Civil Engineering

## THESIS ACCEPTANCE STATEMENT

On behalf of the Graduate Committee for Alex Duguay, I affirm that this manuscript is the final and accepted thesis. Signatures of all committee members are on file with the Graduate School at the University of Maine, 5755 Stodder Hall, Orono Maine.

..... April, \_\_\_\_ 2011

Habib J. Dagher, Ph. D., P.E.

Professor of Civil Engineering

Committee Chair

## **LIBRARY RIGHTS STATEMENT**

In presenting this thesis in partial fulfillment of the requirements for an advanced degree at The University of Maine, I agree that the Library shall make it freely available for inspection. I further agree that permission for “fair use” copying of this thesis for scholarly purposes may be granted by the Librarian. It is understood that any copying or publication of this thesis for financial gain shall not be allowed without my written permission.

Signature:

Date:

**EXFOLIATED GRAPHITE NANOPATELET-FILLED  
IMPACT MODIFIED POLYPROPYLENE  
NANOCOMPOSITES**

By Alex Duguay

Thesis Co-Advisors: Dr. Habib J. Dagher and Dr. Douglas J. Gardner

An Abstract of the Thesis Presented  
in Partial Fulfillment of the Requirements for the  
Degree of Master of Science  
(in Civil Engineering)  
May, 2011

Exfoliated graphite nanoplatelets (xGnP)-filled polymer composites have demonstrated superior electrical, mechanical, physical and thermal properties and are becoming a major focus for both academic and industrial research and development (R&D) activities. The main objective of this study was to characterize the influence of xGnP particle diameter, filler loading and the addition of coupling agents on the mechanical, rheological and thermal properties of xGnP-filled impact modified polypropylene (IMPP) composites. IMPP is currently being used at the AEWC Advanced Structures and Composites Center in polymer impregnated (pre-preg) fiber reinforced polymer (FRP) tapes consisting of an IMPP matrix polymer and E-glass continuous fibers. These tapes are layered and pressed into blast protection panels currently being used by the U.S. military. This research aims to implement nanotechnology and unique experimental methodology to increase modulus and strength of neat IMPP while either

conserving or improving the uniquely tailored impact properties of the existing IMPP used.

The nanoparticles used in this research were xGnP with three different sizes: xGnP<sup>5</sup> has an average thickness of 10 nm, and an average platelet diameter of 5 μm, whereas xGnP<sup>15</sup> and xGnP<sup>25</sup> have the same thickness but average diameters are 15 and 25 μm, respectively. The coupling agent used in this study was polypropylene-graft-maleic anhydride (PP-g-MA).

Mechanical characterization of the composites was completed via American Society for Testing and Materials (ASTM) testing standards for flexure, tension and Izod impact. Test results show that nanocomposites with smaller xGnP diameter exhibited better flexural, tensile and impact properties for both neat and composites containing coupling agent. For composites containing a coupling agent, tensile and flexural modulus and strength increased with the addition of xGnP. In the case of neat composites, both tensile and flexural modulus and strength decreased at higher filler loading levels. Increasing xGnP loading resulted in reduction of elongation at break for both neat and composites containing coupling agent. Similarly, unnotched and notched impact strengths as well as fracture initiation resistance were dramatically deteriorated with the introduction of xGnP. Explanation for this brittle behavior in a nanoplatelet-filled IMPP is presented throughout this thesis using scanning electron microscopy (SEM), transmission electron microscopy (TEM), and melt flow index testing.

The thermal behavior of the composites was investigated using differential scanning calorimetry (DSC) and thermogravimetric analysis (TGA). The DSC results indicated that the addition of xGnP slightly increased the melting temperature ( $T_m$ ) and increased the crystallization temperature ( $T_c$ ) of IMPP by 2 to 3 °C which is attributed to the heterogeneous nucleation of the xGnP. The TGA results indicated that the degradation temperature of IMPP is lowered with the addition of PP-g-MA, indicative of the poor thermal stability of PP-g-MA. However, the thermal stability of the composites increases with xGnP loading because of the high thermal stability of the xGnP and the hypothesized “tortuosity effect” that the graphite nanoplatelets was inhibiting diffusion of oxygen and volatile products throughout the composites during thermal decomposition.

## ACKNOWLEDGEMENTS

I would like to assert my deepest gratitude to my advisors Dr. Habib J. Dagher and Dr. Douglas J. Gardner for their valuable guidance, wealth of knowledge, unwavering support and instilled confidence provided to me throughout the completion of my graduate thesis. The journey would have been much less rewarding without their collaborative advice and direction. I would also like to thank my other thesis committee members Dr. Eric N. Landis and Dr. Roberto Lopez-Anido for their important role in my development as an engineer, both through educating me and providing support since my arrival at The University of Maine.

I owe many thanks to Jacques W. Nader for the confidence and trust he has given me throughout my development from an undergraduate employee to a graduate research assistant at the AEWC Advanced Structures and Composites Center. Jacques has provided me with opportunities that foster intellectual independence and ingrained a desire and demand for excellence in all that I produce.

I am extremely fortunate to have had the opportunity to work in the presence of the AEWC Nanocomposites Research Group. This team is provided with world class management by Jacques W. Nader and first-rate polymer composite expertise by Dr. Douglas J. Gardner, Dr. Yousoo Han and Dr. Han-Seung Yang. Much of the research work is carried out by Ph. D students Alper Kiziltas and Yucheng Peng. Undergraduate employees Joel Parent, Gregory Macallister and William Curnan deserve a great deal of my appreciation for all of their hard work in preparing and characterizing



nanocomposites with the upmost quality assurance in mind. All of those mentioned have provided significant research assistance as well as personally impacted my life for the better.

I would also like to thank the U.S. Army Corps of Engineers, Engineer Research and Development Center (ERDC) for their financial support and valuable insight. In particular, I extend many thanks to Toney K. Cummins and Dr. Todd S. Rushing for the opportunity to present and share my work and for their input and direction during their visits to The University of Maine. The content and information within this thesis does not necessarily reflect the position of this funding agency.

Last but certainly not least, I would like to dedicate this thesis to my family. This research would not have been possible without the love and support they have provided throughout my six years of undergraduate and graduate schooling. My parents, Cynthia and Mark Duguay, have encouraged me to take risks and succeed even when the fear of failure is overwhelming. My brother, Desmond Duguay, has given me courage, praise and wisdom. I am truly fortunate to have our unique bond. My sister, Jennifer Duguay, is a beautiful and intelligent philanthropist excelling in her undergraduate studies at Northeastern University. She has given me so much hope and confidence for the continued success of our entire family by traveling the world, taking chances and breaking down cultural barriers. And finally, my grandmother, Eleanor Mitchell, not a holiday has gone by in the past six years where I have not received a card with love, advice and a little money! *I love you guys and thank you for all the support!*

## TABLE OF CONTENTS

ACKNOWLEDGEMENTS .....	iii
LIST OF TABLES .....	ix
LIST OF FIGURES .....	xi
Chapter 1 – BACKGROUND/MOTIVATION .....	1
1.1. Background .....	1
1.1.1. Definition of Polymer Nanocomposite .....	1
1.1.2. Advantages of Nanoparticles .....	2
1.1.3. Challenges in Polymer Nanocomposites .....	5
1.1.3.1. Nanoparticle Dispersion .....	5
1.1.3.2. Nanoparticle Orientation .....	7
1.1.3.3. Cost Effectiveness .....	9
1.1.3.4. Health and Safety Concerns .....	11
1.2. Overview of the Project .....	13
1.2.1. Why IMPP and xGnP? .....	13
1.2.2. Project Motivation .....	18
1.2.3. Objectives.....	19
1.3. Structure of Thesis .....	20
1.3.1. Mechanical and Rheological Properties of xGnP-Filled IMPP .....	20
1.3.2. Thermal Properties of xGnP-Filled IMPP .....	21
1.4. Economic Feasibility of xGnP-Filled IMPP .....	22
1.5. References .....	24

Chapter 2 – FLEXURAL AND TENSILE PROPERTIES OF XGNP-FILLED IMPP NANOCOMPOSITES .....	29
2.1. Chapter Summary .....	29
2.2. Introduction .....	30
2.3. Experimental Procedures .....	33
2.3.1. Materials .....	33
2.3.2. Sample Preparation .....	34
2.3.3. Mechanical Characterization .....	37
2.3.4. Morphological Characterization .....	38
2.3.5. Statistical Analysis .....	39
2.4. Results and Discussion .....	39
2.4.1. Flexural Properties .....	39
2.4.2. Tensile Properties .....	46
2.5. Conclusions .....	64
2.6. References .....	65
Chapter 3 – IMPACT PROPERTIES AND RHEOLOGICAL BEHAVIOR OF XGNP-FILLED IMPP NANOCOMPOSITES .....	70
3.1. Chapter Summary .....	70
3.2. Introduction .....	71
3.3. Experimental Procedures .....	73
3.3.1. Materials .....	73
3.3.2. Sample Preparation .....	74
3.3.3. Mechanical Characterization .....	77

3.3.4. Morphological Characterization .....	78
3.3.5. Melt Flow Characterization .....	78
3.3.6. Statistical Analysis .....	79
3.4. Results and Discussion .....	79
3.4.1. Impact Properties .....	79
3.4.2. Melt Flow Behavior .....	90
3.5. Conclusions .....	97
3.6. References .....	98
 Chapter 4 – THERMAL PROPERTIES OF XGNP-FILLED IMPP	
NANOCOMPOSITES .....	101
4.1. Chapter Summary .....	101
4.2. Introduction .....	102
4.3. Experimental Procedures .....	105
4.3.1. Materials .....	105
4.3.2. Sample Preparation .....	106
4.3.3. Thermal Characterization .....	108
4.4. Results and Discussion .....	109
4.4.1. Differential Scanning Calorimetry (DSC) .....	109
4.4.2. Thermogravimetric analysis (TGA) .....	113
4.5. Conclusions .....	120
4.6. References .....	122

Chapter 5 – CONCLUSIONS AND RECOMMENDATIONS .....	127
5.1. Conclusions .....	127
5.2. Recommendations for Future Work .....	130
BIBLIOGRAPHY .....	133
BIOGRAPHY OF THE AUTHOR .....	139

## LIST OF TABLES

Table 1.1 Geometrical, physical, mechanical and cost characteristics of common fillers .....	18
Table 1.2 Costs of neat materials and different loading levels of xGnP-filled IMPP .....	23
Table 2.1 Summary of materials used in current study .....	34
Table 2.2 Basic operating parameters of the Brabender rheomixer .....	35
Table 2.3 Designated labels and compositions of xGnP-filled neat composites .....	35
Table 2.4 Designated labels and compositions of xGnP-filled composites with the addition of coupling agents .....	36
Table 2.5 Summary of flexural mechanical properties and statistical significance of all compounded materials .....	45
Table 2.6 Summary of tensile mechanical properties and statistical significance of all compounded materials .....	63
Table 3.1 Summary of materials used in current study .....	74
Table 3.2 Basic operating parameters of the Brabender rheomixer .....	75
Table 3.3 Designated labels and compositions of xGnP filled neat composites .....	75
Table 3.4 Designated labels and compositions of xGnP filled compatibilized composites .....	76
Table 3.5 Summary of impact mechanical properties and statistical significance of all compounded materials .....	89
Table 3.6 Summary of melt flow behavior for all compounded materials .....	96
Table 4.1 Summary of materials used in current study .....	106
Table 4.2 Basic operating parameters of the Brabender rheomixer .....	107

Table 4.3 Designated labels and compositions of neat IMPP, neat coupling agents, IMPP/PP-g-MA blends and coupled xGnP-filled IMPP compounded materials discussed .....	107
Table 4.4 DSC summary of $T_m$ , $T_c$ , $\Delta H_m$ , $\Delta H_c$ and $X_c$ for neat IMPP, neat coupling agents, IMPP/PP-g-MA blends and xGnP-filled IMPP composites .....	109
Table 4.5 Thermogravimetric data for neat IMPP, neat coupling agents, IMPP/PP-g-MA blends and xGnP-filled IMPP composites analyzed from ambient temperature to 600 °C .....	114

## LIST OF FIGURES

Figure 1.1 Common particle morphologies and corresponding surface area-to-volume ratios .....	3
Figure 1.2 Surface area-to-volume ratio vs. platelet thickness for layered exfoliated graphite .....	4
Figure 1.3 Illustration of three commonly considered terms to describe dispersion quality .....	6
Figure 1.4 Illustration of randomly oriented and controlled alignment of graphite platelets in a polymer medium .....	9
Figure 1.5 TEM images showing the similarity between morphology of a chrystile asbestos fiber and a MWCNT .....	12
Figure 1.6 Scanning electron micrograph of xGnP <sup>25</sup> showing bulk morphology and average platelet diameter of 25 $\mu\text{m}$ .....	15
Figure 1.7 Scanning electron micrograph of xGnP <sup>15</sup> showing bulk morphology, average platelet diameter of 15 $\mu\text{m}$ and a stacked structure .....	16
Figure 1.8 Scanning electron micrograph of xGnP <sup>5</sup> showing bulk morphology, average platelet diameter of 15 $\mu\text{m}$ and a layered structure .....	17
Figure 2.1 Three categories of nano-reinforcing fillers based on particle geometry .....	31
Figure 2.2 Normalized flexural modulus experimental results for xGnP <sup>5</sup> -filled composites .....	40
Figure 2.3 Normalized flexural modulus experimental results for xGnP <sup>15</sup> -filled composites .....	41
Figure 2.4 Normalized flexural modulus experimental results for xGnP <sup>25</sup> -filled composites .....	41
Figure 2.5 Normalized flexural strength experimental results for xGnP <sup>5</sup> -filled composites .....	42



Figure 2.6 Normalized flexural strength experimental results for xGnP <sup>15</sup> -filled composites .....	43
Figure 2.7 Normalized flexural strength experimental results for xGnP <sup>25</sup> -filled composites .....	43
Figure 2.8 Normalized tensile modulus experimental results for xGnP <sup>5</sup> -filled composites .....	47
Figure 2.9 Normalized tensile modulus experimental results for xGnP <sup>15</sup> -filled composites .....	47
Figure 2.10 Normalized tensile modulus experimental results for xGnP <sup>25</sup> -filled composites .....	48
Figure 2.11 Transmission electron micrographs of IMPP_xGnP <sup>5</sup> _2% and IMPP_WL9100_xGnP <sup>5</sup> _2% .....	50
Figure 2.12 Comparison of Halpin-Tsai prediction of tensile modulus with experimental results for neat xGnP <sup>5</sup> -filled composites .....	52
Figure 2.13 Comparison of Halpin-Tsai prediction of tensile modulus with experimental results for SA9100 coupled xGnP <sup>5</sup> -filled composites .....	52
Figure 2.14 Comparison of Halpin-Tsai prediction of tensile modulus with experimental results for WL9100 coupled xGnP <sup>5</sup> -filled composites .....	53
Figure 2.15 Transmission electron micrograph of IMPP_SA9100_xGnP <sup>25</sup> _4% showing evidence of platelet buckling .....	54
Figure 2.16 Normalized tensile strength experimental results for xGnP <sup>5</sup> -filled composites .....	55
Figure 2.17 Normalized tensile strength experimental results for xGnP <sup>15</sup> -filled composites .....	56
Figure 2.18 Normalized tensile strength experimental results for xGnP <sup>25</sup> -filled composites .....	56
Figure 2.19 Normalized elongation at break experimental results for xGnP <sup>5</sup> -filled composites .....	57
Figure 2.20 Normalized elongation at break experimental results for xGnP <sup>15</sup> -filled composites .....	58

Figure 2.21 Normalized elongation at break experimental results for xGnP <sup>25</sup> - filled composites .....	58
Figure 2.22 Scanning electron micrographs illustrating poor particle/matrix adhesion in tensile fracture surface of IMPP_xGnP <sup>25</sup> _4% at 1200x, 6200x and 13000x magnification .....	60
Figure 2.23 Scanning electron micrographs illustrating progressively brittle failure surfaces in tensile fracture surfaces of Neat IMPP, IMPP_xGnP <sup>25</sup> _2%, IMPP_xGnP <sup>25</sup> _4% and IMPP_xGnP <sup>25</sup> _6% .....	61
Figure 3.1 Conventional toughening mechanisms: inelastic void growth, localized shear yielding or shear crazing, and cavitation of the rubber particles .....	72
Figure 3.2 Normalized unnotched impact strength experimental results for xGnP <sup>5</sup> filled composites .....	81
Figure 3.3 Normalized unnotched impact strength experimental results for xGnP <sup>15</sup> filled composites .....	82
Figure 3.4 Normalized unnotched impact strength experimental results for xGnP <sup>25</sup> filled composites .....	82
Figure 3.5 Normalized notched impact strength experimental results for xGnP <sup>5</sup> filled composites .....	84
Figure 3.6 Normalized notched impact strength experimental results for xGnP <sup>15</sup> filled composites .....	84
Figure 3.7 Normalized notched impact strength experimental results for xGnP <sup>25</sup> filled composites .....	85
Figure 3.8 Transmission electron micrograph with arrow indicating evidence of elastomeric impact modification phase .....	86
Figure 3.9 Conceptual illustration of proposed failure mechanism in xGnP filled IMPP .....	87
Figure 3.10 Melt flow index experimental results for xGnP <sup>5</sup> filled composites .....	91
Figure 3.11 Melt flow index experimental results for xGnP <sup>15</sup> filled composites .....	91

Figure 3.12 Melt flow index experimental results for xGnP <sup>25</sup> filled composites .....	92
Figure 3.13 Correlation of melt flow index with filler loading for IMPP_WL9100_xGnP <sup>5</sup> composites .....	93
Figure 3.14 Correlation of impact properties with melt flow index for IMPP_WL9100_xGnP <sup>5</sup> composites .....	94
Figure 4.1 Effect of particle size on DSC behavior of 96:4 wt./wt. xGnP-filled IMPP composites .....	110
Figure 4.2 Effect of filler loading on DSC behavior of xGnP <sup>5</sup> -filled IMPP composites manufactured with the WL9100 coupling agent .....	112
Figure 4.3 Effect of coupling agents on DSC behavior of neat IMPP and xGnP <sup>5</sup> -filled IMPP composites .....	113
Figure 4.4 Effect of particle size on the TGA behavior of 96:4 wt./wt. xGnP-filled IMPP composites .....	115
Figure 4.5 Effect of particle size on the TGA temperatures at 10% and 50% weight loss of 96:4 wt./wt. xGnP-filled IMPP composites .....	116
Figure 4.6 Effect of filler loading on TGA behavior of xGnP <sup>5</sup> -filled IMPP composites manufactured with the WL9100 coupling agents .....	117
Figure 4.7 Effect of filler loading on TGA temperature at 10% and 50% weight loss of IMPP/xGnP <sup>5</sup> composites manufactured with the WL9100 coupling agent .....	118
Figure 4.8 Effect of coupling agents on the TGA and DTG behavior of neat IMPP and xGnP <sup>5</sup> -filled IMPP composites .....	119
Figure 4.9 Effect of coupling agents on TGA temperature at 10% and 50% weight loss of neat IMPP and xGnP <sup>5</sup> -filled IMPP composites .....	120

## **Chapter 1**

### **BACKGROUND/MOTIVATION**

#### **1.1. Background**

A vast array of inorganic and organic microparticles such as mineral and glass fillers, carbon black and wood flour have been used as fillers in thermoplastic composites to improve stiffness, decrease density, improve long-term mechanical performance and reduce costs (Chen and Gardner 2008). Over the past two decades the rising cost of engineering thermoplastics have invigorated the research and development community to find alternatives via incorporating nanoscale fillers into less expensive commodity thermoplastics to target specific electrical, mechanical, and thermal properties (Houphouet-Boigny 2007; Maniar 2004). The resulting composites are known as polymer nanocomposites (PNCs).

##### **1.1.1. Definition of Polymer Nanocomposite**

The term PNC as used in this thesis is defined as a multiphase polymer-based material where at least one phase exhibits one, two or three dimensions below 100 nm.

### **1.1.2. Advantages of Nanoparticles**

PNCs are one component of the broad field of nanotechnology research and show significantly improved mechanical and thermal properties at far lower reinforcement volume fractions when compared to conventional micro and macro composites (Giannelis 1996; Hussain et al. 2006; Pavlidou and Papaspyrides 2008). The high reinforcement efficiency of some nanoparticles is credited to their high aspect ratio (Hussain et al. 2006). However, it is thought that the need for far lower reinforcement volume fractions stems from the fact that dramatic changes in physical properties of reinforcing particles occur as they depart from microscale classification and approach the nanoscale realm. The specific interfacial area of nanoparticles can reach upwards of hundreds of  $\text{m}^2/\text{g}$ , resulting in high surface area-to-volume ratios. This phenomenon results in relatively high interphase content in nanocomposites (Houphouet-Boigny 2007; Sharma et al. 2002). Many important chemical and physical interactions are governed by surface properties. Therefore a nanocomposite can exhibit significantly different properties even at low filler contents when compared to traditional micro and macro composites (Luo and Daniel 2002).

There is a broad range of nanoparticles that are now commercially available. These include cellulose, clays, carbon, metals, silica, titania, zirconia and the list continues to grow. The potential polymer/nanoparticle combinations and targetable properties are seemingly endless (Vaia et al. 2007). Common particle morphologies and their corresponding surface area-to-volume ratios (Hussain et al. 2006) are depicted in

Figure 1.1. From this figure we can see that the surface area-to-volume ratios are inversely proportional to the particle radius for spheres, rods, tubes and whiskers. Similarly, the surface area-to-volume ratio for a plate-like layered structure is inversely proportional to the platelet thickness. According to Hussain et al., the second terms for rods and layered structures ( $2/l$  and  $4/l$ ) are commonly ignored because the first terms ( $2/r$  and  $2/t$ ) predominately control.


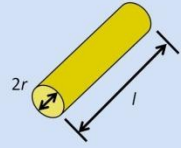
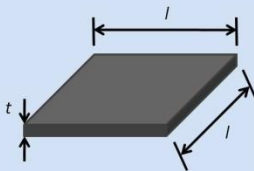
<b>Morphology</b>	Spherical	Rods, Tubes and Whiskers	Layered Structures
<b>Dimensions</b>			
<b>Surface area-to-volume</b>	$\frac{3}{r}$	$\frac{2}{r} + \frac{2}{l}$	$\frac{2}{t} + \frac{4}{l}$

Figure 1.1 Common particle morphologies and corresponding surface area-to-volume ratios. (Reproduced from Hussain et al. 2006).

Figure 1.2 illustrates the exponential increase of surface area-to-volume ratio for layered structures with decreasing platelet thickness. Recognizing this behavior is important because the exfoliated graphite nanoplatelets used throughout this research exhibit an average platelet thickness equal to 10 nm. Therefore we can see that for a traditional microscale platelet with thickness equal to 100 nm (0.1  $\mu\text{m}$ ), the surface area-

to-volume ratio is equal to 0.021. Meanwhile, for a nanoplatelet exhibiting a thickness of just 10 nm, the surface area-to-volume ratio is nearly an order of magnitude larger and is equal to 0.201.

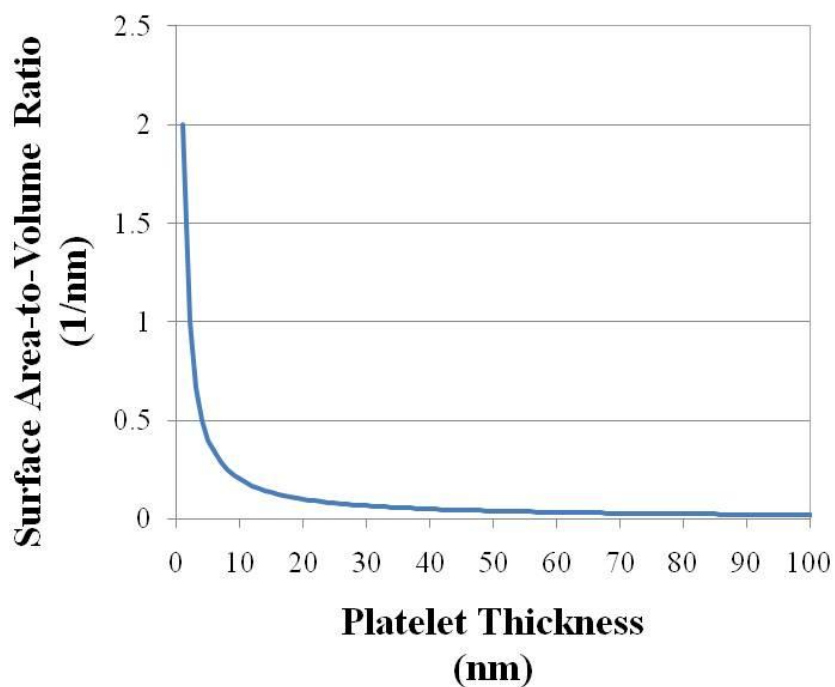


Figure 1.2 Surface area-to-volume ratio vs. platelet thickness for layered exfoliated graphite.

With the advantage of nanoplatelet's high surface area-to-volume ratio as well as high aspect ratio, the development of advanced thermoplastic PNCs remains promising. However, there are significant challenges involved with developing nanocomposite formulations and material-specific fabrication processes. The major challenges associated with polymer nanocomposites are highlighted in the following section.

### **1.1.3. Challenges in Polymer Nanocomposites**

There are many challenges associated with the development and optimization of PNCs. The most prevalent throughout PNC literature are discussed in this section. This includes the uniform dispersion of nanoparticles, the control of nanoparticle orientation, cost effectiveness and health and safety concerns.

#### **1.1.3.1. Nanoparticle Dispersion**

The uniform dispersion of nanoparticles is the first major hurdle scientists face when producing a nanocomposite. Van der Waals forces and differences in polymer/nanoparticle surface energies often cause nanoparticles to have greater affinity towards each other compared to the polymer matrix they are being introduced into. This high affinity between nanoparticles leads to the problem of agglomeration (Thostenson et al. 2005). An illustrative figure to describe the various degrees of dispersion is provided in nearly all nanocomposite literature involving a polymer reinforced with layered structured nanoparticles. Figure 1.3 is provided to illustrate the three commonly considered descriptors of dispersion quality.



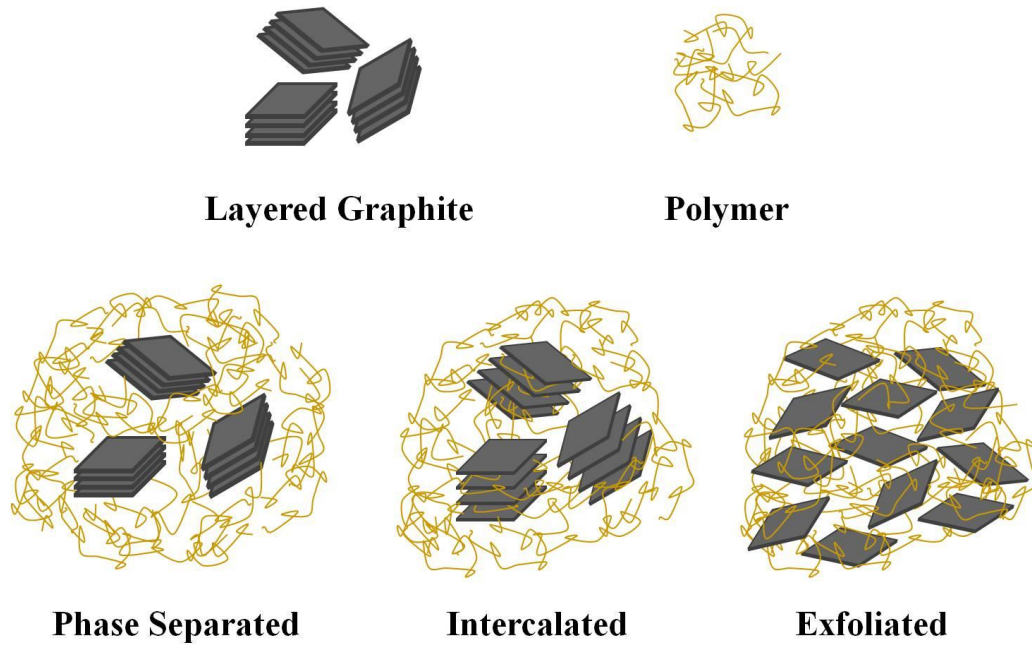


Figure 1.3 Illustration of three commonly considered terms to describe dispersion quality.

The first level of dispersion considered is phase-separated. In this case, the polymer chains are unable to penetrate between the individual graphene sheets (reinforcement phase). In the phase-separated state, the composite may be characterized as a microcomposite because the effective particle sizes can be greater than 100 nm. The reinforcement efficiency of the layered graphite will not be maximized and therefore the mechanical properties will increase only slightly or deteriorate all together. The second level of dispersion considered is a composite exhibiting intercalated morphology. In this case, the polymer chains are able to penetrate between the individual graphene sheets (reinforcement phase). In the intercalated state, the composite may be characterized as a nanocomposite because the effective particle sizes are below 100 nm. The reinforcement efficiency of the layered graphite is improved compared to a phase-separated microcomposite. The third level of dispersion considered is a fully exfoliated composite.

In this case, the polymer chains are able to penetrate between the individual graphene sheets (reinforcement phase) and completely disperse the individual graphene sheets in a continuous polymer matrix. In the exfoliated state, the composite may be characterized as a nanocomposite and the reinforcement efficiency of the layered graphite is maximized (Luo and Daniel 2003; Hussain et al. 2006; Houphouet-Boigny 2007; Thostenson et al. 2005).

The exfoliation of layered structured nanoparticles such as clays and graphite is imperative to maximize their reinforcing efficiency. It has been demonstrated that the magnitude of inherent stress concentrations decreases as the thickness at the tip of graphite agglomerates decreases (Thostenson et al. 2005; Sharma et al. 2002). Improvement in degree of exfoliation results in smaller thickness of effective particles. Therefore an improved degree of exfoliation results in larger surface area-to-volume ratios, lower stress concentrations and subsequently higher performance mechanical properties. Appropriate composite formulations (polymer, coupling agent and nanomaterial) and processing methods must be implemented to achieve dispersion of the individual layers of nanoplatelets such that effective reinforcing particles achieve thicknesses below 100 nm.

### **1.1.3.2. Nanoparticle Orientation**

Control of nanoparticle orientation in a polymer medium is extremely difficult because of the small size of nanoparticles (Thostenson et al. 2005; Vaia et al. 2007;

Wang and Stein 2008; Okamoto et al. 2001). Often times beyond maximizing the dispersion of nanoparticles, the orientation of the nanoparticles is essentially uncontrolled resulting in nanocomposites exhibiting isotropy. This is undesirable when our goal is to target specific electrical, mechanical, and thermal properties and create spatially engineered, designed and tailored materials (Vaia et al. 2007).

Randomly oriented and aligned nanoplatelets in a polymer medium are shown in Figure 1.4. Both images illustrate an exfoliated (well dispersed) nanocomposite. However, the image on the left (randomly oriented) represents the typical morphology of layered structure nanoparticle-reinforced polymers. This morphology has been described as a “house of cards structure” by researchers at the Toyota Technology Institute (Okamoto et al. 2001). Rather than tailoring the nanocomposite for mechanical loading in a specific principle material direction, the nanoplatelets are providing mediocre reinforcement in many different planes. According to Vaia et al., this random arrangement of nanoparticles will not provide optimized electrical, thermal or optical performance as nanocomposite applications extend beyond commodity thermoplastics and enter high-technology components (Vaia et al. 2007). The image on the right (aligned) represents an ideal, controlled morphology of a layered structure nanoparticle-reinforced polymer. In this image, individual reinforcing sheets can be seen well-aligned in one principal material direction. In this case, the nanoplatelet reinforcing efficiency is maximized for mechanical loading in this specific principal material direction. Similarly, the efficiency of a networked structure is maximized for electrical conductance applications in the alignment direction.

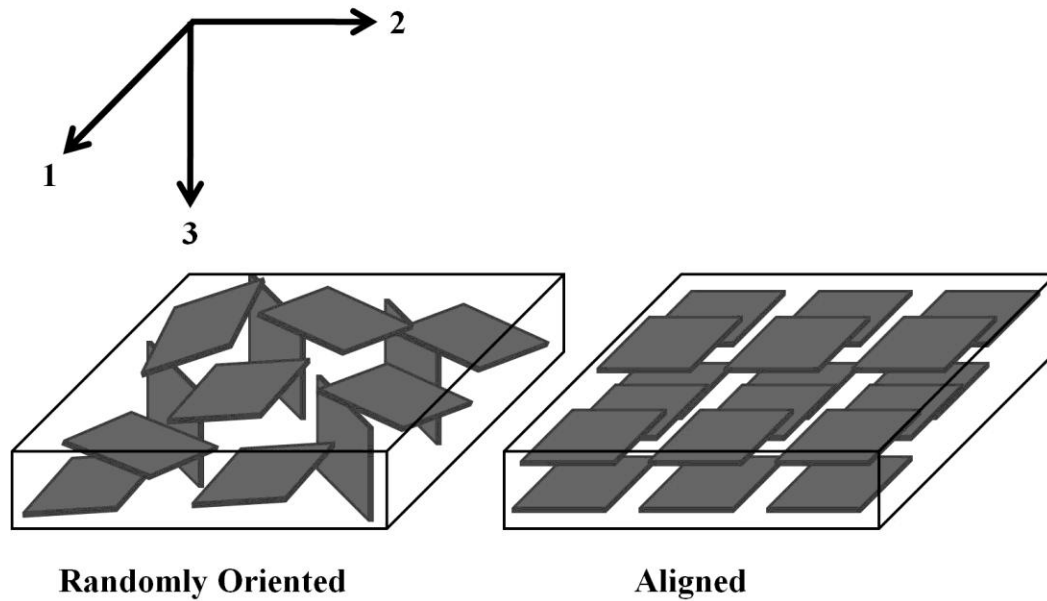


Figure 1.4 Illustration of randomly oriented and controlled alignment of graphite platelets in a polymer medium.

Controlling the morphology of PNCs will become imperative as nanocomposites become more prevalent in high performance applications. As researchers gain further insight into the manipulation of PNC morphology, new processing methods will undoubtedly arise. It is suspected that the technology to develop a scalable method of preferred alignment of nanoparticles will dramatically accelerate the implementation of nanocomposites in both commercial and national defense applications.

### 1.1.3.3. Cost Effectiveness

There are two critical issues in the development of commercially viable nanocomposites. The first critical issue is the development of high volume and high rate fabrication. The second critical issue is the cost of the nano-reinforcement itself.

High volume and high rate fabrication methods will be paramount for the future of nanocomposites in commercial and national defense applications. Similar to the birth of traditional fiber-reinforced polymers (FRPs), highly engineered and efficient processing will successfully transition PNCs into industrial applications (Thostenson et al. 2005; Savage 2004).

Perhaps the most critical challenge in producing commercially viable nanocomposites is the cost of the nano-reinforcement material itself. The most frequently studied nanoscale fillers for polymer resins are nanoclays and carbon nanotubes (CNTs) (Kim et al. 2010; Sherman 2004; Kalaitzidou 2006). While CNTs have outstanding thermal, electrical and mechanical properties, they are very expensive (250-500 \$/lb), which is one of the most serious drawbacks in developing CNT-filled PNCs. The high cost can be linked to low yield and low production and purification rates commonly associated with all of the current CNT preparation processes (Sherman 2007; Kim and Drzal 2009a; Kumar et al. 2010). However, nanoclay-filled PNCs have already made it to commercial applications in the field of lightweight plastics for automobiles. The trend of PNC research is often traced back to 1987 with the work done by researchers from Toyota, Fukushima and Inagaki (Patel et al. 2005). According to Sherman, some of the latest applications include the cargo bed of the 2005 GM Hummer H2 SUT. The vehicle bed uses approximately seven pounds of molded-in-color nanocomposite parts for its center bridge, sail panel, and box-rail protector. The nanocomposite used was Basell's Profax CX-284 reactor TPO with nanoclay. The reason nanoclay-filled PNCs have made

it to industrial applications is certainly due to their outstanding balance between desirable mechanical properties and low cost (2.25-3.25 \$/lb) (Sherman 2004).

#### **1.1.3.4. Health and Safety Concerns**

As nanotechnology's materials and applications continue to grow, more concerns arise about the potential health and environmental implications of exposure to production and use of nanocomposites.

According to Roco, success of nanotechnology will not be defined by only good R&D in academic and industrial environments. Instead, true success of nanotechnology will be a coordination of successful product development with a clear understanding of the societal implications. Advancements in electronic, medical and structural technologies and economies are key factors driving nanotechnology research. However, the negative consequences of nanotechnology, mainly health and safety concerns, are also being vigorously researched (Roco 2003).

Powell and Kanarek explain the very properties that make nanoparticles advantageous, as discussed above, also come into play when recognizing the health risks associated with nanoparticles. That is, because of nanoparticles high surface area-to-volume ratios a large percentage of atoms are on their surface. This allows the atoms to more readily react with adjacent atoms and substances including tissues in the body, and travel easily throughout the body and environmental barriers, such as traditional personal

protective equipment (PPE) (Powell and Kanarek 2006a). Brouwer equates the potential dangers of multi-wall carbon nanotubes (MWCNTs) to the long-term detrimental effects the human race as seen from mass exposure to chrysotile asbestos. Figure 1.5 shows TEM images of a chrysotile asbestos fiber and a typical MWCNT. The similarities between the two fibers morphologies are undeniable. But the question still remains whether the toxicity of MWCNTs to the human respiratory system is the same as asbestos (Brouwer 2009).

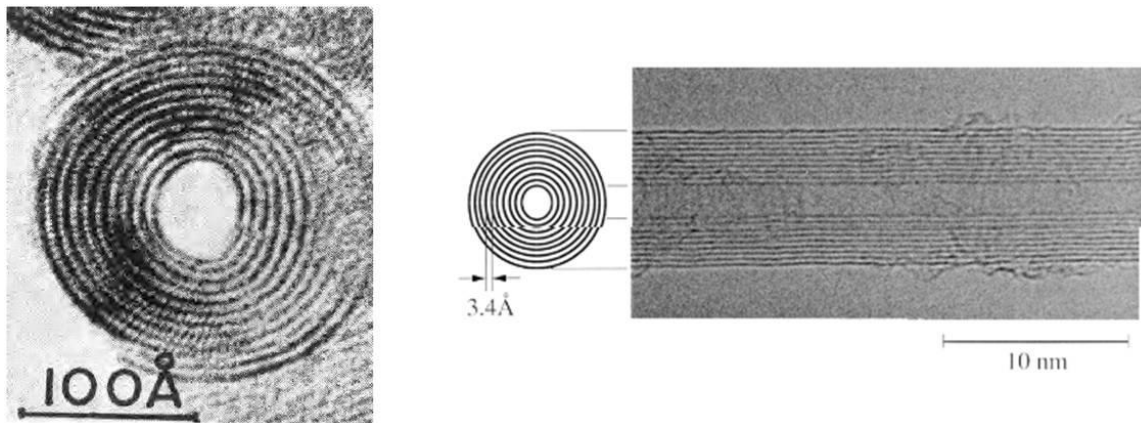


Figure 1.5 TEM images showing the similarity between morphology of a chrysotile asbestos fiber (left) and a MWCNT (right). (Images from Brouwer 2009)

The majority of research conducted regarding the toxicological issues involved with nanomaterials all reports the same current status: there are currently gaps in data which do not allow scientists to make decisive conclusions on the health and safety concerns involved with nanomaterials of all elemental make-up and morphology. Until the necessary research is funded and completed, current personnel working with nanomaterials should take available safety precautions (Powell and Kanarek 2006b; Hutchison 2008; Albrecht et al. 2006; Brouwer 2009). For example, exposure to powder

forms of nanoparticles should be accompanied by appropriate respiratory protection such as a respirator with nano-grade filters as well as epidermal (skin) protection such as latex gloves. Future understanding gained in the health and safety concerns of nanomaterials will produce a consensus on and implementation of strict universal procedures to manage the exposure and risk involved with all nanomaterials.

## **1.2. Overview of the Project**

This section is included to provide justification for the materials chosen for this study, introduce the motivation of the project and the state the objectives this thesis aims to address.

### **1.2.1. Why IMPP and xGnP?**

The increasing cost of engineering thermoplastics is leading researchers to allocate time and resources towards finding alternatives. Commodity thermoplastics are inexpensive, easy to process and well understood, but have lower performance mechanical properties when compared to engineering thermoplastics. It has been shown that we can improve strength and stiffness of commodity thermoplastics by reinforcing them with nanomaterials. Ultimately we would like to increase the performance of the neat commodity thermoplastic such that it performs equally or better than commercially available engineering thermoplastics at a lower cost.



Impact modified polypropylene (IMPP) is currently being used at the AEWCA Advanced Structures and Composites Center. Pre-preg FRP tapes consisting of an IMPP matrix polymer and E-glass continuous fibers are layered and pressed into blast protection panels currently being used by the U.S. military. IMPP was developed to be extremely efficient in absorbing energy in high impact loading scenarios. However a price is paid with the impact modification. IMPP exhibits a significantly lower modulus and strength when compared to neat polypropylene homopolymer (Ahmad et al. 2007; Lim et al. 2008), which is the foundation of IMPP. Herein lays a great opportunity to utilize nanotechnology to increase modulus and strength while either preserving or improving the uniquely tailored impact properties of the existing IMPP used.

The nanoparticles chosen for this study were exfoliated graphite nanoplatelets (xGnP) with three different sizes: xGnP<sup>5</sup> has an average thickness of 10 nm, and an average platelet diameter of 5 μm, whereas xGnP<sup>15</sup> and xGnP<sup>25</sup> have the same thickness but average diameters are 15 and 25 μm, respectively. Scanning electron micrographs provided in Figure 1.6 illustrates the bulk morphology of xGnP<sup>25</sup>. Similarly, Figure 1.7 and Figure 1.8 illustrate the bulk morphology of xGnP<sup>15</sup> and xGnP<sup>5</sup>, respectively. It is shown clearly that each brand of xGnP exhibits an average particle diameter corresponding to the brand name. Furthermore in Figure 1.7 and Figure 1.8 you can see clearly that the bulk morphology of xGnP is in fact agglomerates of prepared expanded graphite (EG) which consists of in some case thousands of individual graphene sheets or graphite nanoplatelets. The stacks of individual graphene sheets readily exfoliate when

introduced under the proper conditions and upon the introduction of mechanical shearing during the melt compounding process.

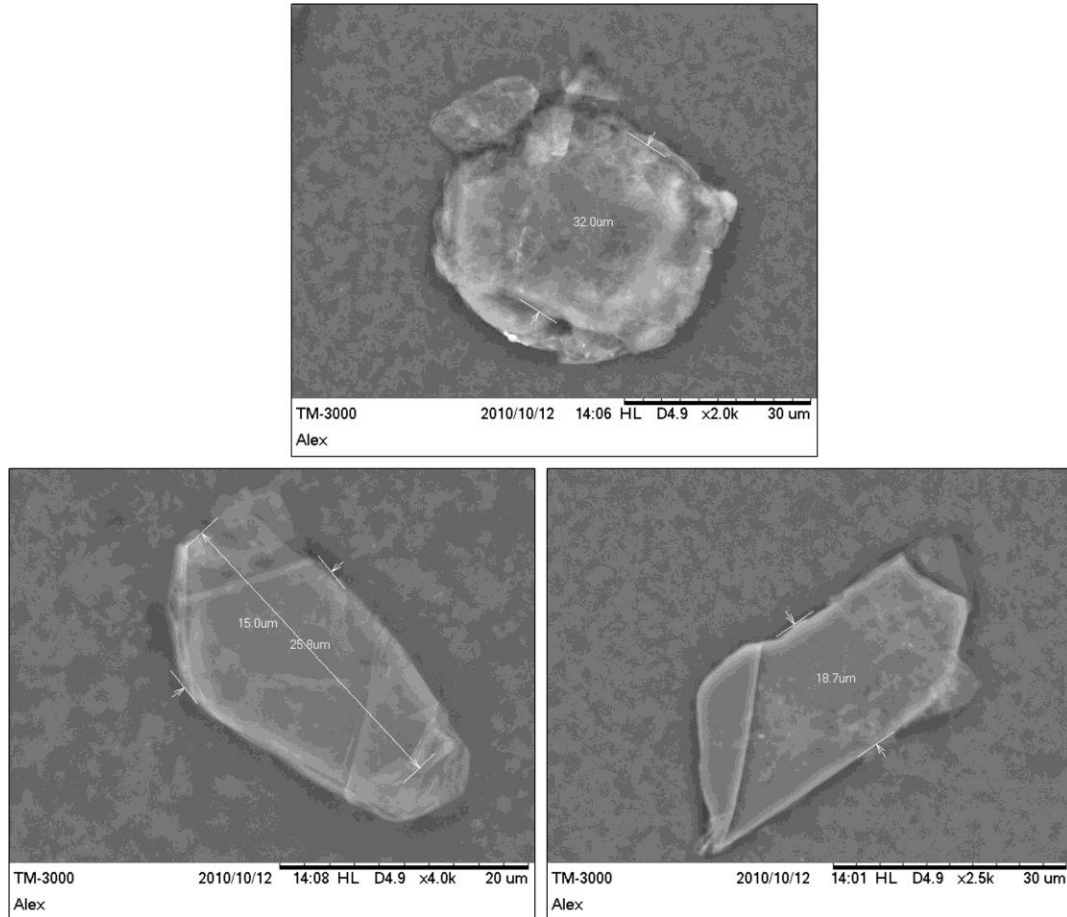


Figure 1.6 Scanning electron micrograph of xGnP<sup>25</sup> showing bulk morphology and average platelet diameter of 25 μm.

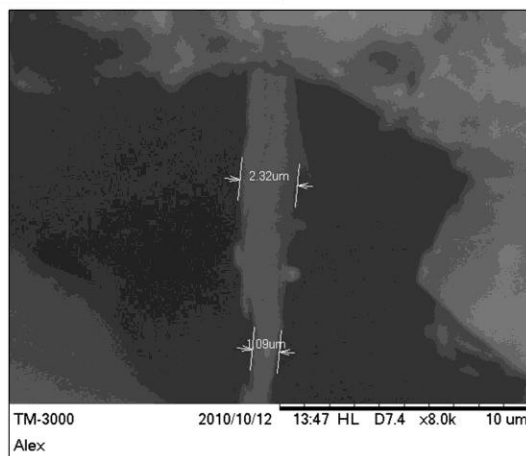
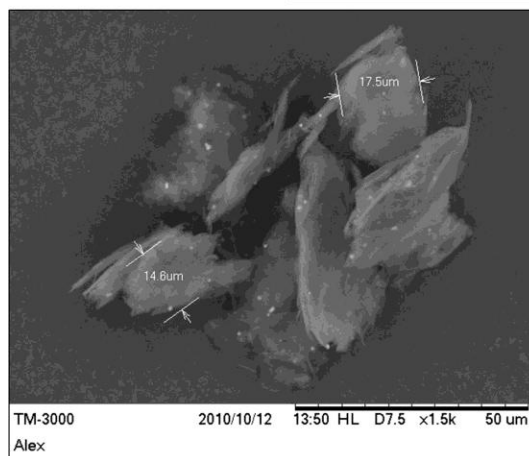
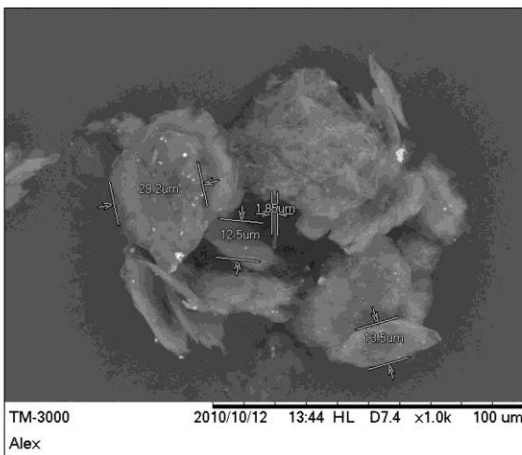


Figure 1.7 Scanning electron micrograph of xGnP<sup>15</sup> showing bulk morphology, average platelet diameter of 15 μm (top and bottom left) and a stacked structure (bottom right).

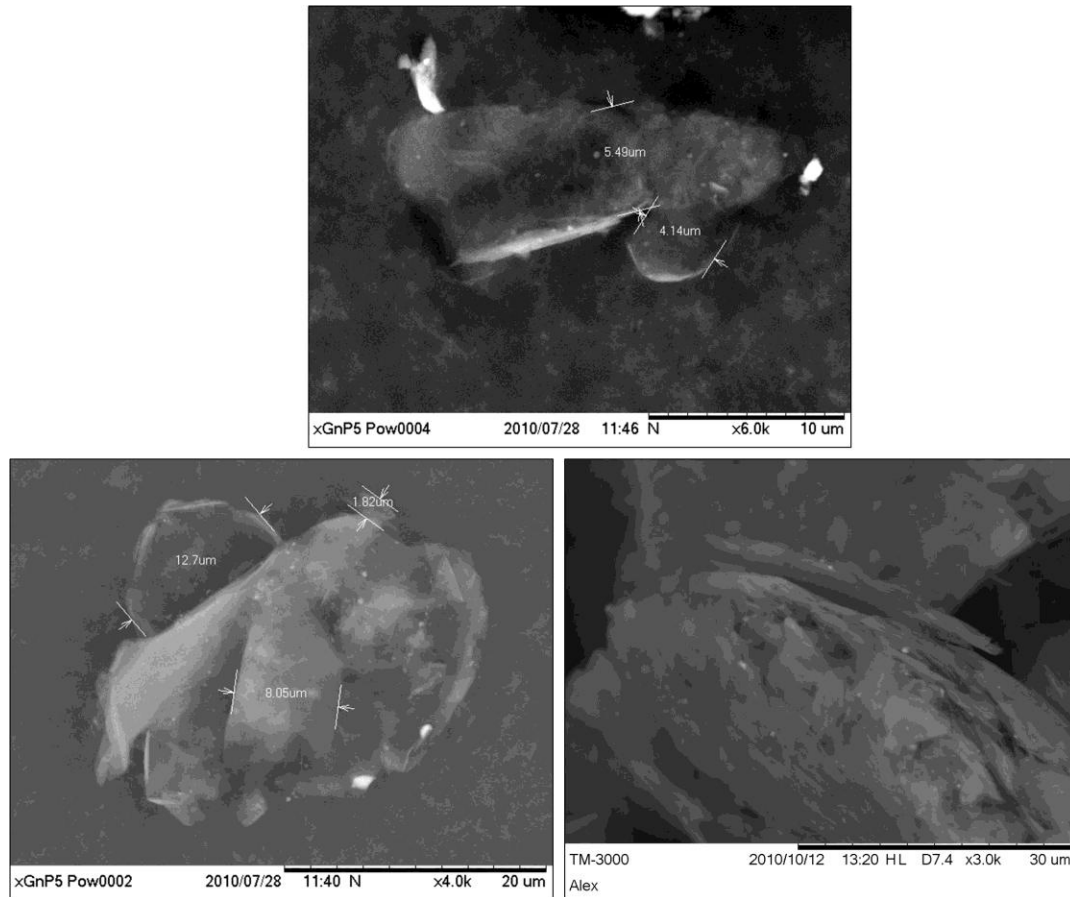


Figure 1.8 Scanning electron micrograph of xGnP<sup>5</sup> showing bulk morphology, average platelet diameter of 15 μm (top and bottom left) and a layered structure (bottom right).

Previous work with nanoclay-filled IMPP has been completed at the AEW. The impact properties were found to remain intact while the stiffness and strength of IMPP was improved slightly. Table 1.1 provides a comparison of common fillers for polymer composites. It can be easily inferred that the xGnP combine unique properties (high aspect ratio, high surface area, high modulus) exhibited by SWCNTs at a considerably lower cost. Although the cost of xGnP is still extremely high compared to clays and carbon black, there is a potential for significant mechanical and thermal enhancement of IMPP at comparably lower filler content. Aside from compressive, flexural and tensile

improvement, there are proposed theoretical mechanism which could cause high aspect ratio nanomaterials to improve impact and fracture properties of PNCs. Crack branching, bridging and pinning are amongst these mechanisms (Lesser 2009; Jiang and Drzal 2010).

Table 1.1 Geometrical, physical, mechanical and cost characteristics of common fillers.

Material	Length (µm)	Diameter (µm)	Thickness (µm)	Aspect Ratio	Surface area (m <sup>2</sup> /g)	Density (g/cm <sup>3</sup> )	Modulus (GPa)	Cost (\$/lb)
xGnP <sup>5</sup>	---	5 <sup>a</sup>	<0.01 <sup>ab</sup>	~500 <sup>a</sup>	60-150 <sup>a</sup>	2 <sup>b</sup>	~1,000 <sup>a</sup>	159
xGnP <sup>15</sup>	---	15 <sup>a</sup>	<0.01 <sup>ab</sup>	~1,500 <sup>ab</sup>	60-150 <sup>a</sup>	2 <sup>b</sup>	~1,000 <sup>a</sup>	159
xGnP <sup>25</sup>	---	25 <sup>a</sup>	<0.01 <sup>ab</sup>	~2,500 <sup>a</sup>	60-150 <sup>a</sup>	2 <sup>b</sup>	~1,000 <sup>a</sup>	159
PAN CF	175 <sup>b</sup>	7.2 <sup>b</sup>	---	~24 <sup>b</sup>	16 <sup>b</sup>	1.81 <sup>b</sup>	531 <sup>c</sup>	5-6 <sup>b</sup>
VGCF	50-100 <sup>b</sup>	0.15 <sup>b</sup>	---	300-700 <sup>b</sup>	25 <sup>b</sup>	2 <sup>b</sup>	680-1,000 <sup>c</sup>	40-50 <sup>b</sup>
CB	0.4-0.5 <sup>b</sup>	0.4-0.5 <sup>b</sup>	---	1 <sup>b</sup>	1,400 <sup>b</sup>	1.8 <sup>b</sup>	---	12 <sup>b</sup>
Clays	---	10-20 <sup>b</sup>	0.05 <sup>b</sup>	300 <sup>b</sup>	>750 <sup>f</sup>	2.85 <sup>b</sup>	170 <sup>f</sup>	2.25-3.25 <sup>d</sup>
SWCNT	3-30 <sup>h</sup>	~0.001 <sup>h</sup>	---	3,000-30,000 <sup>h</sup>	~1,100 <sup>h</sup>	1.3-1.4 <sup>c</sup>	~1,000 <sup>c</sup>	250-500 <sup>g</sup>

<sup>a</sup> Values obtained from XG Sciences Inc.

<sup>b</sup> Values obtained from Kalaitzidou et al. 2007d

<sup>c</sup> Values obtained from Wikipedia

<sup>d</sup> Values obtained from Sherman 2004

<sup>e</sup> Values obtained from Jacobsen 1995

<sup>f</sup> Values obtained from Southern Clay Products Inc.

<sup>g</sup> Values obtained from Sherman 2007

<sup>h</sup> Values obtained from Cheap Tubes Inc.

### 1.2.2. Project Motivation

Both industrial and national defense applications demand materials exhibiting high specific strength and modulus, which can allow decreased material usage and subsequently decreased weight of structures. Graphene-filled polymers are becoming a

highly researched topic in the field of PNCs. The main advantages of graphene are high modulus (~1TPa), high aspect ratio, layered structure, high thermal stability and electrical conductivity. With this wide range of mechanical, physical and thermal properties, graphene is being focused on to create multifunctional nanocomposites. xGnP is expected to provide sufficient reinforcement and toughening while improving the thermal stability of neat IMPP because of the high modulus, high aspect ratio and high thermal stability of graphene.

### **1.2.3. Objectives**

The main objective of this research is to produce well-dispersed nanocomposites which exhibit high specific strength and modulus, high energy absorption capabilities and high thermal stability using melt blending followed by injection molding. Specific research objectives are summarized as shown below.

- Fabricate xGnP-filled IMPP nanocomposites via melt compounding and injection molding.
- Characterize the effect of particle diameter, filler loading and the addition of coupling agents on the mechanical, rheological and thermal properties of xGnP-filled IMPP nanocomposites.
- Utilize electron microscopy techniques as well as traditional mechanics models to draw conclusions regarding degree of xGnP dispersion within the matrix IMPP.

- Correlate mechanical results with rheological behavior to gain insight into optimizing nanocomposite formulations.

### **1.3. Structure of Thesis**

In this thesis, the fabrication methods of thermoplastic nanocomposites are described. The effects of xGnP particle diameter, filler loading and the addition of coupling agent on the performance of xGnP-filled IMPP nanocomposites are investigated. Specifically, this thesis focuses on the effect of these variables on mechanical, rheological and thermal properties that are important in thermoplastic characterization. The thesis is separated into three papers. The first paper investigates the flexural and tensile behaviors of xGnP-filled IMPP nanocomposites. The second paper investigates the impact properties of xGnP-filled IMPP nanocomposites and correlates these impact properties with the rheological behavior of the nanocomposites. Finally the third paper explains the implications on thermal performance when creating xGnP-filled IMPP nanocomposites.

#### **1.3.1. Mechanical and Rheological Properties of xGnP-Filled IMPP**

In chapter 2 the effects of xGnP particle diameter, filler loading and coupling agents on the flexural and tensile properties of IMPP are investigated. The flexural modulus and strength were studied using ASTM D 790-07 which is the standard test method for determining flexural properties of unreinforced and reinforced plastics.

Similarly, the tensile modulus, strength and elongation at break were studied using ASTM D 638-03 which is the standard test method for determining tensile properties of plastics. In chapter 3 the effects of xGnP particle diameter, filler loading and coupling agents on the impact properties and rheological behavior of IMPP is investigated. The unnotched and notched impact strengths as well as fracture initiation resistance were studied using ASTM D 256-06 which is the standard test method for determining the Izod impact properties of plastics. The melt flow index was studied using ASTM D 1238-04c which is the standard test method for determining the melt flow rates of thermoplastics. Both scanning electron microscopy (SEM) and transmission electron microscopy (TEM) were used throughout chapters 2 and 3 where morphological characterization was imperative to understanding the quality of dispersion and the failure mechanisms occurring in the composites.

### **1.3.2. Thermal Properties of xGnP-Filled IMPP**

In chapter 4 the effects of xGnP particle diameter, filler loading and coupling agents on the thermal properties of IMPP are investigated. The melting temperature, crystallization temperature, heat of fusion and degree of crystallinity were studied by means of differential scanning calorimetry (DSC). The peak degradation temperature, weight loss at peak degradation temperature and residual mass after 600 °C was determined using thermogravimetric analysis (TGA).



#### 1.4. Economic Feasibility of xGnP-Filled IMPP

To justify the commercialization of new composite materials with high performance nano fillers, the development efforts must improve working properties and extend the base polymer's range of applications all in a cost efficient manner. Incorporating low loading levels of nanoscale reinforcing fillers into polymer matrices is a promising approach to achieve these goals.

The cost of different blends of xGnP-filled IMPP pellets can be calculated according to Equation 1.1 (Rowell 1998).

$$\$/lb = \frac{PCT(X) + PG(Y) + C}{E} \quad \text{Equation 1.1}$$

Where PCT is the percentage of commodity thermoplastic in the composite by weight, X is the cost of the commodity thermoplastic in dollars per pound, PG is the percentage of graphene in the composite by weight, Y is the cost of the graphene filler in dollars per pound, PCA is the percentage of coupling agent in the composite by weight, Z is the cost of the coupling agent in dollars per pound, C is the cost of compounding the composite in dollars per pound, and E is the efficiency of the composite fabrication process.

Table 1.2 shows the resulting nanocomposite costs in dollars per pound for different loading levels of xGnP-filled IMPP nanocomposites manufactured using a composite fabrication process with an efficiency (E) equal to 1 and a process which cost

0.20 \$/lb of composite material compounded (C). From this table and the conclusions developed throughout this thesis it is suspected that there is a potential for low filler loading level (<0.5 wt. %) xGnP-filled IMPP.

Table 1.2 Costs of neat materials and different loading levels (wt. %) of xGnP-filled IMPP.

Material	Cost (\$/lb)
IMPP	1.10
PP-g-MA	2.25
xGnP	159
IMPP_PP-g-MA_xGnP_0.01%	1.32
IMPP_PP-g-MA_xGnP_0.05%	1.38
IMPP_PP-g-MA_xGnP_0.10%	1.46
IMPP_PP-g-MA_xGnP_0.50%	2.09
IMPP_PP-g-MA_xGnP_1.00%	2.88
IMPP_PP-g-MA_xGnP_2.00%	4.47
IMPP_PP-g-MA_xGnP_4.00%	7.64
IMPP_PP-g-MA_xGnP_6.00%	10.81
IMPP_PP-g-MA_xGnP_8.00%	13.98

## 1.5. References

Ahmad S.H., Rasid R., Surip S.N., Anuar H., Czigany T., Abdul Razak S.B. “Mechanical and Fracture Toughness Behavior of TPNR Nanocomposites.” *Journal of Composite Materials*, 41(17) (2007): 2147-2159.

Brouwer, Derk. “Potential for exposure to (manufactured) nano-objects (particles) in workplaces.” *Proceedings of NSF Summer Institute on Nanomechanics, Nanomaterials, and Micro/Nanomanufacturing*, University of Massachusetts Lowell (2009).

Chen J. & Gardner D.J. “Dynamic mechanical properties of extruded nylon-wood composites.” *Polymer Composites*, 29 (4) (2008): 372–379.

Houphouet-Boigny, Chrystèle. Fiber Reinforced Polypropylene Nanocomposites. PhD Dissertation, Lausanne, Switzerland: Institute of Technology (EPFL) (2007).

Giannelis, Emmanuel P. “Polymer Layered Silicate Nanocomposites.” *Advanced Materials*, 8 (1) (1996): 29-35.

Hussain F., Hojjati M., Okamoto M. and Gorga R.E. “Review article: Polymer-matrix Nanocomposites, Processing, Manufacturing, and Application: An Overview.” *Journal of Composite Materials*, 40 (17) (2006): 1511-1575.

Jacobsen R.L., Tritt T.M., Guth J.R., Ehrlich A.C. and Gillespie D.J. “Mechanical Properties of Vapor-Grown Carbon Fiber” *Carbon*, 33 (9) (1995): 1217-1221.

Jiang X. & Drzal L. T. “Multifunctional High Density Polyethylene Nanocomposites Produced by Incorporation of Exfoliated Graphite nanoplatelets 1: Morphology and Mechanical Properties.” *Polymer Composites*, (2010): 1091-1098.

Kalaitzidou, Kyriaki. Exfoliated Graphite Nanoplatelets as Nanoreinforcement for Multifunctional Polypropylene Nanocomposites. PhD Dissertation, East Lansing, MI, USA: Michigan State University (2006).

Kalaitzidou K., Fukushima H., Drzal L. T. “Mechanical properties and morphological characterization of exfoliated graphite-polypropylene nanocomposites.” *Composites: Part A*, 38 (2007d): 1675-1682.

Kim S. & Drzal L. T. “High latent heat storage and high thermal conductive phase change materials using exfoliated graphite nanoplatelets.” *Solar Energy Materials & Solar Cells*, 93 (2009a): 136-142.

Kim S., Do I. & Drzal L.T. “Thermal Stability and Dynamic Mechanical Behavior of Exfoliated Graphite Nanoplatelets LLDPE Nanocomposites.” *Polymer composites*, 31 (5) (2010): 755-761.

Kumar S., Sun L.L., Caceres S., Li B., Wood W., Pereguni A., Maguire R.G. & Zhong W.H. “Dynamic synergy of graphitic nanoplatelets and multi-walled carbon nanotubes in polyetherimide nanocomposites.” *Nanotechnology*, 21 (10) (2010): 105702 (9pp).

Lesser A.J. “Fundamentals in Toughening.” *Proceedings of NSF Summer Institute on Nanomechanics, Nanomaterials, and Micro/Nanomanufacturing*, University of Massachusetts Lowell (2009).

Lim J.W., Hassan A., Rahmat A.R., Wahit M.U. “Phase Morphology and Mechanical Properties of Rubber-Toughened Polypropylene Nanocomposites: Effect of Elastomer Polarity.” *Polymer-Plastics Technology and Engineering*, 47 (2008): 411-419.

Luo J-J. & Daniel I.M. “Characterization and modeling of mechanical behavior of polymer/clay nanocomposites.” *Composites Science and Technology*, 63 (2008): 1607–1616.

Maniar, Ketan K. “Polymeric Nanocomposites: A Review.” *Polymer-Plastics Technology and Engineering*, 43 (2) (2004): 427–443.

Okamoto M., Nam H.P., Maiti P., Kotaka T., Hasegawa N. and Usuki A. “A House of Cards Structure in Polypropylene/Clay Nanocomposites under Elongational Flow” *Nano Letters*, 1 (6) (2001): 295-298.

Pavlidou S. & Papaspyrides C.D. "A review on polymer-layered silicate nanocomposites." *Progress in Polymer Science*, 33 (12) (2008): 1119–1198.

Patel H.A., Somani R.S., Bajaj H.C. and Jasra R.V. "Nanoclays for polymer nanocomposites, paints, inks, greases and cosmetic formulations, drug delivery vehicle and waste water treatment." *Bulletin of Material Science*, 29 (2) (2006): 133-145.

Powell M.C. & Kanarek M.S. "Nanomaterial Health Effects – Part 1: Background and Current Knowledge." *Wisconsin Medical Journal*, 105 (2) (2006a): 16-20.

Powell M.C., Kanarek M.S. "Nanomaterial Health Effects – Part 2: Uncertainties and Recommendations for the Future." *Wisconsin Medical Journal*, 105 (3) (2006b): 18-23.

Roco, M.C. "Broader societal issues of nanotechnology." *Journal of Nanoparticle Research*, (5) (2003): 181-189.

Rowell, Roger M. "Economic Opportunities in Natural Fiber-Thermoplastic Composites." In *Science and Technology of Polymers and Advanced Materials: Emerging Technologies and Business Opportunities*, 869-872. New York: Plenum Press, 1998.

Savage S.J. "Defence applications of nanocomposite materials." FOI Swedish Defence Research Agency. User Report. December 2004. pp. 1-20.

Sharma P., Ganti S., and Bhate N. "Effect of surfaces on size-dependent elastic state of nano-inhomogeneities." *Applied Physics Letters*, 82 (4) (2003): 535–537.

Sherman, Lilli Manolis. "Chasing Nanocomposites." *Plastics Technology*, 50 (11) (2004): 56-61.

Sherman, Lilli Manolis. "Carbon nanotubes: Lots of potential-If the price is right" *Plastic Technology*, 53 (2007): 68-73.

Thostenson E. T., Li C., Chou T.W. "Nanocomposites in context." *Composites Science and Technology*, 65 (2005): 491-516.

Vaia R., Koerner H., Lu W., Manias E. "Polymer Nanocomposites With Prescribed Morphology: Going Beyond Nanoparticle-filled Polymers." *Chemistry of Materials*, 19 (11) (2007): 2736-2751.

Wang Z. & Stein A. "Morphology Control of Carbon, Silica, and Carbon/Silica Nanocomposites: From 3D Ordered Macro-/Mesoporous Monoliths to Shaped Mesoporous Particles." *Chemistry of Materials*, 20 (3) (2008): 1029-1040.

## Chapter 2

### FLEXURAL AND TENSILE PROPERTIES OF XGNP-FILLED IMPP NANOCOMPOSITES

#### 2.1. Chapter Summary

xGnP-filled IMPP composites were prepared at 2, 4, 6, and 8 wt. % xGnP with and without the addition of a coupling agent and manufactured using melt mixing followed by injection molding. The coupling agent used in this study was polypropylene-graft-maleic anhydride (PP-g-MA). The nanoparticles used were xGnP with three different sizes: xGnP5 has an average thickness of 10 nm, and an average platelet diameter of 5  $\mu\text{m}$ , whereas xGnP15 and xGnP25 have the same thickness but average diameters are 15 and 25  $\mu\text{m}$ , respectively. Test results show that nanocomposites with smaller xGnP diameter exhibited better flexural and tensile properties for both neat and compatibilized composites. For composites containing a coupling agent, tensile and flexural modulus and strength increased with the addition of xGnP. In the case of neat composites, both tensile and flexural modulus and strength decreased at higher filler loading levels. Increasing xGnP loading resulted in reduction of elongation at break for both neat and composites containing coupling agent. Explanation of this brittle behavior in a nanoplatelet filled IMPP is presented using scanning electron microscopy and transmission electron microscopy.



## 2.2. Introduction

Polymer nanocomposites (PNCs) are continuing to be of great interest in the thermoplastics industry. Nano-reinforcing fillers can be divided into three categories based on particle morphologies as illustrated in Figure 2.1. The first category is made up of spherical particles exhibiting three dimensions on the nanoscale. A few examples of these are gold, titanium oxide and silica dioxide particles. The second category consists of rods, tubes and whiskers having two dimensions on the nanoscale. Some examples of these are gold and silver nano rods, multi-wall and single-wall carbon nanotubes and cellulose nanowhiskers. Finally the third category contains layered structural fillers exhibiting one dimension on the nanoscale. Typical fillers from this category used for mechanical enhancement are exfoliated graphite nanoplatelets, mica and nanoclays (Kim et al. 2010a). Incorporating nanoscale fillers into polymer matrices can be a simple and economical process to enhance the properties of the neat matrix material (Ahmad et al. 2007). In fact, dramatic improvements in mechanical and thermal properties have been documented with as little as 2 to 6 weight percentage of nanoparticles introduced into thermoplastic matrices via melt compounding. Currently, the most commonly used nano reinforcement phase is layered silicate nanoclays and carbon nanotubes (CNTs) (Sherman 2004).

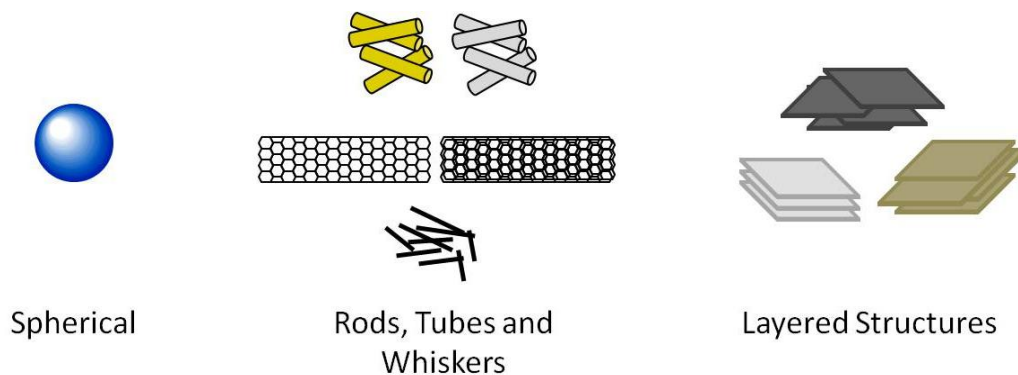


Figure 2.1 Three categories of nano-reinforcing fillers based on particle geometry.

Recently there has been increasing interest in the use of exfoliated graphite nanoplatelets (xGnP) as a multifunctional reinforcement phase for PNCs. These graphitic nanoplatelets, derived from expanded graphite (EG), combine the low-cost and stacked or layered structures of nanoclays with a unique plethora of properties usually exhibited by CNTs including electrical conductivity, and superior mechanical, physical, and thermal properties. (Kim et al. 2010a-b; Kalaitzidou et al. 2007a-d; Stankovich et al. 2006; Kim and Drzal 2009a-b; Chen et al. 2001; Park et al. 2007; Miloago et al. 2005; Jiang and Drzal 2010) Unfortunately, similar to nanoclay dispersions, in the absence of a coupling agent the stacks of nano-thin graphite sheets do not readily exfoliate when incorporated into thermoplastic matrices. Rather than exfoliating into individual graphene sheet reinforcements, the stacks of xGnP tend to remain agglomerated, exhibiting an intercalated dispersion (Ratnayake et al. 2009).

Polypropylene (PP) is among the most commonly used thermoplastics in the world with a vast range of applications in the automobile and construction industries (Teng et. al 2008). PP is non polar and does not interact with chemically inert graphite.

Therefore, producing graphite-reinforced PP nanocomposites is very difficult because of the lack of affinity between the two constituents. This issue can be overcome by adding a coupling agent such as propylene-graft-maleic anhydride (PP-g-MA) (Gopakumar and Page 2004; Spoljaric et al. 2009). According to a study by Page et al., XRD and SEM results indicate that the functionalization of PP by addition of PP-g-MA leads to an excellent dispersion of graphite, and improvement in flexural properties of the material (Page and Gopakumar 2006).

The objective of this study was to investigate the influence of (1) particle diameter, (2) filler loading, and (3) coupling agent, on the flexural and tensile mechanical properties of xGnP filled IMPP composites. The ultimate goal is to enhance the stiffness, strength and overall toughness of IMPP using xGnP. All compounded materials were manufactured using melt mixing followed by injection molding and were prepared at 2, 4, 6, and 8 wt. % xGnP. The weight ratio of filler-to-coupling agent was held constant at 2:1 throughout this study. Mechanical characterization was accomplished via flexural and tensile tests. Morphological characterization was conducted by means of scanning electron microscopy (SEM) and transmission electron microscopy (TEM).

## 2.3. Experimental Procedures

### 2.3.1. Materials

The IMPP was supplied as polymer pellets by Polystrand Inc., USA. The IMPP had a density of  $0.900 \text{ g/cm}^3$  and melt flow index of 35 g/10 min. The xGnP fillers were supplied by XG Sciences Inc., USA. Three xGnP fillers in powder form were used as the reinforcement with different particle diameters 5, 15, and 25  $\mu\text{m}$ . Average platelet thickness ranges from about 5 to 15 nanometers. This translates into an average particle surface area ranging from about 60 to 150  $\text{m}^2/\text{g}$ . The bulk density of all three xGnP fillers is reported to be 0.18-0.25  $\text{g/cm}^3$ . Two different PP-g-MA were used as coupling agents, labeled for this study as SA9100 and WL9100, provided by Sigma-Aldrich Co., USA and West Lake Chemical Co., USA, respectively. Both coupling agents had a density of  $0.934 \text{ g/cm}^3$ , molecular weight of 9,100 by GPC, and acid number of 45-47. SA9100 and WL9100 coupling agents differed in that their maleic anhydride content was 8-10% and <0.7%, respectively. Materials used in this study are summarized in Table 2.1.

Table 2.1 Summary of materials used in current study.

Material/Supplier	Label	Density (g/cm <sup>3</sup> )	MA Content (%)	M <sub>w</sub>	Acid #
Impact Modified Polypropylene/ <i>Polystrand Inc.</i>	IMPP	0.900	---	---	---
Exfoliate Graphite Nanoplatelets 5μ/ <i>XG Sciences Inc.</i>	xGnP <sup>5</sup>	2	---	---	---
Exfoliate Graphite Nanoplatelets 15μ/ <i>XG Sciences Inc.</i>	xGnP <sup>15</sup>	2	---	---	---
Exfoliate Graphite Nanoplatelets 25μ/ <i>XG Sciences Inc.</i>	xGnP <sup>25</sup>	2	---	---	---
Polypropylene-g-Maleic Anhydride/ <i>Sigma-Aldrich Co.</i>	SA9100	0.934	8-10	9100	47
Polypropylene-g-Maleic Anhydride/ <i>West Lake Chemical Co.</i>	WL9100	0.934	< 0.7	9100	45

### 2.3.2. Sample Preparation

The matrix polymer IMPP was mixed with the xGnP fillers. The compounding was carried out with a Brabender Prep-mixer® equipped with a mixing bowl. The basic processing parameters used in this study are summarized in Table 2.2. The temperature was set to 180 °C and mixing speed was set at 60 rpm. All composite formulations were prepared in 150 g batches and all constituents were added to the mixer simultaneously. Mixing was done for 20 minutes; this was an optimum processing time as determined from preliminary experiments.

Table 2.2 Basic operating parameters of the Brabender rheomixer.

Batch Size (g)	Temperature (°C)	RPM	Compounding Time (min)
150	180	60	20

All composite compounds were then granulated using a lab scale grinder. The ground particles were then injection molded into ASTM test samples using a barrel temperature of 246 °C and injection pressure of 2,500 psi. The designated labels and compositions of all compounded materials with and without the addition of a coupling agent are shown in Table 2.3 and Table 2.4, respectively.

Table 2.3 Designated labels and compositions of xGnP-filled neat composites.

Study Label	Content Per Batch (g)					
	IMPP	SA9100	WL9100	xGnP <sup>5</sup>	xGnP <sup>15</sup>	xGnP <sup>25</sup>
IMPP_xGnP <sup>5</sup> _2%	147	---	---	3	---	---
IMPP_xGnP <sup>5</sup> _4%	144	---	---	6	---	---
IMPP_xGnP <sup>5</sup> _6%	141	---	---	9	---	---
IMPP_xGnP <sup>5</sup> _8%	138	---	---	12	---	---
IMPP_xGnP <sup>15</sup> _2%	147	---	---	---	3	---
IMPP_xGnP <sup>15</sup> _4%	144	---	---	---	6	---
IMPP_xGnP <sup>15</sup> _6%	141	---	---	---	9	---
IMPP_xGnP <sup>15</sup> _8%	138	---	---	---	12	---
IMPP_xGnP <sup>25</sup> _2%	147	---	---	---	---	3
IMPP_xGnP <sup>25</sup> _4%	144	---	---	---	---	6
IMPP_xGnP <sup>25</sup> _6%	141	---	---	---	---	9
IMPP_xGnP <sup>25</sup> _8%	138	---	---	---	---	12

Table 2.4 Designated labels and compositions of xGnP-filled composites with the addition of coupling agents.

Study Label	Content Per Batch (g)					
	IMPP	SA9100	WL9100	xGnP <sup>5</sup>	xGnP <sup>15</sup>	xGnP <sup>25</sup>
IMPP_SA9100_xGnP <sup>5</sup> _2%	145.5	1.5	---	3	---	---
IMPP_SA9100_xGnP <sup>5</sup> _4%	141	3	---	6	---	---
IMPP_SA9100_xGnP <sup>5</sup> _6%	136.5	4.5	---	9	---	---
IMPP_SA9100_xGnP <sup>5</sup> _8%	132	6	---	12	---	---
IMPP_SA9100_xGnP <sup>15</sup> _2%	145.5	1.5	---	---	3	---
IMPP_SA9100_xGnP <sup>15</sup> _4%	141	3	---	---	6	---
IMPP_SA9100_xGnP <sup>15</sup> _6%	136.5	4.5	---	---	9	---
IMPP_SA9100_xGnP <sup>15</sup> _8%	132	6	---	---	12	---
IMPP_SA9100_xGnP <sup>25</sup> _2%	145.5	1.5	---	---	---	3
IMPP_SA9100_xGnP <sup>25</sup> _4%	141	3	---	---	---	6
IMPP_SA9100_xGnP <sup>25</sup> _6%	136.5	4.5	---	---	---	9
IMPP_SA9100_xGnP <sup>25</sup> _8%	132	6	---	---	---	12
IMPP_WL9100_xGnP <sup>5</sup> _2%	145.5	---	1.5	3	---	---
IMPP_WL9100_xGnP <sup>5</sup> _4%	141	---	3	6	---	---
IMPP_WL9100_xGnP <sup>5</sup> _6%	136.5	---	4.5	9	---	---
IMPP_WL9100_xGnP <sup>5</sup> _8%	132	---	6	12	---	---
IMPP_WL9100_xGnP <sup>15</sup> _2%	145.5	---	1.5	---	3	---
IMPP_WL9100_xGnP <sup>15</sup> _4%	141	---	3	---	6	---
IMPP_WL9100_xGnP <sup>15</sup> _6%	136.5	---	4.5	---	9	---
IMPP_WL9100_xGnP <sup>15</sup> _8%	132	---	6	---	12	---
IMPP_WL9100_xGnP <sup>25</sup> _2%	145.5	---	1.5	---	---	3
IMPP_WL9100_xGnP <sup>25</sup> _4%	141	---	3	---	---	6
IMPP_WL9100_xGnP <sup>25</sup> _6%	136.5	---	4.5	---	---	9
IMPP_WL9100_xGnP <sup>25</sup> _8%	132	---	6	---	---	12

### 2.3.3. Mechanical Characterization

Tensile tests were conducted according to the American Society of Testing and Materials (ASTM) standard D 638-03, "Standard Test Method for Tensile Properties of Plastics". The tensile behaviors of composites were measured using an Instron 8801 with a 5 kN load cell. All the tension tests were conducted at a rate of 5.08 mm/min. An extensometer was used for elongation determinations. Tensile modulus of the polymer composites was determined from the slope of the linear portion of the stress-strain curve. Tensile strength was calculated from the maximum load of the load-displacement curve divided by the specimen original cross-sectional area. Elongation at break was also reported. At least five samples were tested for each composition and the results are presented as an average for tested samples.

Flexural tests were conducted according to ASTM D 790-07, "Standard Test Methods for Flexural Properties of Unreinforced and Reinforced Plastics and Electrical Insulating Materials", Procedure A. This test consisted of a three-point loading system introducing mid-span loading using an Instron 8801 with a 225 N load cell. The support span was 52.8 mm, resulting in a span-to-depth ratio of 16 ( $\pm 1$ ). All flexural tests were conducted at a rate of 1.27 mm/min. Flexural modulus of the polymer composites was determined using Equation 2.1 and inputting the slope of the linear portion of the load-deflection curve for the variable  $m$ . Flexural strength was calculated using Equation 2.2 and inputting the maximum load of the load-displacement curve for the variable  $P$ . The other variables in the equation are  $L$ ,  $b$  and  $d$ , which is the span, width and depth of the



beam specimen, respectively. At least five samples were tested for each composition and the results are presented as an average for tested samples.

$$E_b = \frac{L^3 m}{4bd^3} \quad \text{Equation 2.1}$$

$$\sigma_f = \frac{3PL}{2bd^2} \quad \text{Equation 2.2}$$

#### **2.3.4. Morphological Characterization**

Studies regarding the microscopic morphology of the tensile fracture surfaces of the composites were carried out using an AMR 1000 (AMRay Co.) scanning electron microscope. Images were taken at 10 kV with 1200 X, 6200 X and 13000 X SEM micrograph magnifications. All samples were sputter coated with gold before the microscopic observations were obtained.

The nanoscale morphology of the PNCs was completed using a Phillips CM10 transmission electron microscope. Images were taken at magnifications of 130 kX, 245 kX and 450 kX. Sectioning of thermoplastics is a difficult task because of their inherently soft characteristics. In the absence of low temperature ultra-cryotome technology, a method for obtaining ultrathin sections was necessary. Thin slivers of our composites were shaved and embedded in an epoxy matrix to aid in sectioning the soft plastic. The embedded sample was then sectioned using a Leica EM UC6 ultra-microtome equipped

with a diamond knife. Specimens were sectioned with thickness on the order of 50-75 nm.

### **2.3.5. Statistical Analysis**

The flexural modulus, flexural strength, tensile modulus, tensile strength and elongation at break were compared using a one-way analysis of variance followed by Tukey-Kramer Honestly Significant Differences (HSD) test at a confidence value equal to 0.05 with JMP statistical analysis program (JMP 9).

## **2.4. Results and Discussion**

### **2.4.1. Flexural Properties**

The flexural behavior of all compounded composites was characterized via the flexural testing methods describe in Section 2.3.3. Neat IMPP was determined to have flexural modulus and flexural strength equal to 1.1 GPa and 33.7 MPa, respectively.

Normalized flexural modulus results for neat and xGnP<sup>5</sup>-filled composites with coupling agent as a function of filler loading level up to 8% are presented in Figure 2.2. Similar plots are provided for neat and xGnP<sup>15</sup> and xGnP<sup>25</sup>-filled composites with coupling agent in Figure 2.3 and Figure 2.4, respectively. In general, flexural modulus

was found to increase with decreasing xGnP particle diameter and increased filler loading for both neat and xGnP-filled composites containing coupling agent. However, flexural modulus increased with filler loading much more efficiently at higher loading levels for composites containing coupling agent. In general, the optimum formulation to improve flexural modulus for filler loading levels 2, 4, 6 and 8 wt. % is IMPP\_WL9100\_xGnP<sup>15</sup> composites. The resulting improvement from neat IMPP is 16, 24, 35 and 50%, respectively.

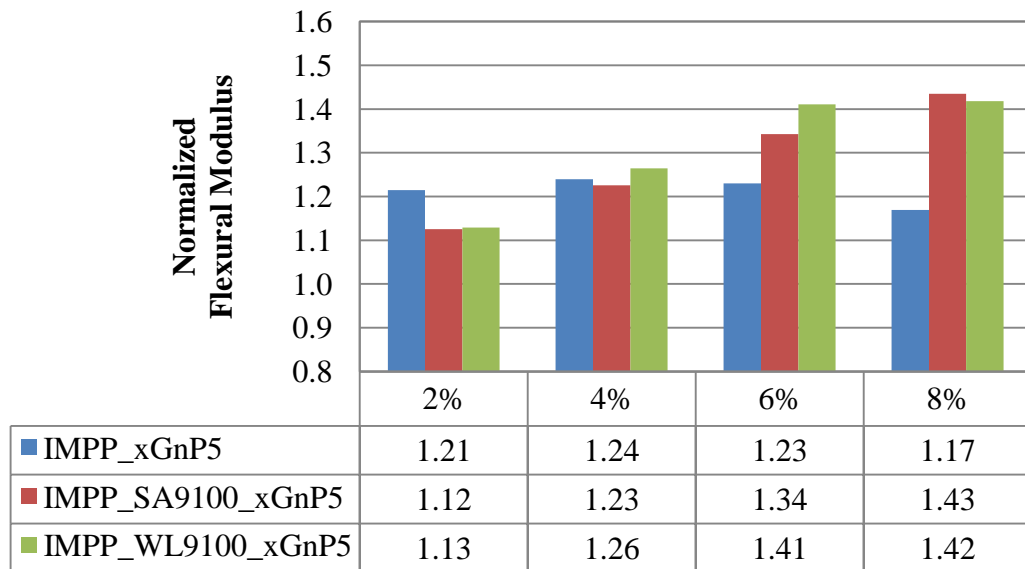


Figure 2.2 Normalized flexural modulus experimental results for xGnP<sup>5</sup>-filled composites.

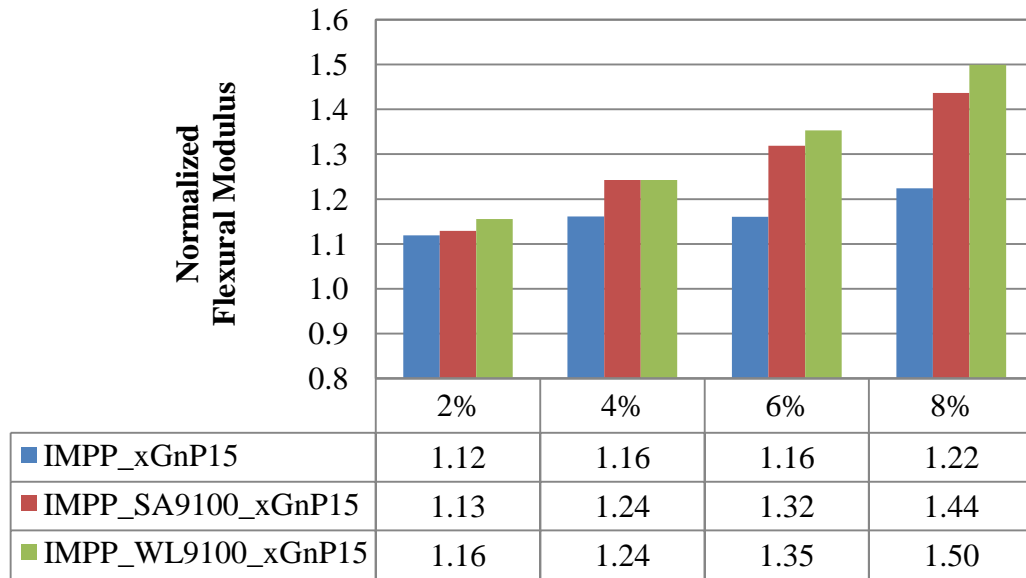


Figure 2.3 Normalized flexural modulus experimental results for xGnP<sup>15</sup>-filled composites.

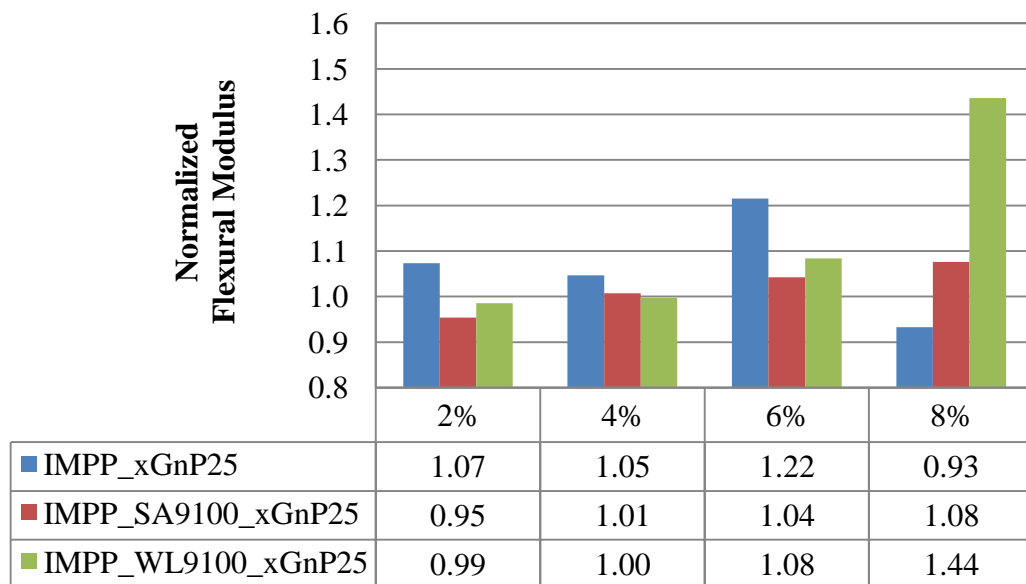


Figure 2.4 Normalized flexural modulus experimental results for xGnP<sup>25</sup>-filled composites.

Normalized flexural strength results for neat and xGnP<sup>5</sup>-filled composites with coupling agent as a function of filler loading level up to 8% are presented in Figure 2.5. Similar plots are provided for neat and xGnP<sup>15</sup> and xGnP<sup>25</sup>-filled composites with coupling agent in Figure 2.6 and Figure 2.7, respectively. Flexural strength was found to increase with decreasing xGnP particle diameter for all filler loading values of both neat and xGnP-filled composites containing coupling agent. Flexural strength increases with filler loading for all xGnP-filled composites containing coupling agent. However, flexural strength decreased with increased filler loading for neat composites. The optimum formulation to improve flexural strength for filler loading levels 2, 4, 6 and 8 wt. % is IMPP\_WL9100\_xGnP<sup>5</sup> composites. The resulting improvement from neat IMPP is 4, 8, 12 and 9%, respectively.

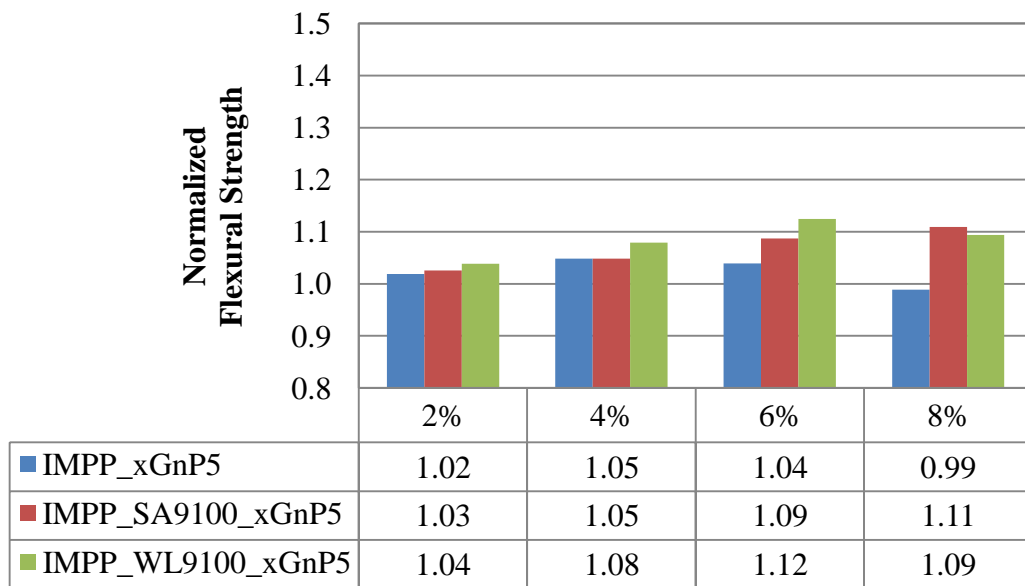


Figure 2.5 Normalized flexural strength experimental results for xGnP<sup>5</sup>-filled composites.

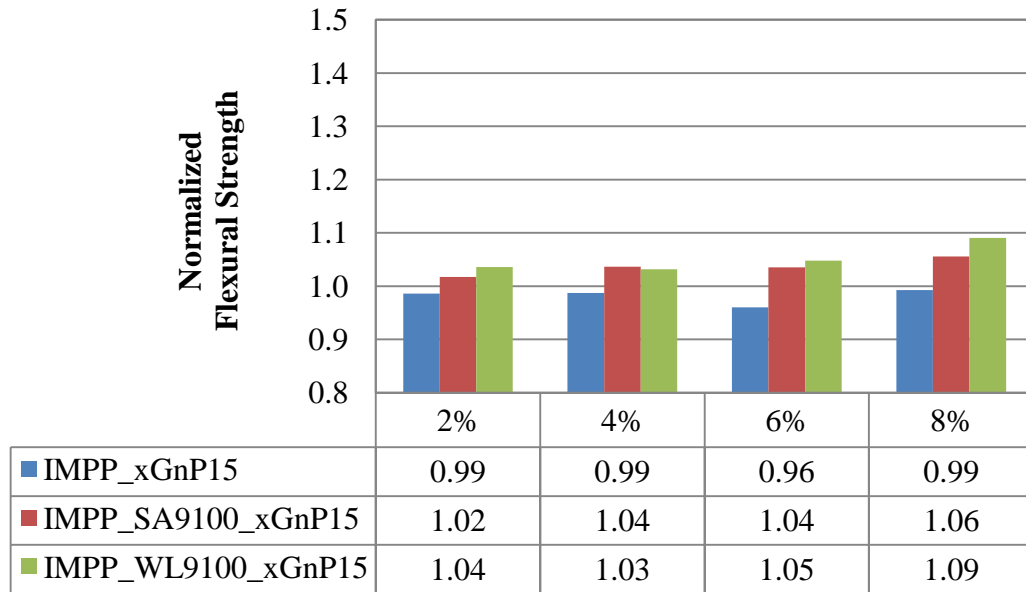


Figure 2.6 Normalized flexural strength experimental results for xGnP<sup>15</sup>-filled composites.

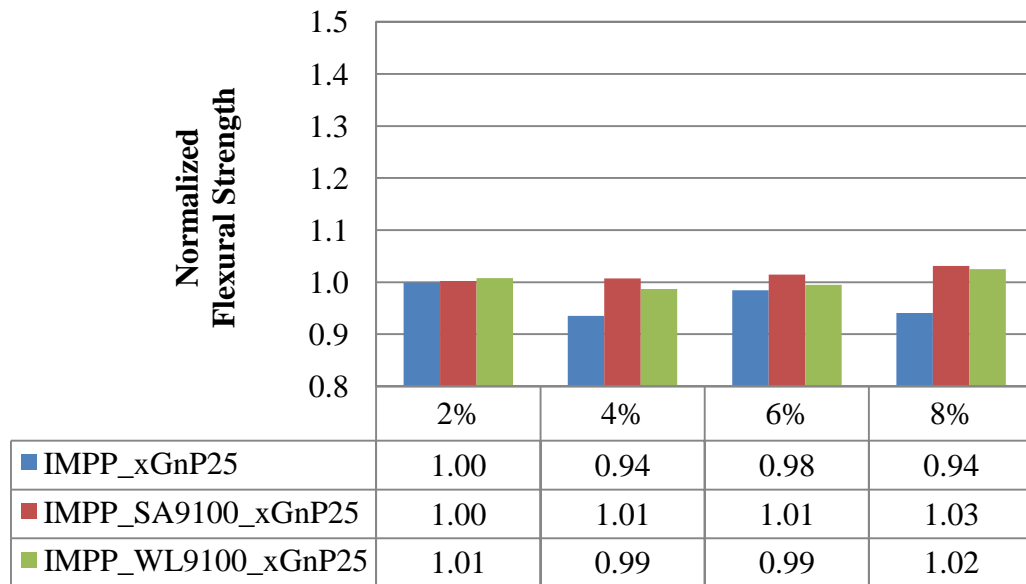


Figure 2.7 Normalized flexural strength experimental results for xGnP<sup>25</sup>-filled composites.

Research performed by Kalaitzidou et al. showed much greater improvement in flexural modulus compared to results shown here. Using xGnP<sup>1</sup> in polypropylene homopolymer, they obtained flexural modulus improvement of ~900% at a loading of 20 vol% (~6 wt. %) (Kalaitzidou et al. 2007 c,d). Such a large improvement may be attributed to the five-fold decrease in xGnP particle diameter. The importance of the dispersion of the reinforcing filler was also a highlight of this article. Kalaitzidou found that xGnP<sup>15</sup> was susceptible to agglomeration and fiber buckling or rollup. On the contrary, when xGnP<sup>1</sup> was incorporated into the polypropylene matrix, although some agglomerations were present, they appear in much smaller effective particle sizes (Kalaitzidou et al. 2007 a,b,d). These findings are very similar to this study's morphological findings presented below in Section 2.4.2.

This study proved feasibility of improving flexural modulus and strength of IMPP using xGnP as a nano reinforcement phase and PP-g-MA as a coupling agent. However, it is suspected that incorporation of xGnP with an average particle diameter smaller than 5  $\mu\text{m}$  would inevitably lead to largely increased improvements in flexural properties. Table 2.5 shows a summary of flexural mechanical properties and statistical significance of all compounded materials.

Table 2.5 Summary of flexural mechanical properties and statistical significance (Tukey-Kramer HSD comparison at  $\alpha = 0.05$ ) of all compounded materials.

Study Label	Flexural Properties			
	Modulus		Strength	
		(GPa)		(MPa)
Neat IMPP	LMN	1.08 (0.06)	JKLMNO	33.7 (1.0)
IMPP_xGnP <sup>5</sup> _2%	FGH	1.31 (0.04)	GHIJKL	34.3 (1.4)
IMPP_xGnP <sup>5</sup> _4%	F	1.33 (0.03)	EF	35.3 (0.7)
IMPP_xGnP <sup>5</sup> _6%	F	1.32 (0.04)	EFG	35.0 (0.5)
IMPP_xGnP <sup>5</sup> _8%	GHI	1.26 (0.02)	MNO	33.3 (0.4)
IMPP_SA9100_xGnP <sup>5</sup> _2%	IJ	1.21 (0.02)	FGHIJK	34.6 (0.5)
IMPP_SA9100_xGnP <sup>5</sup> _4%	FG	1.32 (0.01)	EF	35.3 (0.3)
IMPP_SA9100_xGnP <sup>5</sup> _6%	D	1.44 (0.02)	BC	36.6 (0.2)
IMPP_SA9100_xGnP <sup>5</sup> _8%	B	1.54 (0.01)	AB	37.4 (0.3)
IMPP_WL9100_xGnP <sup>5</sup> _2%	IJ	1.21 (0.02)	EFG	35.0 (0.3)
IMPP_WL9100_xGnP <sup>5</sup> _4%	EF	1.36 (0.02)	CD	36.4 (0.5)
IMPP_WL9100_xGnP <sup>5</sup> _6%	BC	1.52 (0.02)	A	37.9 (0.4)
IMPP_WL9100_xGnP <sup>5</sup> _8%	B	1.53 (0.03)	BC	36.9 (0.8)
IMPP_xGnP <sup>15</sup> _2%	IJ	1.20 (0.01)	NO	33.2 (0.3)
IMPP_xGnP <sup>15</sup> _4%	HI	1.25 (0.01)	NO	33.3 (0.3)
IMPP_xGnP <sup>15</sup> _6%	FG	1.25 (0.04)	LMNO	32.4 (0.6)
IMPP_xGnP <sup>15</sup> _8%	FG	1.32 (0.02)	LMNO	33.5 (0.3)
IMPP_SA9100_xGnP <sup>15</sup> _2%	IJ	1.21 (0.02)	GHIJKLM	34.3 (0.4)
IMPP_SA9100_xGnP <sup>15</sup> _4%	F	1.34 (0.02)	EFGH	34.9 (0.3)
IMPP_SA9100_xGnP <sup>15</sup> _6%	DE	1.42 (0.01)	EFGHI	34.9 (0.2)
IMPP_SA9100_xGnP <sup>15</sup> _8%	B	1.55 (0.04)	DE	35.6 (0.7)
IMPP_WL9100_xGnP <sup>15</sup> _2%	I	1.24 (0.01)	EFGH	34.9 (0.2)
IMPP_WL9100_xGnP <sup>15</sup> _4%	F	1.34 (0.01)	EFGHI	34.8 (0.2)
IMPP_WL9100_xGnP <sup>15</sup> _6%	CD	1.46 (0.04)	EF	35.3 (0.6)
IMPP_WL9100_xGnP <sup>15</sup> _8%	A	1.61 (0.03)	BC	36.8 (0.4)
IMPP_xGnP <sup>25</sup> _2%	JK	1.15 (0.08)	KLMNO	33.7 (1.0)
IMPP_xGnP <sup>25</sup> _4%	KL	1.13 (0.05)	P	31.5 (0.5)
IMPP_xGnP <sup>25</sup> _6%	FGH	1.31 (0.02)	O	33.2 (0.5)
IMPP_xGnP <sup>25</sup> _8%	O	1.00 (0.03)	P	31.7 (1.0)
IMPP_SA9100_xGnP <sup>25</sup> _2%	NO	1.03 (0.01)	JKLMNO	33.8 (0.3)
IMPP_SA9100_xGnP <sup>25</sup> _4%	LMN	1.08 (0.01)	IJKLMNO	33.9 (0.3)
IMPP_SA9100_xGnP <sup>25</sup> _6%	KLM	1.12 (0.01)	GHIJKLMN	34.2 (0.4)
IMPP_SA9100_xGnP <sup>25</sup> _8%	JK	1.16 (0.01)	EFGHIJ	34.7 (0.4)
IMPP_WL9100_xGnP <sup>25</sup> _2%	MNO	1.06 (0.03)	HJKLMNO	34.0 (0.9)
IMPP_WL9100_xGnP <sup>25</sup> _4%	LMN	1.07 (0.01)	NO	33.3 (0.4)
IMPP_WL9100_xGnP <sup>25</sup> _6%	JK	1.17 (0.13)	LMNO	33.5 (0.8)
IMPP_WL9100_xGnP <sup>25</sup> _8%	B	1.54 (0.04)	FGHIJK	34.5 (0.5)

Parenthesis indicates standard deviation.

Presence of the same letter indicates no statistical difference.



### 2.4.2. Tensile Properties

The tensile behavior of all compounded materials were characterized via the tensile testing methods describe in Section 2.3.3. Neat IMPP was determined to have tensile modulus, tensile strength and elongation at break equal to 1.29 GPa, 21.3 MPa and 33.8%, respectively.

Normalized tensile modulus results for neat and xGnP<sup>5</sup>-filled composites with coupling agent as a function of filler loading level up to 8% are presented in Figure 2.8. Similar plots are provided for neat and xGnP<sup>15</sup> and xGnP<sup>25</sup>-filled composites with coupling agent in Figure 2.9 and Figure 2.10, respectively. Tensile modulus was found to increase with decreasing xGnP particle diameter for all filler loading values of both neat and xGnP-filled composites containing coupling agent. Tensile modulus remains statistically unchanged with increased filler loading for neat xGnP-filled composites. However, tensile modulus consistently increases with increased filler loading for all SA9100 and WL9100 coupled xGnP filled composites. In general, the optimum formulation to improve tensile modulus for filler loading levels 2, 4, 6 and 8 wt. % is IMPP\_WL9100 \_ xGnP<sup>5</sup> composites. The resulting improvement from neat IMPP is 6, 18, 24 and 31%, respectively.

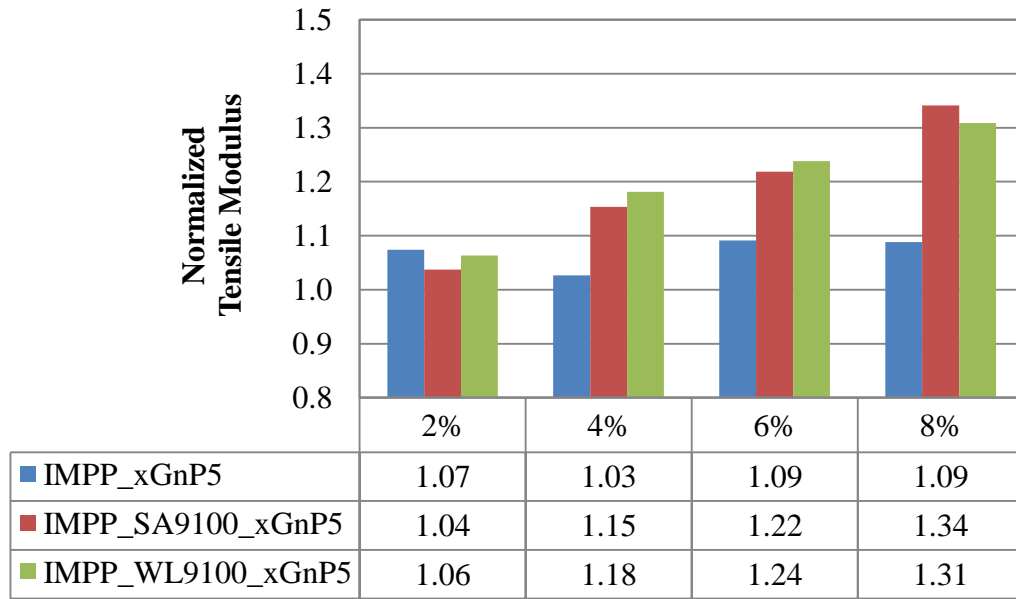


Figure 2.8 Normalized tensile modulus experimental results for xGnP<sup>5</sup>-filled composites.

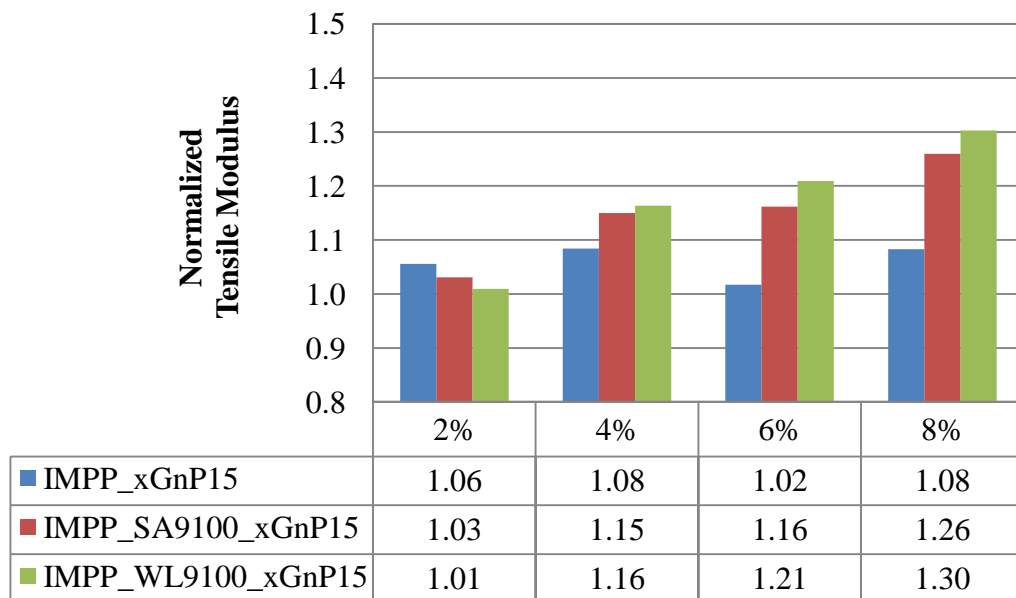


Figure 2.9 Normalized tensile modulus experimental results for xGnP<sup>15</sup>-filled composites.

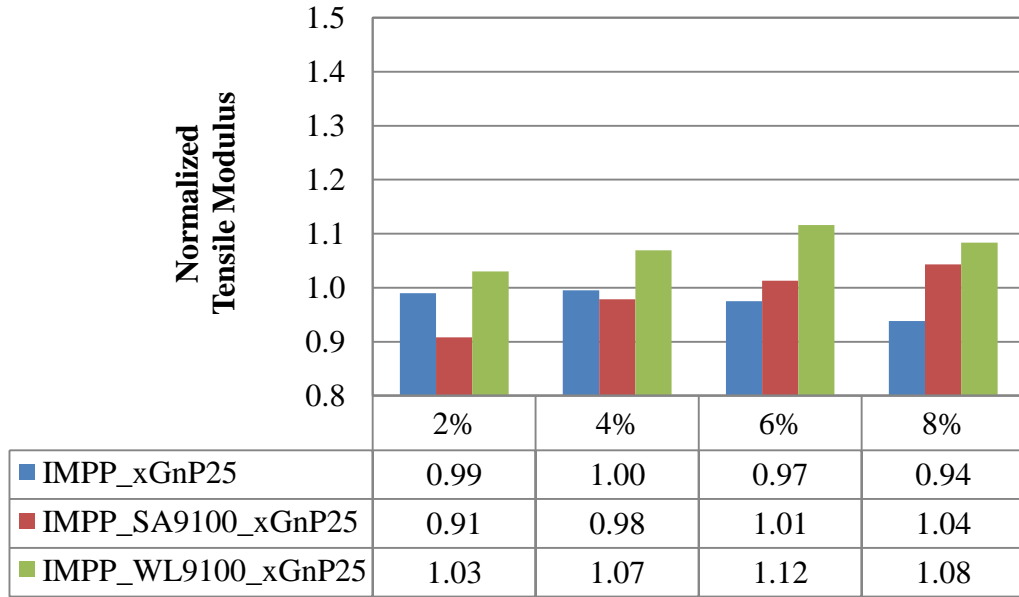


Figure 2.10 Normalized tensile modulus experimental results for xGnP<sup>25</sup>-filled composites.

Test results show that PP-g-MA is extremely beneficial to dispersion, particularly at higher filler loading levels. As discussed by Hussain et al., the degree of dispersion is one of the most critical aspects of layered nanomaterial reinforcement. In the absence of perfect exfoliation the nano reinforcement phase will not provide improved mechanical properties. In fact, poorly dispersed nano fillers can greatly deteriorate the mechanical properties when compared to the neat polymer matrix (Hussain et al. 2006). As described by Thostenson et al., the individual graphene platelets have greater affinity to themselves compared to the polymer matrix. For this reason, perfect dispersion (exfoliation) of the nano particles is very difficult. Furthermore, it has been demonstrated that the magnitude of inherent stress concentrations decreases as the thickness at the tip of the graphite agglomerates decreases (Thostenson et al. 2005). Improvement in degree of exfoliation

results in smaller thickness of graphite effective particles. Therefore an improved degree of exfoliation results in lower stress concentrations and subsequently higher performance mechanical properties. TEM investigations are necessary to draw further conclusions regarding the influence of PP-g-MA coupling agent on the degree of dispersion within our composites.

TEM images are shown in Figure 2.11 and illustrate the obvious improvement in quality of dispersion in properly compatibilized composites. In Figure 2.11 a and b individual platelets can be seen and their individual thickness of 10 nm is confirmed. However, the individual platelets are present in stacks ranging from 50 to 200 nm in thickness. This nanoscale morphology is described as intercalated dispersion at best. Figure 2.11 c and d show with the addition of WL9100 coupling agent, individual platelets are visible at 10 nm thick, and polymer is also seen penetrating much of the gallery spacing among platelets resulting in stacks of only two or three platelets. This nanoscale morphology can be described as a partially exfoliated dispersion.

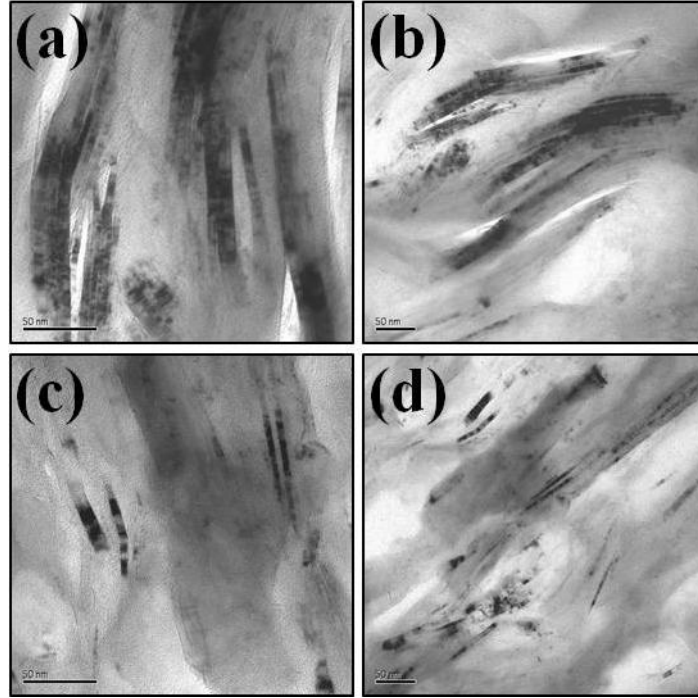


Figure 2.11 Transmission electron micrographs of (a & b) IMPP\_xGnP<sup>5</sup>\_2% and (c & d) IMPP\_WL9100\_xGnP<sup>5</sup>\_2%.

The Halpin-Tsai equation was introduced to predict the tensile longitudinal modulus of unidirectional fiber-reinforced composites. The Halpin-Tsai prediction of tensile modulus was calculated using Equation 2.3 through Equation 2.5 as shown:

$$E = E_m \frac{1 + \eta \xi V_f}{1 - \eta V_f} \quad \text{Equation 2.3}$$

$$\eta = \frac{\frac{E_f}{E_m} - 1}{\frac{E_f}{E_m} + \xi} \quad \text{Equation 2.4}$$

$$\xi = \frac{2}{3a} \quad \text{Equation 2.5}$$

Where the parameter  $E_m$  is the neat IMPP Young's modulus,  $E_f$  is the elastic modulus of the fiber reinforcement phase, and  $V_f$  is the fiber volume fraction. The variable  $\xi$  shown here is an adaptation for the case of platelet shaped fillers and is a function of the filler's aspect ratio,  $a$ . Assumptions of the Halpin-Tsai equation include perfect exfoliation to attain the aspect ratio input into Equation 2.5, as well as perfect contact between filler and matrix (Kalaitzidou et al. 2007c).

For the case of xGnP<sup>5</sup>, variables  $E_f$  and  $a$  were taken as 1 TPa and 500, respectively. The predicted tensile modulus of various composites can then be plotted as a function of fiber volume fraction. Figure 2.12, Figure 2.13 and Figure 2.14 illustrate a comparison of Halpin-Tsai prediction of tensile modulus and experimental results fit to 2nd-order polynomials for neat and compatibilized xGnP<sup>5</sup>-filled composites. Figure 2.12 depicts a very poor agreement between the Halpin-Tsai prediction and experimental results for neat xGnP<sup>5</sup>-filled composites. On the contrary, both Figure 2.13 and Figure 2.14 show rather good agreement between the Halpin-Tsai prediction and experimental results for both SA9100 and WL9100 coupled xGnP<sup>5</sup>-filled composites. The 2nd-order polynomial fit to the experimental data exhibited correlation coefficients,  $R^2$ , for composites containing coupling agent greater than 0.975. Coupled composites show excellent agreement with the modeled prediction, particularly at higher filler loading levels when compared with neat composites.

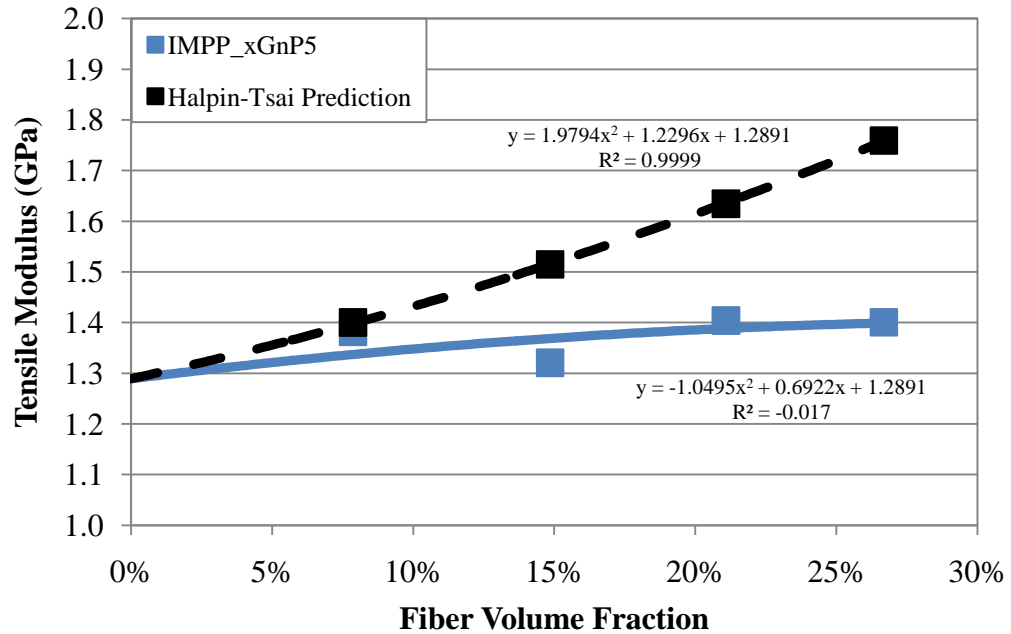


Figure 2.12 Comparison of Halpin-Tsai prediction of tensile modulus with experimental results for neat xGnP<sup>5</sup>-filled composites.

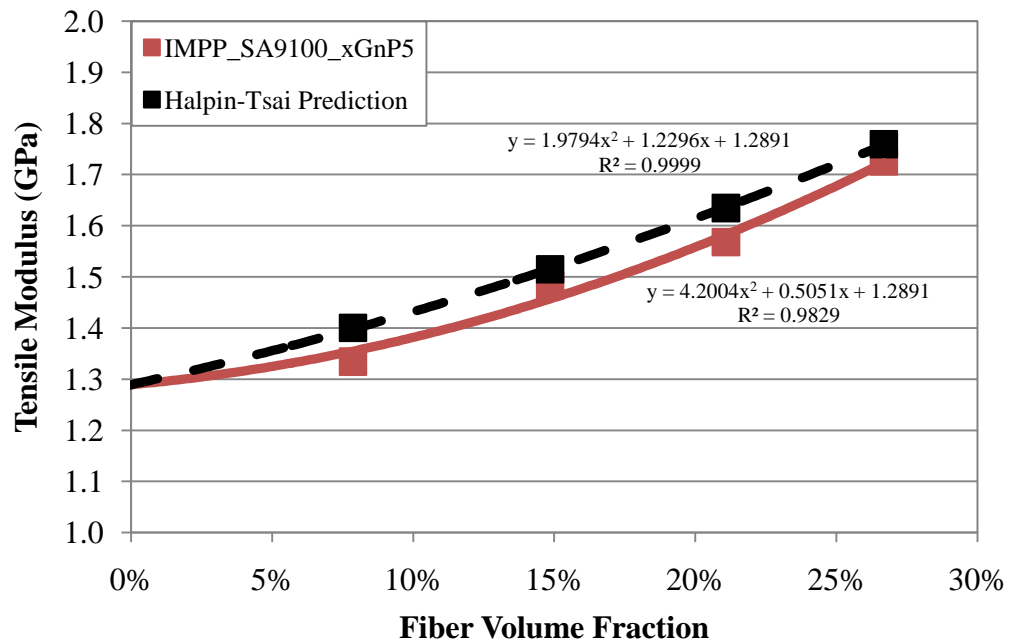


Figure 2.13 Comparison of Halpin-Tsai prediction of tensile modulus with experimental results for SA9100 coupled xGnP<sup>5</sup>-filled composites.

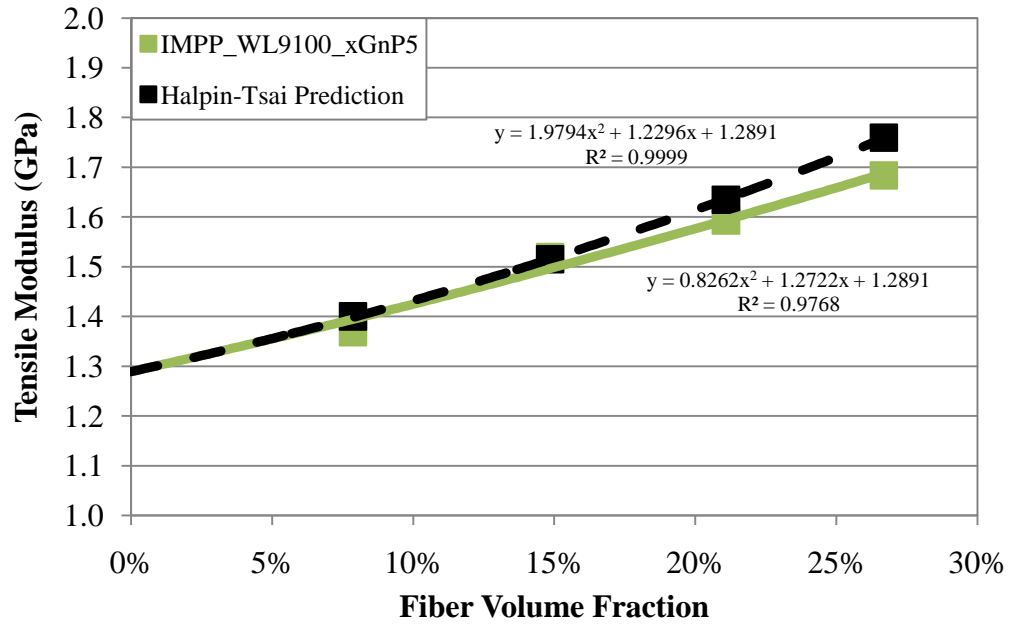


Figure 2.14 Comparison of Halpin-Tsai prediction of tensile modulus with experimental results for WL9100 coupled xGnP<sup>5</sup>-filled composites.

The Halpin-Tsai model slightly over-predicts the composite tensile modulus. This is similar to other findings in the literature, where over-predictions of modulus using Halpin-Tsai equation are attributed to the theoretical aspect ratio that was input into the model. In actuality, agglomerations and distortion (e.g. buckling, folding, roll-up) of the platelets during melt compounding can lead to effective aspect ratios much smaller than calculated based on perfect exfoliation. Instead of perfectly exfoliated 10 nm thick individual graphene sheets aligned in the injection mold flow direction, the effective particle thickness could be at least an order of magnitude larger and no longer in a planar geometric shape (Ahmad et al. 2007; Kalaitzidou et al. 2007a-d; Kim H. et al. 2010). Evidence of this phenomenon occurring in this study is shown in Figure 2.15 and is indicated by the red arrow. Analogous to slenderness in a structural column, the xGnP<sup>25</sup> particle is relatively long and thin. Thus, the platelet is inherently susceptible to buckling,



folding and roll-up during the intensive shear mixing induced during melt compounding. The other source of deviation from the Halpin-Tsai prediction is attributed to the assumption of perfect contact between the filler and the matrix.

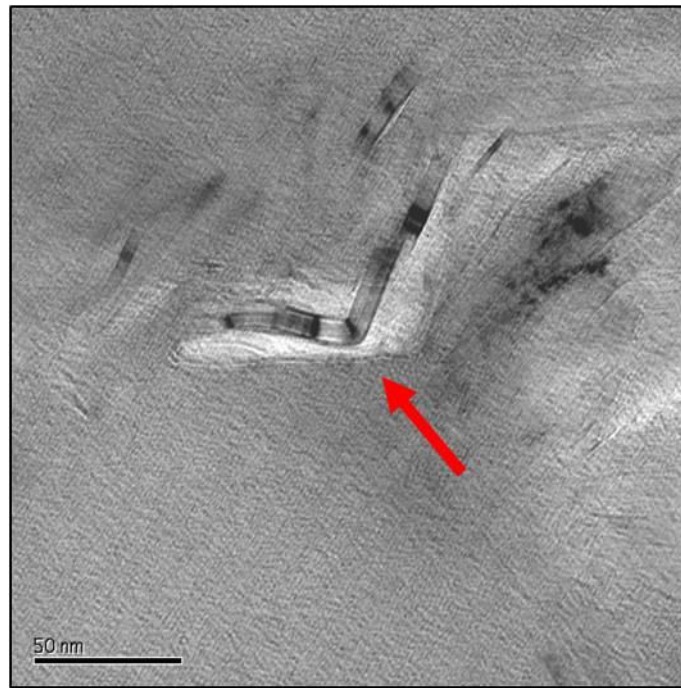


Figure 2.15 Transmission electron micrograph of IMPP\_SA9100\_xGnP<sup>25</sup>\_4% showing evidence of platelet buckling.

Normalized tensile strength results for neat and xGnP<sup>5</sup>-filled composites with coupling agent as a function of filler loading level up to 8% are presented in Figure 2.16. Similar plots are provided for neat and xGnP<sup>15</sup> and xGnP<sup>25</sup>-filled composites with coupling agent in Figure 2.17 and Figure 2.18, respectively. Tensile strength was found to increase with decreasing xGnP particle diameter for all filler loading values of both neat and xGnP-filled composites containing coupling agent. Tensile strength decreased with increased filler loading for all neat xGnP-filled composites. However, tensile

strength is statistically higher than neat IMPP at all filler loading level for WL9100 coupled xGnP<sup>5</sup>-filled composites. In general, the optimum formulation to improve tensile strength for filler loading levels 2, 4, 6 and 8 wt. % is IMPP\_WL9100 \_ xGnP<sup>5</sup> composites. The resulting improvement from neat IMPP is 12, 6, 5 and 5%, respectively.

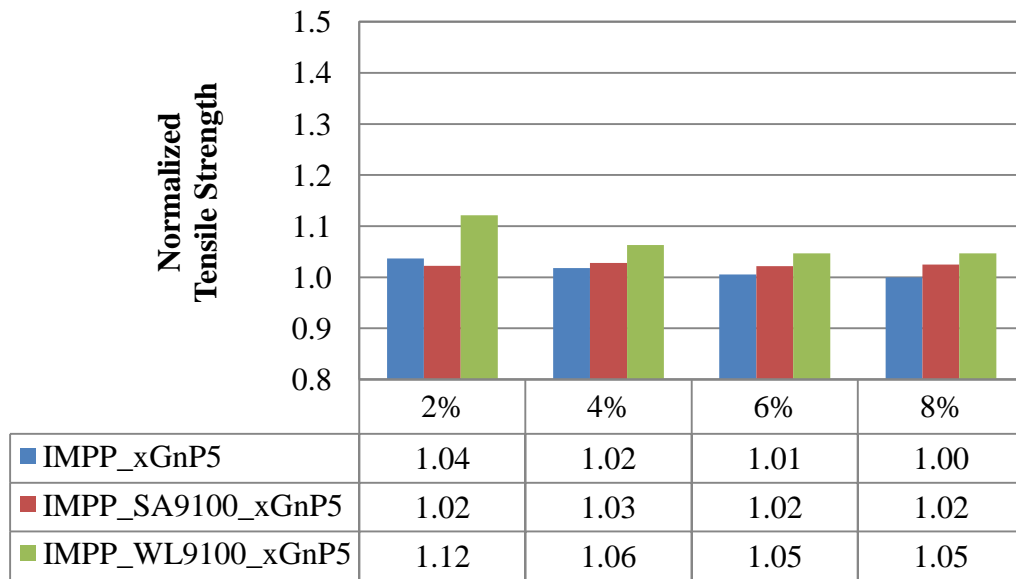


Figure 2.16 Normalized tensile strength experimental results for xGnP<sup>5</sup>-filled composites.

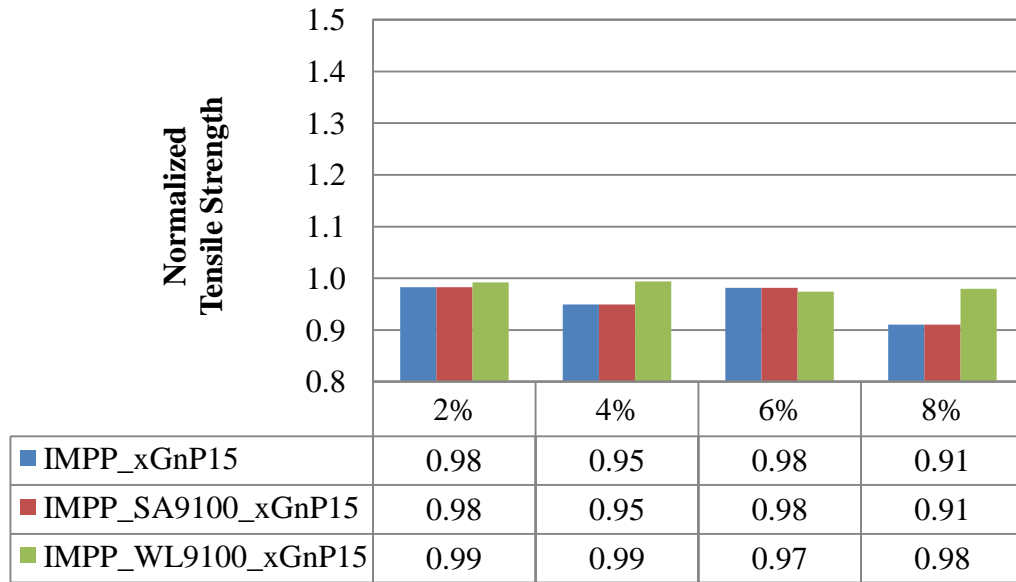


Figure 2.17 Normalized tensile strength experimental results for xGnP<sup>15</sup>-filled composites.

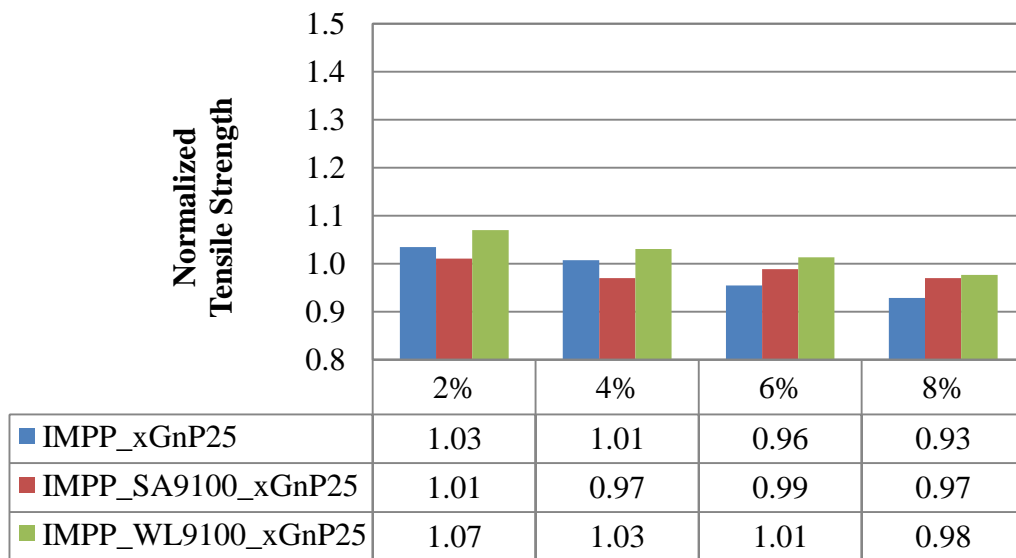


Figure 2.18 Normalized tensile strength experimental results for xGnP<sup>25</sup>-filled composites.

Normalized elongation at break results for neat and xGnP<sup>5</sup>-filled composites with coupling agent as a function of filler loading level up to 8% are presented in Figure 2.19. Similar plots are provided for neat and xGnP<sup>15</sup> and xGnP<sup>25</sup>-filled composites with coupling agent in Figure 2.20 and Figure 2.21, respectively. In general, elongation at break increased with decreasing xGnP particle diameter for all filler loading values of both neat and xGnP-filled composites containing coupling agent. However, elongation at break decreased with increased filler loading for all neat and xGnP-filled composites containing coupling agent. It is important to note that the addition of coupling agent caused lower elongation at break and therefore a more brittle behaving composite. The optimum formulation to obtain the least degradation of elongation at break for filler loading levels 2, 4, 6 and 8 wt. % is IMPP\_xGnP<sup>5</sup> composites. The resulting degradation when compared to neat IMPP is 13, 29, 44 and 41%, respectively.

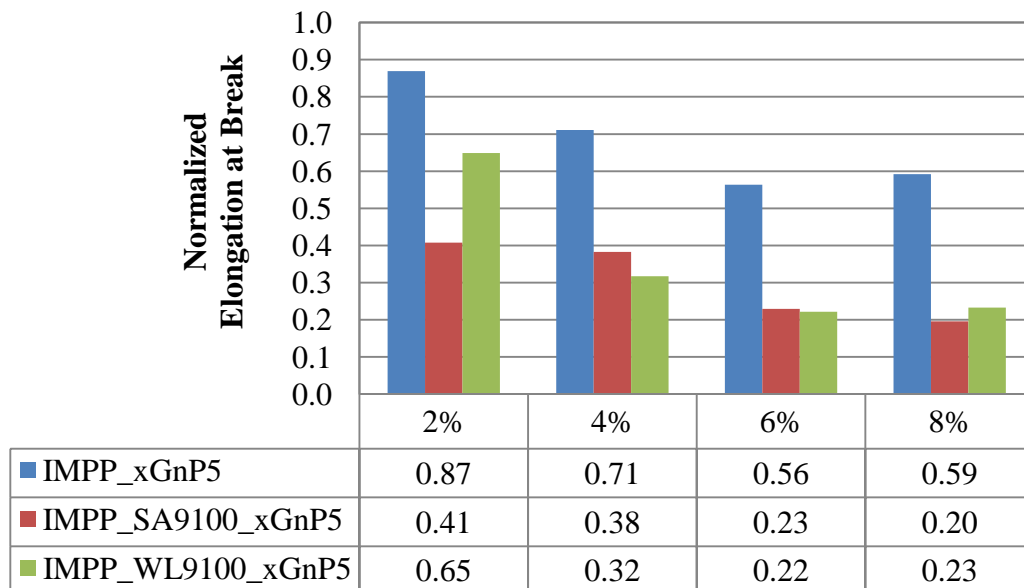


Figure 2.19 Normalized elongation at break experimental results for xGnP<sup>5</sup>-filled composites.

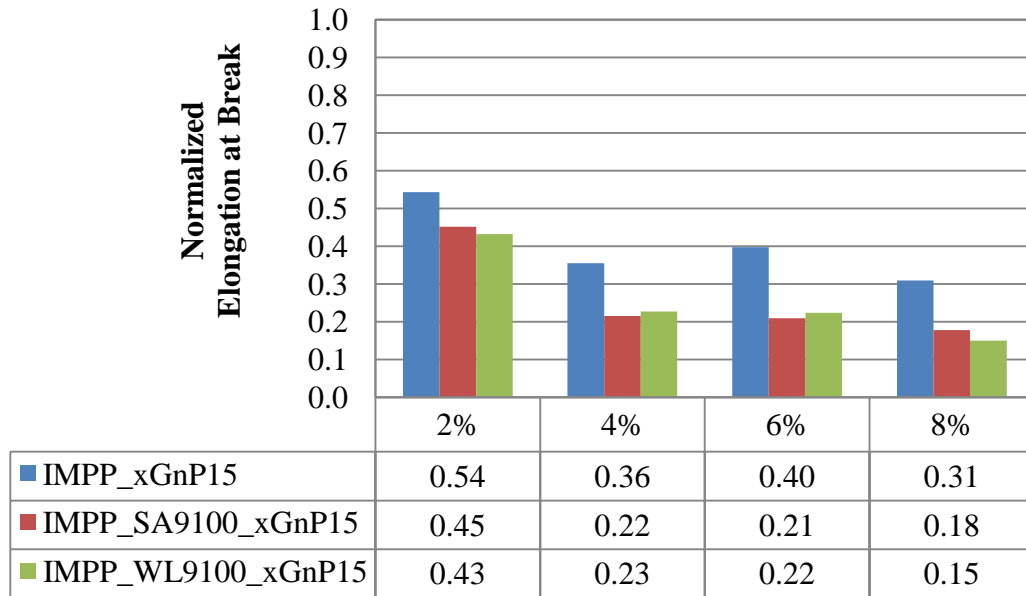


Figure 2.20 Normalized elongation at break experimental results for xGnP<sup>15</sup>-filled composites.

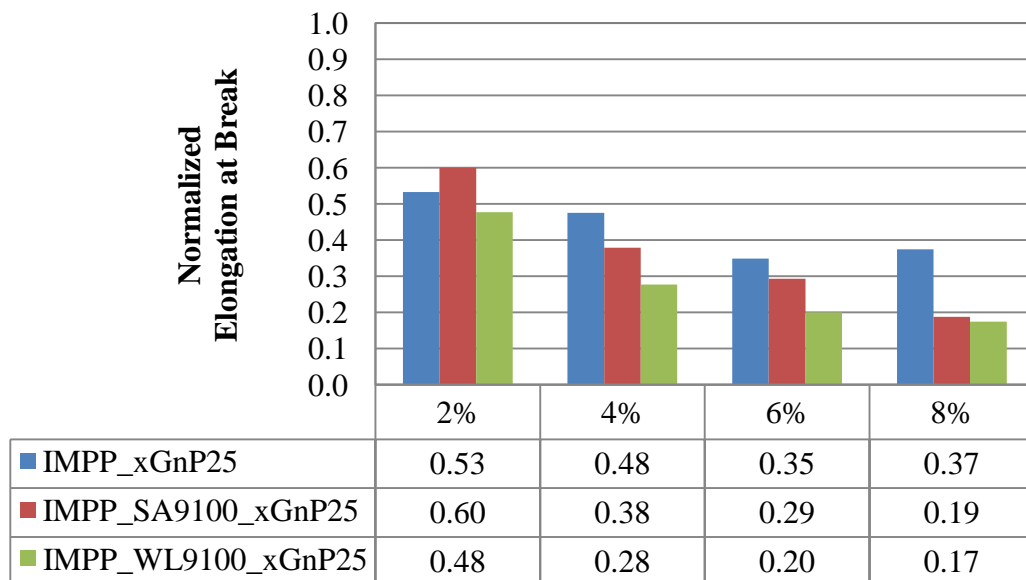


Figure 2.21 Normalized elongation at break experimental results for xGnP<sup>25</sup>-filled composites.

According to Ahmad et al., nearly any filled polymer will show an increase in modulus and strength while concurrently producing a more brittle behaving composite (Ahmad et al. 2007). The xGnP is an extremely rigid particle. Therefore, nearly all elongation of the specimen during the tensile test will occur in the matrix. When there is good adhesion between the filler and the matrix, a significant decrease in elongation at break can be expected even at small filler loading levels. In the case of poor adhesion, the decrease in elongation at break is expected to be more gradual (Oksman and Clemons 1998). This study's composites containing coupling agent have been proven to exhibit improved dispersion and are expected to exhibit improved adhesion at the particle/matrix interface as proposed in the previously discussed Halpin-Tsai comparison plots. Poor particle/matrix adhesion can be seen in SEM images of tensile fracture surfaces where no polymer is found to be attached to or coating embedded fillers. This phenomenon is seen here as shown in Figure 2.22 and is indicated by the red arrow where the tensile fracture surface of IMPP\_xGnP<sup>25</sup>\_4% clearly indicates poor adhesion between the filler and the matrix in the absence of PP-g-MA. Thus the decrease in elongation at break for this neat composite and the comparably larger decrease in elongation at break for similar composites containing coupling agent is explained and justified.

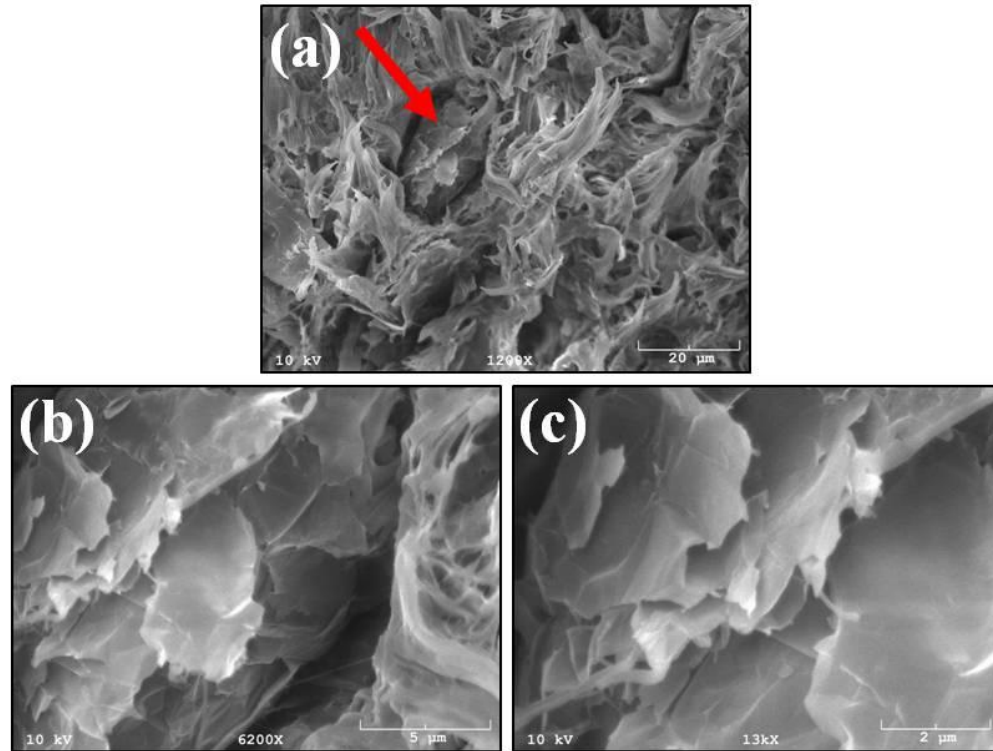


Figure 2.22 Scanning electron micrographs illustrating poor particle/matrix adhesion in tensile fracture surface of IMPP\_xGnP<sup>25</sup>\_4% at (a) 1200x, (b) 6200x and (c) 13000x magnification.

Figure 2.23 is provided to illustrate the change in microscopic morphology of the tensile fracture surface with increased filler loading. In Figure 2.23a the neat IMPP is seen to exhibit a fracture surface consisting of many elongated ligaments of polymer, indicating a considerably ductile failure. Figure 2.23 b and c shows neat xGnP<sup>25</sup>-filled composites at 2% and 4% filler loading, respectively. At 2% filler loading a decrease is seen in the amount of elongated polymer present on the fracture surface as well as a cavity, indicated by the red arrow, where an agglomeration of xGnP<sup>25</sup> platelets have pulled-out. At 4% filler loading we can see a further decrease in the density of elongated polymer on the fracture surface as well as an agglomeration of xGnP<sup>25</sup> platelets, indicated

by the red arrow, which again illustrate poor adhesion in the absence of PP-g-MA. Finally, in Figure 2.23d at 6% filler loading there is essentially no presence of elongated ligaments of polymer. Instead there is very smooth fracture surface, indicative of a considerably brittle failure.

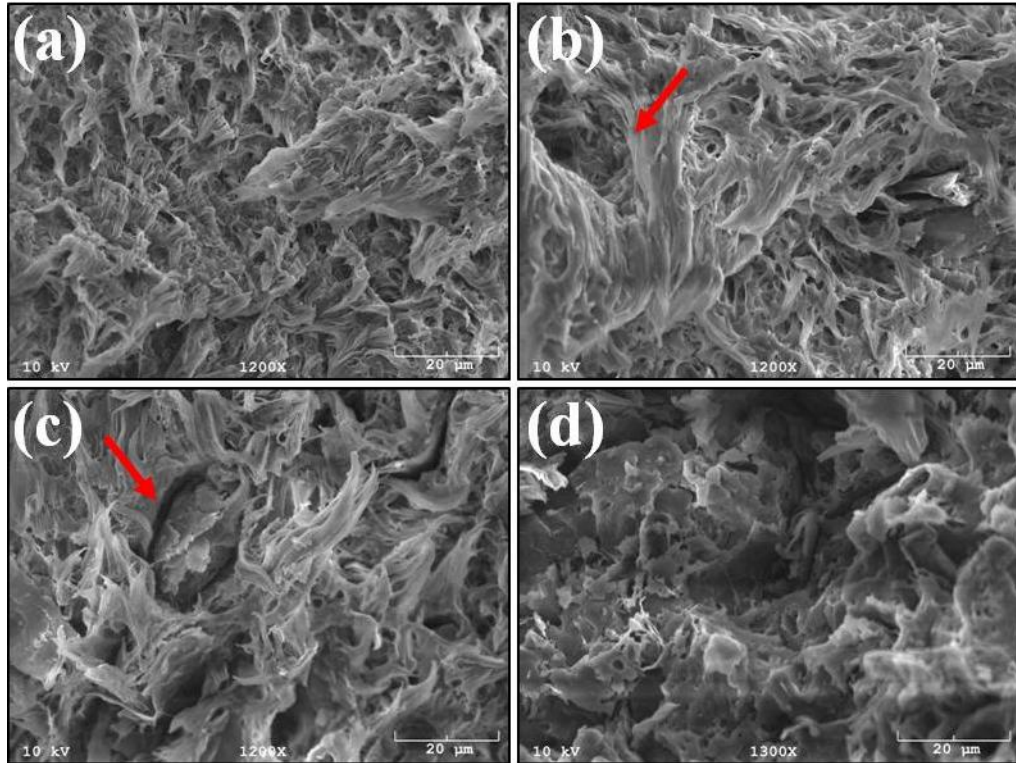


Figure 2.23 Scanning electron micrographs illustrating progressively brittle failure surfaces in tensile fracture surfaces of (a) Neat IMPP, (b) IMPP\_xGnP<sup>25</sup>\_2%, (c) IMPP\_xGnP<sup>25</sup>\_4% and (d) IMPP\_xGnP<sup>25</sup>\_6%.

This study proved the feasibility of improving tensile modulus and strength of IMPP using xGnP as a nano reinforcement phase and PP-g-MA as a coupling agent. The benefit of both SA9100 and WL9100 can be attributed to improved dispersion and particle/matrix interaction. However, it is suspected that upon mechanical loading



residual agglomerated stacks of nanoplatelets act as very stiff inclusions. These stiff inclusions redirect stress concentrations from the elastomeric impact modification (toughening) phase of the IMPP to the much larger and stiffer effective graphite particles. In addition, these agglomerated stacks provide non ideal transfer of stresses between matrix and filler, therefore resulting in early failure or low values of elongation at break compared to the very tough IMPP. Table 2.6 shows a summary of tensile mechanical properties and statistical significance of all compounded materials.

Table 2.6 Summary of tensile mechanical properties and statistical significance (Tukey-Kramer HSD comparison at  $\alpha = 0.05$ ) of all compounded materials.

Study Label	Tensile Properties				
	Elastic Modulus		Strength		Elongation at break
		(GPa)		(MPa)	(%)
Neat IMPP	LMNOPQR	1.29 (0.04)	HIJKLMNO	21.3 (0.3)	A 33.8 (5.4)
IMPP_xGnP <sup>5</sup> _2%	HIJKLMN	1.38 (0.06)	CDE	22.1 (0.3)	AB 29.4 (10.5)
IMPP_xGnP <sup>5</sup> _4%	LMNOPQ	1.32 (0.13)	EFGHIJ	21.7 (0.3)	BC 24.0 (10.4)
IMPP_xGnP <sup>5</sup> _6%	GHIJKL	1.40 (0.05)	HIJKLM	21.5 (0.2)	CDEFG 19.0 (3.4)
IMPP_xGnP <sup>5</sup> _8%	GHIJKL	1.40 (0.04)	IJKLMN	21.3 (0.2)	CDE 20.0 (5.8)
IMPP_SA9100_xGnP <sup>5</sup> _2%	KLMNOP	1.33 (0.04)	DEFGHI	21.8 (0.3)	EFGHIJKL 13.8 (4.3)
IMPP_SA9100_xGnP <sup>5</sup> _4%	EFGHI	1.48 (0.04)	CDEFGH	21.9 (0.2)	FGHIJKLMNO 12.9 (3.2)
IMPP_SA9100_xGnP <sup>5</sup> _6%	CDE	1.57 (0.08)	EFGHI	21.8 (0.2)	JKLMNOP 7.8 (1.6)
IMPP_SA9100_xGnP <sup>5</sup> _8%	A	1.73 (0.04)	CDEFGH	21.9 (0.3)	MNOP 6.6 (1.3)
IMPP_WL9100_xGnP <sup>5</sup> _2%	JKLMN	1.37 (0.04)	A	23.9 (0.3)	CD 21.9 (5.8)
IMPP_WL9100_xGnP <sup>5</sup> _4%	DEF	1.52 (0.07)	B	22.7 (0.2)	IJKLMN 10.7 (3.3)
IMPP_WL9100_xGnP <sup>5</sup> _6%	BCDE	1.59 (0.05)	BC	22.3 (0.5)	KLMNOP 7.5 (2.0)
IMPP_WL9100_xGnP <sup>5</sup> _8%	AB	1.68 (0.05)	BCD	22.3 (0.3)	JKLMNOP 7.9 (1.1)
IMPP_xGnP <sup>15</sup> _2%	KLMNOP	1.36 (0.06)	LMNOP	21.0 (0.3)	CDEF 18.4 (4.4)
IMPP_xGnP <sup>15</sup> _4%	GHIJKL	1.39 (0.05)	TU	20.3 (0.3)	EFGHIJK 12.0 (4.3)
IMPP_xGnP <sup>15</sup> _6%	LMNOPQ	1.31 (0.22)	MNOPQ	21.0 (0.3)	EFGHIJKLM 13.4 (3.6)
IMPP_xGnP <sup>15</sup> _8%	GHIJKLM	1.39 (0.07)	V	19.4 (0.2)	HIJKLMNOP 10.5 (1.3)
IMPP_SA9100_xGnP <sup>15</sup> _2%	KLMNOP	1.33 (0.03)	FGHIJKL	21.0 (0.3)	DEFGHI 15.3 (2.9)
IMPP_SA9100_xGnP <sup>15</sup> _4%	EFGHIJ	1.48 (0.03)	QRST	20.3 (0.3)	LMNOP 7.3 (1.3)
IMPP_SA9100_xGnP <sup>15</sup> _6%	EFGH	1.49 (0.06)	STU	21.0 (0.3)	LMNOP 7.1 (1.0)
IMPP_SA9100_xGnP <sup>15</sup> _8%	ABCD	1.62 (0.07)	QRST	19.4 (0.2)	OP 6.0 (0.9)
IMPP_WL9100_xGnP <sup>15</sup> _2%	KLMNOP	1.30 (0.02)	KLMNOP	21.2 (0.3)	EFGHIJ 14.6 (3.5)
IMPP_WL9100_xGnP <sup>15</sup> _4%	EFG	1.50 (0.04)	JKLMN	21.2 (0.3)	KLMNOP 7.7 (0.9)
IMPP_WL9100_xGnP <sup>15</sup> _6%	DE	1.56 (0.03)	OPQR	20.8 (0.3)	KLMNOP 7.6 (1.0)
IMPP_WL9100_xGnP <sup>15</sup> _8%	ABC	1.68 (0.09)	NOPQ	20.9 (0.3)	P 5.1 (0.4)
IMPP_xGnP <sup>25</sup> _2%	MNOPQR	1.27 (0.05)	CDEF	22.1 (0.3)	CDEFGH 18.0 (5.1)
IMPP_xGnP <sup>25</sup> _4%	LMNOPQR	1.28 (0.06)	GHIJKL	21.5 (0.6)	DEFGHI 16.1 (3.2)
IMPP_xGnP <sup>25</sup> _6%	PQR	1.25 (0.05)	RST	20.4 (0.1)	HIJKLMNOP 11.8 (1.2)
IMPP_xGnP <sup>25</sup> _8%	QR	1.21 (0.03)	UV	19.8 (0.2)	GHIJKLMNO 12.7 (2.3)
IMPP_SA9100_xGnP <sup>25</sup> _2%	R	1.17 (0.03)	FGHIJKL	21.6 (0.2)	CDE 20.3 (8.4)
IMPP_SA9100_xGnP <sup>25</sup> _4%	OPQR	1.26 (0.04)	PQRS	20.7 (0.4)	FGHIJKLMNO 12.8 (3.1)
IMPP_SA9100_xGnP <sup>25</sup> _6%	LMNOPQ	1.30 (0.04)	LMNOP	21.1 (0.3)	IJKLMN 9.9 (1.5)
IMPP_SA9100_xGnP <sup>25</sup> _8%	KLMNOP	1.34 (0.05)	PQRS	20.7 (0.5)	NOP 6.4 (1.0)
IMPP_WL9100_xGnP <sup>25</sup> _2%	KLMNOP	1.33 (0.07)	B	22.8 (0.3)	DEFGHI 16.1 (3.2)
IMPP_WL9100_xGnP <sup>25</sup> _4%	IJKLMNO	1.38 (0.02)	CDEFG	22.0 (0.2)	IJKLMN 9.4 (1.9)
IMPP_WL9100_xGnP <sup>25</sup> _6%	FGHIJK	1.44 (0.08)	EFGHIJK	21.6 (0.2)	MNOP 6.8 (0.5)
IMPP_WL9100_xGnP <sup>25</sup> _8%	GHIJKLM	1.39 (0.04)	NOPQR	20.8 (0.3)	OP 5.9 (0.6)

Parenthesis indicates standard deviation.

Presence of the same letter indicates no statistical difference.

## 2.5. Conclusions

Both xGnP-filled IMPP composites with and without the addition of coupling agent were prepared via melt compounding followed by injection molding. Mechanical and morphological characterization yielded conclusions in understanding the influence of (1) particle diameter, (2) filler loading, and (3) coupling agent, on the flexural and tensile properties of xGnP-filled IMPP composites.

The smallest diameter filler investigated in this study (5 $\mu$ m) performed the best in terms of flexural and tensile mechanical properties of xGnP-filled IMPP composites. It is suspected that incorporation of xGnP with an average particle diameter smaller than 5  $\mu$ m would result in largely increased improvements in flexural and tensile properties. Tensile and flexural moduli and strengths both increased with xGnP filler loading for compatibilized composites. Elongation at break was greatly deteriorated with as little as 2 wt. % xGnP with and without coupling agent. The addition of coupling agent has been proven to dramatically enhance dispersion within xGnP-filled IMPP composites. Enhanced dispersion has been proven indirectly via mechanical testing and Halpin-Tsai modeling comparisons as well as directly via TEM imaging. However, the addition of coupling agent amplifies the degradation of elongation at break because of the improved adhesion between the filler and the matrix.

## 2.6. References

Ahmad S.H., Rasid R., Surip S.N., Anuar H., Czigany T., Abdul Razak S.B. “Mechanical and Fracture Toughness Behavior of TPNR Nanocomposites.” *Journal of Composite Materials*, 41(17) (2007): 2147-2159.

Chen G.H., Wu D.J., Weng W.G., Yan W.L. “Preparation of Polymer/Graphite Conducting Nanocomposite by Intercalation Polymerization.” *Journal of Applied Polymer Science*, 82 (2001): 2506-2513.

Gopakumar T.G. & Page D.J.Y.S. “Polypropylene/Graphite Nanocomposites by Thermo-Kinetic Mixing.” *Polymer Engineering & Science*, 44 (6) (2004): 1162-1169.

Hussain F., Hojjati M., Okamoto M., Gorga R. E. “Review article: Polymer-matrix Nanocomposites, Processing, Manufacturing, and Application: An Overview.” *Journal of Composite Materials*, 40(17) (2006): 1511-1575.

Jiang X. & Drzal L. T. “Multifunctional High Density Polyethylene Nanocomposites Produced by Incorporation of Exfoliated Graphite nanoplatelets 1: Morphology and Mechanical Properties.” *Polymer Composites*, (2010): 1091-1098.

Kalaitzidou K., Fukushima H., Drzal L.T. “A new compounding method for exfoliated graphite-polypropylene nanocomposites with enhanced flexural properties and lower percolation threshold.” *Composites Science and Technology*, 67 (2007a): 2045-2051.

Kalaitzidou K., Fukushima H., Drzal L. T. “Multifunctional polypropylene composites produced by incorporation of exfoliated graphite nanoplatelets.” *Carbon*, 45 (2007b): 1446-1452.

Kalaitzidou K., Fukushima H., Miyagawa H., Drzal L. T. “Flexural and Tensile Moduli of Polypropylene Nanocomposites and Comparison of Experimental Data to Halpin-Tsai and Tandon-Weng Models.” *Polymer Engineering and Science*, 47 (2007c): 1796-1803.

Kalaitzidou K., Fukushima H., Drzal L. T. “Mechanical properties and morphological characterization of exfoliated graphite-polypropylene nanocomposites.” *Composites: Part A*, 38 (2007d): 1675-1682.

Kim S. & Drzal L. T. “High latent heat storage and high thermal conductive phase change materials using exfoliated graphite nanoplatelets.” *Solar Energy Materials & Solar Cells*, 93 (2009a): 136-142.

Kim S., Do I., Drzal L. T. “Multifunctional xGnP/LLDPE Nanocomposites Prepared by Solution Compounding Using Various Screw Rotating Systems.” *Macromolecular Materials and Engineering*, 294 (2009b): 196-205.

Kim S., Do I., Drzal L.T. “Thermal Stability and Dynamic Mechanical Behavior of Exfoliated Graphite Nanoplatelets-LLDPE Nanocomposites.” *Polymer Composites*, 31(5) (2010a): 755-761.

Kim S., Seo J., Drzal L. T. “Improvement of electric conductivity of LLDPE based nanocomposite by paraffin coating on exfoliated graphite nanoplatelets.” *Composites: Part A*, 41 (2010b): 581-587.

Kim H., Abdala A. A., Macosko C. W. “Graphene/Polymer Nanocomposites.” *Macromolecules*, 43(16) (2010): 6515-6530.

Miloaga D. G., Hosein H.A. A., Misra M., Drzal L. T. “Nucleating Effect of Expanded Graphite Nanoplatelets on Poly(Hydroxybutyrate).” Composite Materials & Structures Center, Michigan State University 2005.

Oksman K. & Clemons C. “Mechanical Properties and Morphology of Impact Modified Polypropylene-Wood Flour Composites.” *Journal of Applied Polymer Science*, 67 (1998): 1503-1513.

Page D.J.Y.S. & Gopakumar T.G. “Properties and Crystallization of Maleated Polypropylene/Graphite Flake Nanocomposites.” *Polymer Journal*, 38 (9) (2006): 920-929.

Park H.M., Kalaitzidou K., Fukushima H., Drzal L. T. “Exfoliated Graphite Nanoplatelet (xGnP) /Polypropylene Nanocomposites.” Composite Materials & Structures Center, Michigan State University 2007.

Ratnayake U.N., Haworth B., Hourston D.J. “Preparation of Polypropylene-Clay Nanocomposites by the Co-Intercalation of Modified Polypropylene and Short-Chain Amide Molecules.” *Journal of Applied Polymer Science*, 112 (2009): 320-334.

Sherman, Lilli Manolis. “Chasing Nanocomposites.” *Plastics Technology*, 50(11) (2004): 56-61.

Spoljaric S., Genovese A. & Shank R.A. “Polypropylene–microcrystalline cellulose composites with enhanced compatibility and properties.” *Composites Part A: Applied Science and Manufacturing*, 40 (6-7) (2009): 791-799.

Stankovich S., Dikin D.A., Dommett G.H.B., Kohlhaas K.M, Zimney E.J., Stach E.A., Piner R.D., Nguyen S.T., Ruof R.S. “Graphene-based composite materials.” *Nature*, 442 (2006): 282-286.

Teng C.-C., Ma C.-C. M., Huang Y.W., Yuen S.M., Weng C.-C., Chen C.-H, Su S.F. “Effect of MWCNT content on rheological and dynamic mechanical properties of multiwalled carbon nanotube/polypropylene composites.” *Composites: Part A*, 39 (2008): 1869-1875.

Thostenson E. T., Li C., Chou T.W. "Nanocomposites in context." *Composites Science and Technology*, 65 (2005): 491-516.



## Chapter 3

### IMPACT PROPERTIES AND RHEOLOGICAL BEHAVIOR OF XGNP-FILLED IMPP NANOCOMPOSITES

#### 3.1. Chapter Summary

xGnP-filled IMPP composites were prepared at 2, 4, 6, and 8 wt. % xGnP with and without the addition of a coupling agent and manufactured using melt mixing followed by injection molding. The coupling agent used in this study was polypropylene-graft-maleic anhydride (PP-g-MA). The nanoparticles used were xGnP with three different sizes: xGnP<sup>5</sup> has an average thickness of 10 nm, and an average platelet diameter of 5  $\mu\text{m}$ , whereas xGnP<sup>15</sup> and xGnP<sup>25</sup> have the same thickness but average diameters are 15 and 25  $\mu\text{m}$ , respectively. Test results show that nanocomposites with smaller xGnP diameter exhibited better impact properties for both neat and compatibilized composites. However, unnotched and notched impact strengths as well as fracture initiation resistance were dramatically deteriorated with the introduction of xGnP. Explanation of this brittle behavior in a nanoplatelet filled IMPP is presented using melt flow index and transmission electron microscopy.

### 3.2. Introduction

Polypropylene (PP) is among the most commonly used thermoplastics in the world with applications ranging from automobiles to construction to household appliances (Teng et. al 2008). This is because of its desirable balance between ease of processing, low cost, and mechanical properties (Park et. al 2007; Ratnayake et al. 2009). For this reason, PP is also referred to as a commodity thermoplastic. Typical commodity thermoplastics are inexpensive and well understood, but have lower performance mechanical properties when compared to engineering thermoplastics. Impact modification of commodity plastics with poor impact properties, such as PP, is typical practice for thermoplastic producing companies. The resulting thermoplastic is known as impact modified polypropylene (IMPP).

Although the specific impact modification processes are proprietary, we can deduce the nature of the modification of our IMPP by reviewing the literature. The most effective impact modifiers for PP are ethylene/propylene copolymers (EPM) or ethylene/propylene/diene terpolymer (EPDM). Essentially an elastomeric phase, typically consisting of small (0.1-1 $\mu$ m) spherical rubber particles, is melt blended with a neat PP homopolymer (Oksman and Clemons 1998; Lim et al. 2008). Upon loading, stress concentrations develop between the PP homopolymer and the elastomeric phase. These stress concentrations lead to a number of accepted conventional toughening mechanisms which have the potential to increase energy absorption by an order of magnitude. Three commonly considered mechanisms are illustrated in Figure 3.1. The first toughening

mechanism is the occurrence of plasticized nucleation sites surrounding the particles inducing inelastic void growth of the polymer matrix. The second toughening mechanism is a localized shear yielding or shear crazing of the polymer matrix. The third conventional toughening mechanism is the cavitation of the rubber particles in the elastomeric phase (Lesser 2009). All three of these mechanisms enhance energy dissipation density and therefore result in improved polymer impact properties. The introduction of an elastomeric phase improves the impact strength however simultaneously reduces the elastic modulus and strength of the neat polymer (Ahmad et al. 2007; Lim et al. 2008).

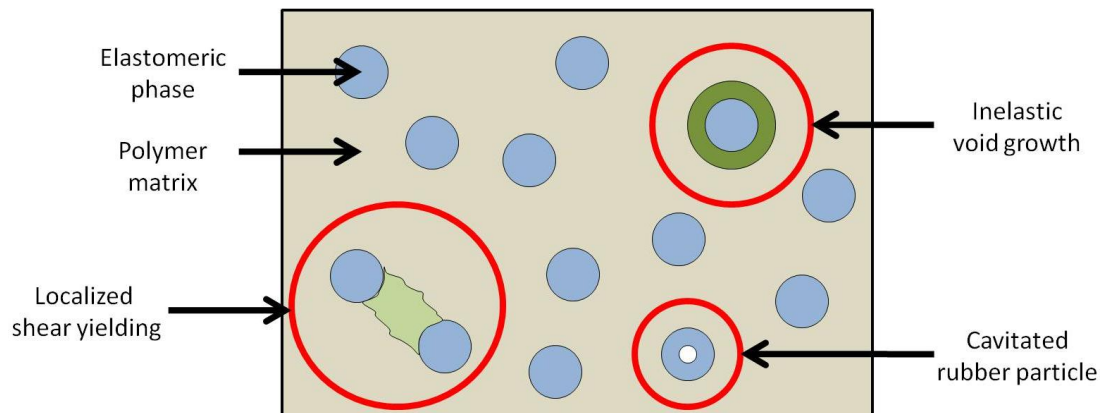


Figure 3.1 Conventional toughening mechanisms: inelastic void growth, localized shear yielding or shear crazing, and cavitation of the rubber particles. (Reproduced from Lesser 2009)

The objective of this study was to investigate the influence of (1) particle diameter, (2) filler loading, and (3) coupling agent, on the impact properties and melt flow behavior of xGnP-filled IMPP composites. The ultimate goal is to preserve or improve the polymer's uniquely tailored energy absorption capabilities. All compounded

materials were manufactured using melt mixing followed by injection molding and were prepared at 2, 4, 6, and 8 wt. % xGnP. The weight ratio of filler-to-coupling agent was held constant at 2:1 throughout this study. Characterization of impact properties was completed via Izod impact tests. Morphological characterization was conducted by means of transmission electron microscopy (TEM). Finally, melt flow behavior characterization was completed using melt flow index (MFI) testing.

### **3.3. Experimental Procedures**

#### **3.3.1. Materials**

The IMPP was supplied as polymer pellets by Polystrand Inc., USA. The IMPP had a density of  $0.900 \text{ g/cm}^3$  and melt flow index of 35 g/10 min. The xGnP fillers were supplied by XG Sciences Inc., USA. Three xGnP fillers in powder form were used as the reinforcement with different particle diameters 5, 15, and 25  $\mu\text{m}$ . Average platelet thickness ranges from about 5 to 15 nanometers. This translates into an average particle surface area ranging from about 60 to  $150 \text{ m}^2/\text{g}$ . The bulk density of all three xGnP fillers is reported to be  $0.18\text{-}0.25 \text{ g/cm}^3$ . Two different PP-g-MA were used as coupling agents, labeled for this study as SA9100 and WL9100, provided by Sigma-Aldrich Co., USA and West Lake Chemical Co., USA, respectively. Both coupling agents had a density of  $0.934 \text{ g/cm}^3$ , molecular weight of 9,100 by GPC, and acid number of 45-47. SA9100 and WL9100 coupling agents differed in that their maleic anhydride content was 8-10% and <0.7%, respectively. Materials used in this study are summarized in Table 3.1.

Table 3.1 Summary of materials used in current study.

Material/Supplier	Label	Density (g/cm <sup>3</sup> )	MA Content (%)	M <sub>w</sub>	Acid #
Impact Modified Polypropylene/ <i>Polystrand Inc.</i>	IMPP	0.900	---	---	---
Exfoliate Graphite Nanoplatelets 5μ/ <i>XG Sciences Inc.</i>	xGnP <sup>5</sup>	2	---	---	---
Exfoliate Graphite Nanoplatelets 15μ/ <i>XG Sciences Inc.</i>	xGnP <sup>15</sup>	2	---	---	---
Exfoliate Graphite Nanoplatelets 25μ/ <i>XG Sciences Inc.</i>	xGnP <sup>25</sup>	2	---	---	---
Polypropylene-g-Maleic Anhydride/ <i>Sigma-Aldrich Co.</i>	SA9100	0.934	8-10	9100	47
Polypropylene-g-Maleic Anhydride/ <i>West Lake Chemical Co.</i>	WL9100	0.934	< 0.7	9100	45

### 3.3.2. Sample Preparation

The matrix polymer IMPP was mixed with the xGnP fillers. The compounding was carried out with a Brabender Prep-mixer® equipped with a mixing bowl. The basic processing parameters used in this study are summarized in Table 3.2. The temperature was set to 180 °C and mixing speed was set at 60 rpm. All composite formulations were prepared in 150 g batches and all constituents were added to the mixer simultaneously. Mixing was done for 20 minutes; this was an optimum processing time as determined from preliminary experiments.

Table 3.2 Basic operating parameters of the Brabender rheomixer.

Batch Size (g)	Temperature (°C)	RPM	Compounding Time (min)
150	180	60	20

All composite compounds were then granulated using a lab scale grinder. The ground particles were then injection molded into ASTM test samples using a barrel temperature of 246°C and injection pressure of 2,500 psi. The designated labels and compositions of all neat and compatibilized compounded materials are shown in Table 3.3 and Table 3.4, respectively.

Table 3.3 Designated labels and compositions of xGnP filled neat composites.

Study Label	Content Per Batch (g)					
	IMPP	SA9100	WL9100	xGnP <sup>5</sup>	xGnP <sup>15</sup>	xGnP <sup>25</sup>
IMPP_xGnP <sup>5</sup> _2%	147	---	---	3	---	---
IMPP_xGnP <sup>5</sup> _4%	144	---	---	6	---	---
IMPP_xGnP <sup>5</sup> _6%	141	---	---	9	---	---
IMPP_xGnP <sup>5</sup> _8%	138	---	---	12	---	---
IMPP_xGnP <sup>15</sup> _2%	147	---	---	---	3	---
IMPP_xGnP <sup>15</sup> _4%	144	---	---	---	6	---
IMPP_xGnP <sup>15</sup> _6%	141	---	---	---	9	---
IMPP_xGnP <sup>15</sup> _8%	138	---	---	---	12	---
IMPP_xGnP <sup>25</sup> _2%	147	---	---	---	---	3
IMPP_xGnP <sup>25</sup> _4%	144	---	---	---	---	6
IMPP_xGnP <sup>25</sup> _6%	141	---	---	---	---	9
IMPP_xGnP <sup>25</sup> _8%	138	---	---	---	---	12

Table 3.4 Designated labels and compositions of xGnP filled compatibilized composites.

Study Label	Content Per Batch (g)					
	IMPP	SA9100	WL9100	xGnP <sup>5</sup>	xGnP <sup>15</sup>	xGnP <sup>25</sup>
IMPP_SA9100_xGnP <sup>5</sup> _2%	145.5	1.5	---	3	---	---
IMPP_SA9100_xGnP <sup>5</sup> _4%	141	3	---	6	---	---
IMPP_SA9100_xGnP <sup>5</sup> _6%	136.5	4.5	---	9	---	---
IMPP_SA9100_xGnP <sup>5</sup> _8%	132	6	---	12	---	---
IMPP_SA9100_xGnP <sup>15</sup> _2%	145.5	1.5	---	---	3	---
IMPP_SA9100_xGnP <sup>15</sup> _4%	141	3	---	---	6	---
IMPP_SA9100_xGnP <sup>15</sup> _6%	136.5	4.5	---	---	9	---
IMPP_SA9100_xGnP <sup>15</sup> _8%	132	6	---	---	12	---
IMPP_SA9100_xGnP <sup>25</sup> _2%	145.5	1.5	---	---	---	3
IMPP_SA9100_xGnP <sup>25</sup> _4%	141	3	---	---	---	6
IMPP_SA9100_xGnP <sup>25</sup> _6%	136.5	4.5	---	---	---	9
IMPP_SA9100_xGnP <sup>25</sup> _8%	132	6	---	---	---	12
IMPP_WL9100_xGnP <sup>5</sup> _2%	145.5	---	1.5	3	---	---
IMPP_WL9100_xGnP <sup>5</sup> _4%	141	---	3	6	---	---
IMPP_WL9100_xGnP <sup>5</sup> _6%	136.5	---	4.5	9	---	---
IMPP_WL9100_xGnP <sup>5</sup> _8%	132	---	6	12	---	---
IMPP_WL9100_xGnP <sup>15</sup> _2%	145.5	---	1.5	---	3	---
IMPP_WL9100_xGnP <sup>15</sup> _4%	141	---	3	---	6	---
IMPP_WL9100_xGnP <sup>15</sup> _6%	136.5	---	4.5	---	9	---
IMPP_WL9100_xGnP <sup>15</sup> _8%	132	---	6	---	12	---
IMPP_WL9100_xGnP <sup>25</sup> _2%	145.5	---	1.5	---	---	3
IMPP_WL9100_xGnP <sup>25</sup> _4%	141	---	3	---	---	6
IMPP_WL9100_xGnP <sup>25</sup> _6%	136.5	---	4.5	---	---	9
IMPP_WL9100_xGnP <sup>25</sup> _8%	132	---	6	---	---	12

### 3.3.3. Mechanical Characterization

Impact tests were conducted according to ASTM D 256-06, “Standard Test Methods for Determining the Izod Pendulum Impact Resistance of Plastics”. The notches were added using a NotchVIS machine manufactured by Ceast. The samples were tested on a Resil 50 B impact test machine, manufactured by Ceast. The sample was clamped in the bottom of the test fixture and the hammer was then released from a controlled height at 150°. A 7.5 J and 2.75 J hammer was used to impact unnotched and notched samples, respectively. Ten samples were tested for each composition and the results are presented as an average for tested samples. All breaks must be completed breaks to count as a data point. Both unnotched and notched impact strength were calculated as impact energy less windage (drag) all divided by the width of specimen less the depth of the notch. Fracture initiation resistance was calculated via Equation 3.1 as shown:

$$\text{FIR} = I_{\text{UN}} - I_{\text{N}} \quad \text{Equation 3.1}$$

Where unnotched impact strength ( $I_{\text{UN}}$ ) represents the energy required to initiate and propagate a crack and notched impact strength ( $I_{\text{N}}$ ) represents the energy required to propagate a crack. Hence, fracture initiation resistance (FIR) represents a characteristic property of the material which defines the energy required for crack initiation and is equal to the difference between unnotched and notched impact strength.



### **3.3.4. Morphological Characterization**

TEM images were obtained using a Phillips CM10 transmission electron microscope. Images were taken at magnifications of 130 kX, 245 kX and 450 kX. Sectioning of thermoplastics is a difficult task because of their inherently soft characteristics. In the absence of low temperature ultra-cryotome technology, a method for obtaining ultrathin sections was necessary. Thin slivers of our composites were shaved and embedded in an epoxy matrix to aid in sectioning the soft plastic. The embedded sample was then sectioned using a Leica EM UC6 ultra-microtome equipped with a diamond knife. Specimens were sectioned with thickness on the order of 50-75 nm.

### **3.3.5. Melt Flow Characterization**

Melt flow index (MFI) testing was conducted according to ASTM D 1238-06, “Standard Test Methods for Melt Flow Rates of Thermoplastics by Extrusion Plastometer”. The samples were tested using a laboratory melt flow tester (indexer), manufactured by Dynisco. Per Section 8.2 of the standard the polypropylene-based composites were tested with procedural conditions, melt temperature and weight, equal to 230°C and 2.16 kg, respectively. The computerized programming capability of the melt flow indexer was implemented to assure accurate melt time and cut time equal to 30 seconds and 15 seconds, respectively. The MFI of an individual sample is calculated as the weight of material extruded divided by the cut time and is traditionally presented in

units of grams per 10 minutes at a specified temperature and weight applied (g/10min @ 230°C/2.16 kg). Three sample runs were completed for each composition. MFI of all compounded materials was reported as an average for tested samples.

### **3.3.6. Statistical Analysis**

The unnotched, notched and FIR impact strengths were compared using a one-way analysis of variance followed by Tukey-Kramer Honestly Significant Differences (HSD) test at a confidence value equal to 0.05 with JMP statistical analysis program (JMP 9).

## **3.4. Results and Discussion**

### **3.4.1. Impact Properties**

The impact properties of all compounded composites was characterized via the impact testing methods described in Section 3.3.3. Neat IMPP was determined to have unnotched impact strength, notched impact strength and fracture initiation resistance equal to 445, 85 and 360 J/m, respectively.

The impact testing of all compounded materials was performed via unnotched and notched Izod impact testing at room temperature. There are some inherent problems often

considered in characterizing impact capacity of structural materials using this test method. The first problem is the fact that the specimen is a relatively short thick beam when compared to typical structural engineering components. Secondly, the Izod impact test is a rapid, destructive test which does not directly replicate low velocity impact events that may occur on many structures while in service. However, the Izod impact test is an appropriate method to rank the impact resistance of a population of composite materials (Cantwell and Morton 1991).

Normalized unnotched impact strength results for neat and xGnP<sup>5</sup>-filled composites with coupling agent as a function of filler loading level up to 8% are presented in Figure 3.2. Similar plots are provided for neat and xGnP<sup>15</sup> and xGnP<sup>25</sup>-filled composites with coupling agent in Figure 3.3 and Figure 3.4, respectively. Unnotched impact strength was found to increase with decreasing xGnP particle diameter for all filler loading values of both neat and xGnP-filled composites containing coupling agent. However, unnotched impact strength decreased dramatically with increased filler loading for all neat and xGnP-filled composites containing coupling agent. In nearly all cases, the addition of coupling agent caused lower unnotched impact strength and therefore a more brittle behaving composite. It is suspected that the reason for this is analogous to the explanation of the same phenomena seen in tensile testing (elongation at break) discussions. That is, when there is improved adhesion between the filler and the matrix (compatibilized), significant decrease in elongation at break (brittle behavior) can be expected even at small filler loading levels. In the case of poor adhesion (neat composite), the decrease in elongation at break (brittle behavior) is expected to be more

gradual (Oksman and Clemons 1998). The optimum formulation to obtain the least degradation of unnotched impact strength for filler loading levels 2, 4, 6 and 8 wt. % is IMPP\_xGnP<sup>5</sup> composites. The resulting degradation when compared to neat IMPP is 54, 65, 70 and 77%, respectively.

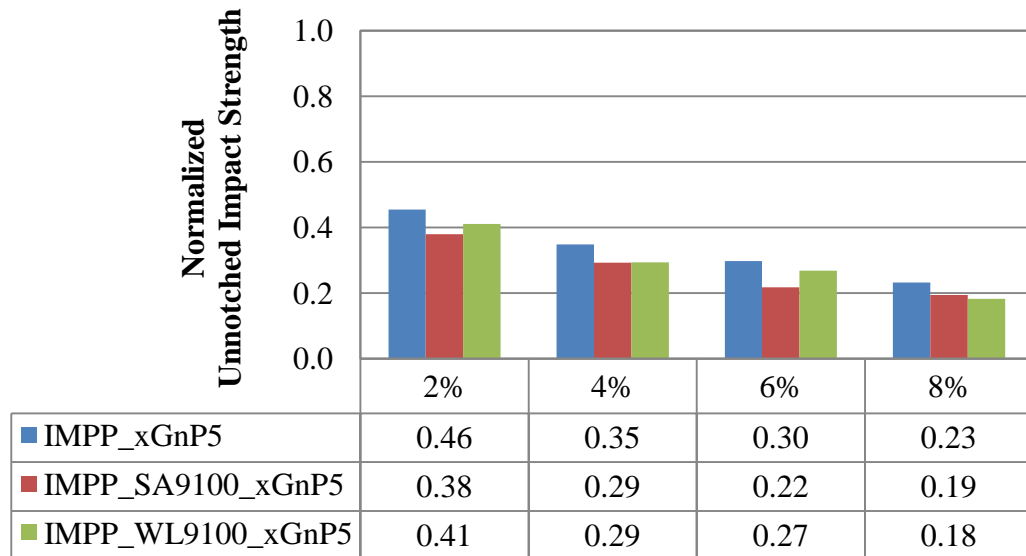


Figure 3.2 Normalized unnotched impact strength experimental results for xGnP<sup>5</sup> filled composites.

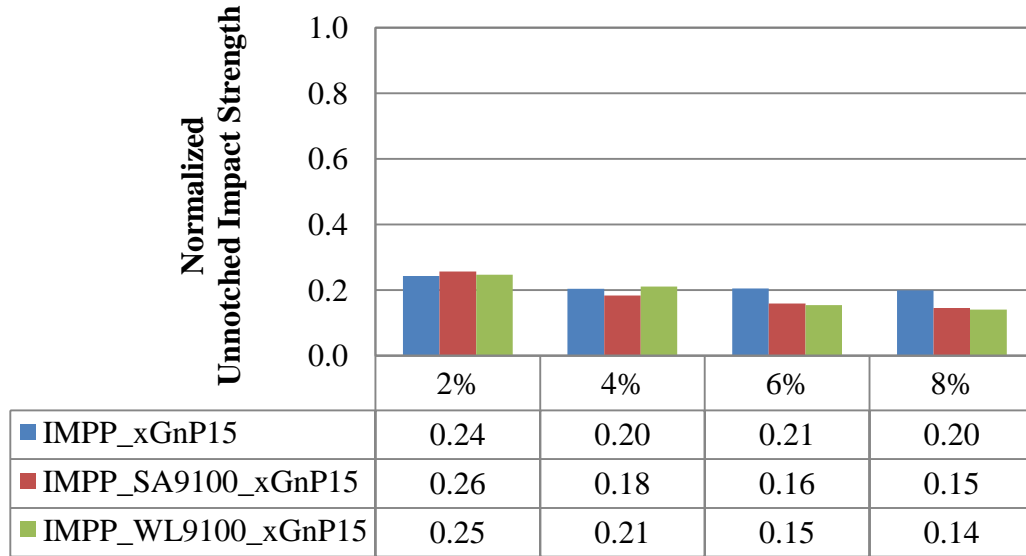


Figure 3.3 Normalized unnotched impact strength experimental results for xGnP<sup>15</sup> filled composites.

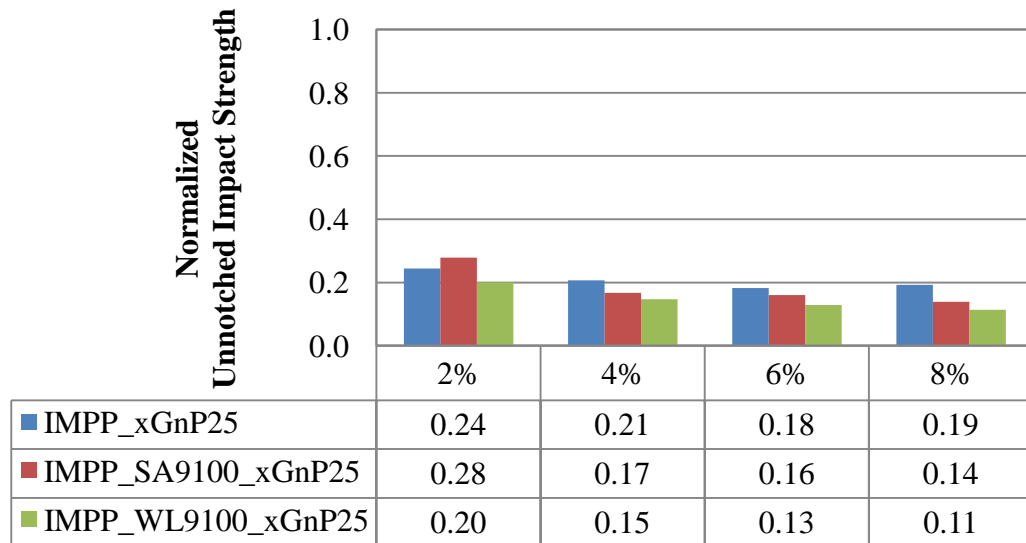


Figure 3.4 Normalized unnotched impact strength experimental results for xGnP<sup>25</sup> filled composites.

Normalized notched impact strength results for neat and xGnP<sup>5</sup>-filled composites with coupling agent as a function of filler loading level up to 8% are presented in Figure 3.5. Similar plots are provided for neat and xGnP<sup>15</sup> and xGnP<sup>25</sup>-filled composites with coupling agent in Figure 3.6 and Figure 3.7, respectively. Notched impact strength was found to increase with decreasing xGnP particle diameter for all filler loading values of both neat and xGnP-filled composites containing coupling agent. Notched impact strength decreased with increased filler loading for all neat and xGnP-filled composites containing coupling agent. The addition of coupling agent caused lower notched impact strength for all xGnP<sup>15</sup> and xGnP<sup>25</sup>-filled composites. Interestingly, the addition of coupling agent resulted in higher notched impact strength for xGnP<sup>5</sup>-filled composites at all filler loading levels below 8 wt. %. The optimum formulation to obtain the least degradation of notched impact strength for filler loading levels 2, 4, 6 and 8 wt. % is IMPP\_WL9100\_xGnP<sup>5</sup> composites. The resulting degradation when compared to neat IMPP is 44, 51, 57 and 77%, respectively.

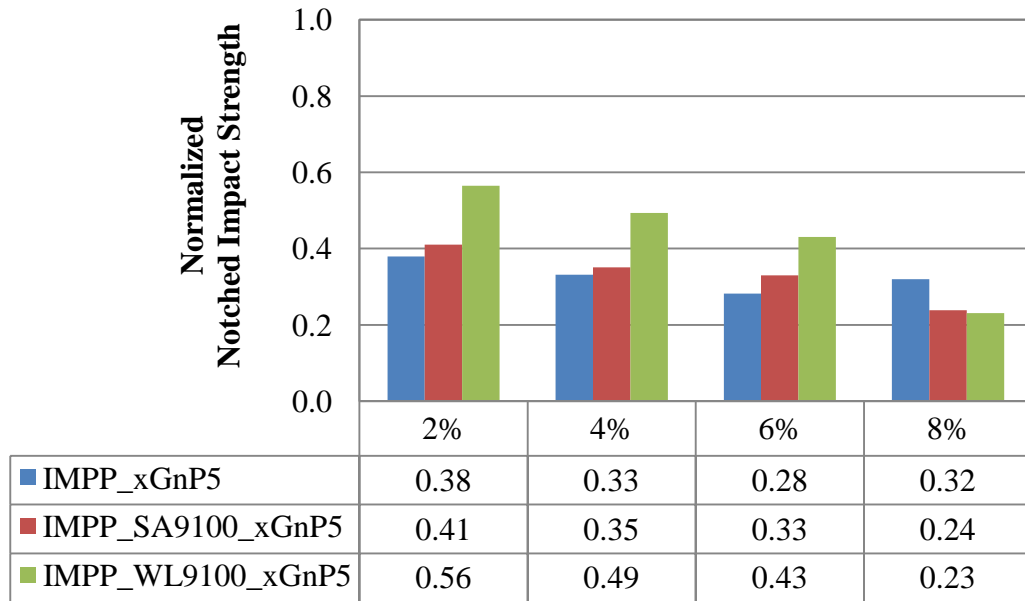


Figure 3.5 Normalized notched impact strength experimental results for xGnP<sup>5</sup> filled composites.

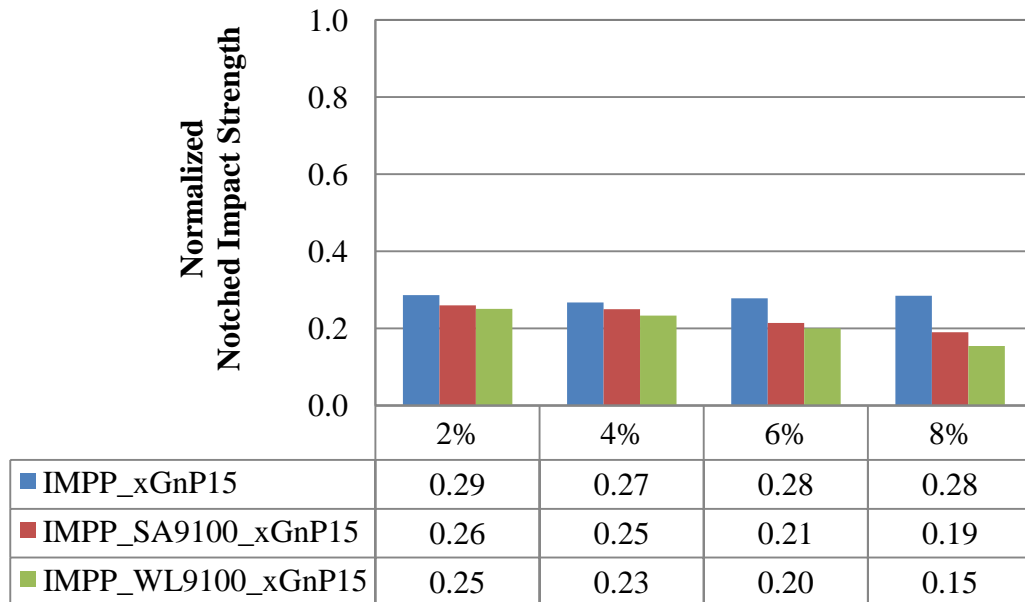


Figure 3.6 Normalized notched impact strength experimental results for xGnP<sup>15</sup> filled composites.

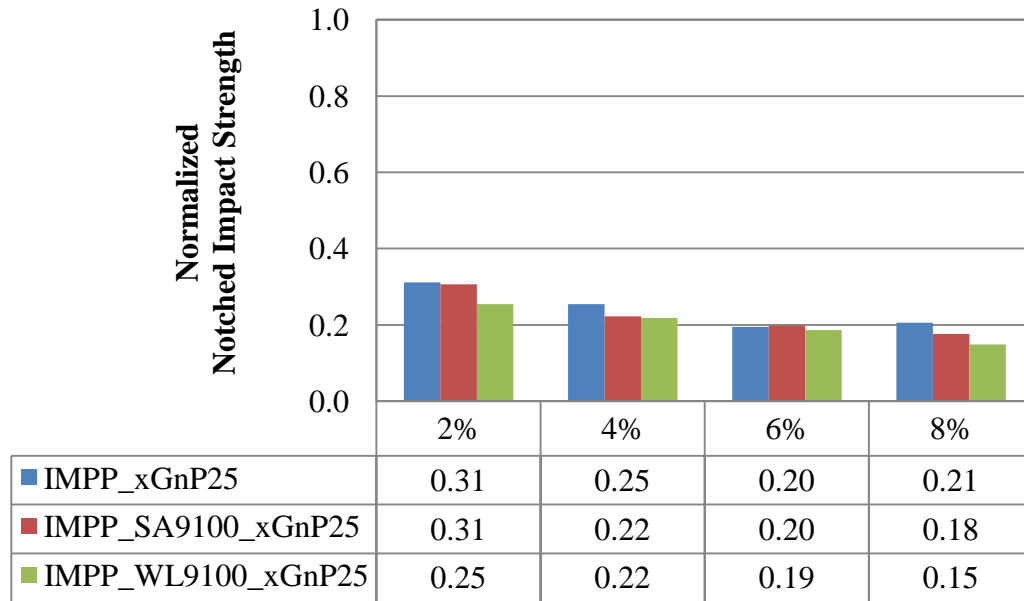


Figure 3.7 Normalized notched impact strength experimental results for xGnP<sup>25</sup> filled composites.

Similar degradation of notched impact strength has been published in recent years. Ahmad et al. investigated nano clay particles incorporated into thermoplastic natural rubbers. Nearly 50% degradation of notched impact strength was observed with the addition of 2 wt. % filler in direct melt compounded composites (Ahmad et. al 2007). Other researchers found degradation of notched impact properties to occur above 5 wt. % filler loading for montmorillonite-filled polypropylene homopolymer reaching nearly 50% degradation at 7 wt. % filler loading (Zhang et al. 2000). Kalaitzidou et al. have shown xGnP<sup>15</sup> and xGnP<sup>1</sup>-filled polypropylene to exhibit significant enhancement (100% for xGnP<sup>1</sup>) of notched impact strength at very low filler loading levels (~3 Vol. %). However, after this point for both fillers further increase of filler loading results in decreasing notched impact strength (Kalaitzidou et al. 2007d).



It has been shown that much lower xGnP content is required to greatly improve impact properties of polypropylene homopolymer. Yet, literature has not shown extreme deterioration of impact strength with the addition of any size particle diameter xGnP. With ~2 wt. % xGnP<sup>15</sup> impact strength was shown to increase slightly from the neat polypropylene homopolymer and with the same filler loading for xGnP<sup>1</sup> impact strength was shown to increase significantly (Kalaitzidou et al. 2007d). Therefore some mechanism must be proposed to justify the massive degradation (71%) seen in this study for our IMPP\_xGnP<sup>15</sup>\_2% composite.

The TEM image shown in Figure 3.8 is provided to illustrate evidence of the elastomeric phase consisting of small (~100 nm) spherical rubber particles, indicated by the red arrow, as predicted by the literature review. Upon impact loading, whether unnotched or notched, the presence of these rubber particles is expected to induce any or all of the three conventional toughening mechanisms illustrated in Figure 3.1, resulting in much higher impact properties when compared to polypropylene homopolymer.

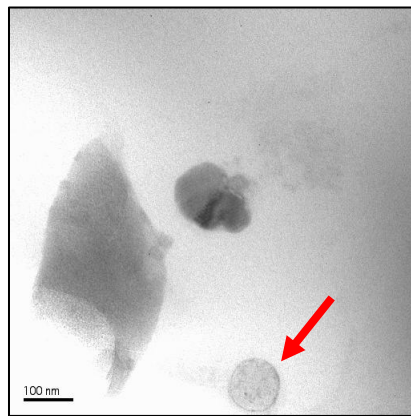


Figure 3.8 Transmission electron micrograph with arrow indicating evidence of elastomeric impact modification phase.

It is proposed that the graphitic nanoplatelets are acting as very stiff inclusions that redirect stress concentrations away from the elastomeric impact modification (toughening) phase. This will not allow the conventional toughening mechanisms to occur. It is expected that stress concentrations instead occur around the xGnP because of the much higher mismatch of modulus between graphite and neat PP. The proposed failure mechanism is detailed in the following steps: (1) stress concentrations occur surrounding the graphite platelets, (2) rapid delamination of the matrix from the filler ensues because of the lack of affinity (poor adhesion) between PP and xGnP and (3) catastrophic crack propagation can occur with little energy applied. A conceptual illustration of this proposed theory and subsequent failure mechanism is shown in Figure 3.9.

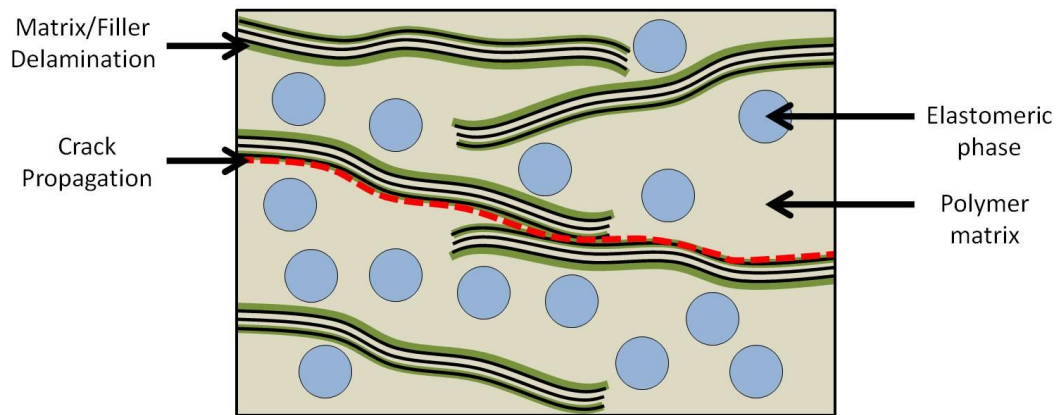


Figure 3.9 Conceptual illustration of proposed failure mechanism in xGnP filled IMPP.

The addition of xGnP has proven catastrophic to the notched and even more so to the unnotched impact strength of the neat IMPP, consequently deteriorating FIR of all xGnP-filled IMPP composites. For these reasons xGnP has been proven not feasible at

filler loading levels 2, 4, 6 and 8 wt. % for use as a reinforcement phase in IMPP composites. Further investigations will be necessary in regards to very low loading levels. In the following section correlation between melt flow index and impact properties will be examined to gain an educated starting point for future xGnP-filled IMPP composites. Table 3.5 shows a summary of impact properties and statistical significance of all compounded materials.

Table 3.5 Summary of impact mechanical properties and statistical significance (Tukey-Kramer HSD comparison at  $\alpha = 0.05$ ) of all compounded materials.

Study Label	Impact Properties					
	Izod Unnotched		Izod Notched		FIR	
		(J/m)		(J/m)		(J/m)
Neat IMPP	A	445.4 (121.8)	A	48.7 (10.9)	A	396.7 (123.5)
IMPP_xGnP <sup>5</sup> _2%	B	202.7 (23.4)	DEF	18.5 (1.5)	B	184.2 (23.2)
IMPP_xGnP <sup>5</sup> _4%	BCD	155.4 (40.3)	EFGH	16.1 (1.8)	BCDE	139.2 (39.9)
IMPP_xGnP <sup>5</sup> _6%	CDE	132.5 (15.1)	GHIJKLM	13.7 (1.8)	CDEF	118.7 (15.5)
IMPP_xGnP <sup>5</sup> _8%	EFGHIJK	103.4 (23.5)	FGHI	15.6 (1.2)	FGHIJKLM	87.8 (23.3)
IMPP_SA9100_xGnP <sup>5</sup> _2%	BC	169.0 (33.1)	DE	20.0 (1.4)	BCD	149.1 (33.6)
IMPP_SA9100_xGnP <sup>5</sup> _4%	CDE	130.7 (25.9)	EFG	17.1 (1.0)	CDEFG	113.6 (26.0)
IMPP_SA9100_xGnP <sup>5</sup> _6%	EFGHIJKL	97.1 (16.9)	FGH	16.1 (1.9)	FGHIJKLM	81.0 (17.0)
IMPP_SA9100_xGnP <sup>5</sup> _8%	EFGHIJKL	86.6 (9.3)	JKLMNOPQ	11.6 (0.8)	FGHIJKLM	74.9 (9.5)
IMPP_WL9100_xGnP <sup>5</sup> _2%	B	183.2 (26.7)	B	27.5 (2.3)	BC	155.7 (26.5)
IMPP_WL9100_xGnP <sup>5</sup> _4%	CDE	130.9 (43.4)	BC	24.0 (1.3)	DEFGHI	106.8 (43.3)
IMPP_WL9100_xGnP <sup>5</sup> _6%	DEFG	119.6 (43.2)	CD	21.0 (2.2)	EFGHIJK	98.6 (42.9)
IMPP_WL9100_xGnP <sup>5</sup> _8%	FGHIJKL	81.6 (10.5)	KLMNOPQR	11.2 (1.5)	GHIJKLM	70.4 (10.5)
IMPP_xGnP <sup>15</sup> _2%	DEFGHIJ	108.1 (11.6)	GHIJKL	13.9 (1.4)	EFGHIJKL	94.2 (11.4)
IMPP_xGnP <sup>15</sup> _4%	EFGHIJKL	91.0 (5.5)	HIJKLMNO	13.0 (0.8)	FGHIJKLM	78.0 (5.5)
IMPP_xGnP <sup>15</sup> _6%	EFGHIJKL	91.3 (13.1)	GHIJKLMN	13.5 (1.7)	FGHIJKLM	77.8 (12.8)
IMPP_xGnP <sup>15</sup> _8%	EFGHIJKL	88.9 (9.54)	GHIJKLM	13.9 (1.2)	FGHIJKLM	75.0 (9.8)
IMPP_SA9100_xGnP <sup>15</sup> _2%	DEFGH	114.3 (13.6)	HIJKLMNOP	12.6 (1.0)	DEFGHIJ	101.7 (13.6)
IMPP_SA9100_xGnP <sup>15</sup> _4%	FGHIJKL	81.7 (4.8)	IJKLMNO	12.2 (0.9)	GHIJKLM	69.6 (4.5)
IMPP_SA9100_xGnP <sup>15</sup> _6%	HIJKL	70.8 (7.9)	LMNOPQRS	10.4 (0.5)	IJKLM	60.4 (8.0)
IMPP_SA9100_xGnP <sup>15</sup> _8%	IJKL	64.8 (7.8)	OPQRS	9.3 (1.3)	JKLM	55.5 (8.0)
IMPP_WL9100_xGnP <sup>15</sup> _2%	DEFGHI	110.0 (17.6)	IJKLMNO	12.2 (2.0)	EFGHIJK	97.8 (17.8)
IMPP_WL9100_xGnP <sup>15</sup> _4%	EFGHIJKL	94.0 (9.0)	JKLMNOPQR	11.3 (0.8)	FGHIJKLM	82.6 (9.7)
IMPP_WL9100_xGnP <sup>15</sup> _6%	HIJKL	68.9 (4.7)	NOPQRS	9.7 (1.2)	IJKLM	59.1 (4.3)
IMPP_WL9100_xGnP <sup>15</sup> _8%	IJKL	62.5 (6.0)	RS	7.5 (1.2)	JKLM	55.0 (6.9)
IMPP_xGnP <sup>25</sup> _2%	DEFGHIJ	108.8 (15.0)	FGHIJ	15.2 (1.0)	EFGHIJKL	93.6 (15.3)
IMPP_xGnP <sup>25</sup> _4%	EFGHIJKL	91.9 (18.5)	HIJKLMNO	12.4 (1.4)	FGHIJKLM	79.5 (18.4)
IMPP_xGnP <sup>25</sup> _6%	FGHIJKL	81.1 (11.4)	OPQRS	9.5 (0.6)	FGHIJKLM	71.6 (11.1)
IMPP_xGnP <sup>25</sup> _8%	EFGHIJKL	85.7 (6.8)	MNOPQRS	10.0 (0.6)	FGHIJKLM	75.7 (6.6)
IMPP_SA9100_xGnP <sup>25</sup> _2%	CDEF	123.9 (17.6)	FGHIJK	14.9 (1.1)	CDEFGH	108.9 (18.2)
IMPP_SA9100_xGnP <sup>25</sup> _4%	GHIJKL	74.7 (9.7)	LMNOPQRS	10.8 (0.9)	HIJKLM	63.8 (9.8)
IMPP_SA9100_xGnP <sup>25</sup> _6%	HIJKL	71.3 (10.1)	OPQRS	9.7 (0.7)	HIJKLM	61.7 (9.9)
IMPP_SA9100_xGnP <sup>25</sup> _8%	JKL	61.9 (17.8)	QRS	8.6 (1.6)	KLM	53.3 (17.2)
IMPP_WL9100_xGnP <sup>25</sup> _2%	EFGHIJKL	89.5 (12.4)	HIJKLMNO	12.4 (1.0)	FGHIJKLM	77.1 (12.8)
IMPP_WL9100_xGnP <sup>25</sup> _4%	IJKL	65.3 (10.6)	LMNOPQRS	10.6 (1.1)	JKLM	54.7 (10.7)
IMPP_WL9100_xGnP <sup>25</sup> _6%	KL	57.3 (6.1)	PQRS	9.1 (1.0)	LM	48.3 (6.3)
IMPP_WL9100_xGnP <sup>25</sup> _8%	L	50.8 (8.2)	S	7.2 (0.7)	M	43.5 (8.0)

Parenthesis indicates standard deviation.

Presence of the same letter indicates no statistical difference.

### 3.4.2. Melt Flow Behavior

The melt flow behavior of all compounded composites was characterized via the melt flow characterization methods described in Section 3.3.5. Neat IMPP was determined to have melt flow index (MFI) equal to 35.4 g/10min @ 230 °C/ 2.16kg.

MFI is an extremely useful technique for the plastics processing industry to determine flow behavior of thermoplastics in the melt form, due to its ease of measurement and repeatability (Teng et al. 2008). MFI results for neat and xGnP<sup>5</sup>-filled composites with coupling agent as a function of filler loading level up to 8% are presented in Figure 3.10. Similar plots are provided for neat and xGnP<sup>15</sup> and xGnP<sup>25</sup>-filled composites with coupling agent in Figure 3.11 and Figure 3.12, respectively. In general, MFI was found to increase with decreasing xGnP particle diameter for both neat and xGnP-filled composites containing coupling agent. However, MFI decreased with increased filler loading for all neat and xGnP-filled composites containing coupling agent. In nearly all cases, the addition of coupling agent caused increased MFI. This behavior is typical of reported results throughout the relevant filled polymer literature discussed below.

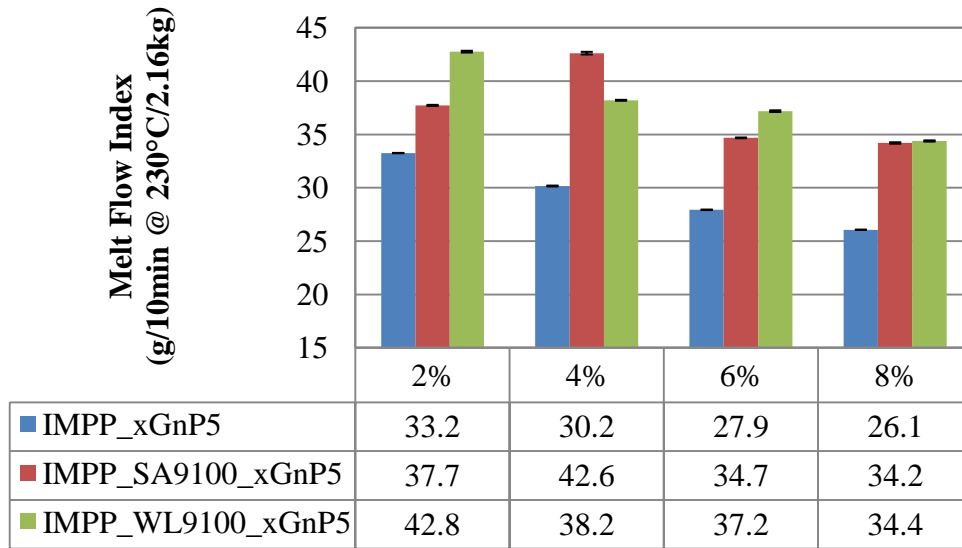


Figure 3.10 Melt flow index experimental results for xGnP<sup>5</sup> filled composites.

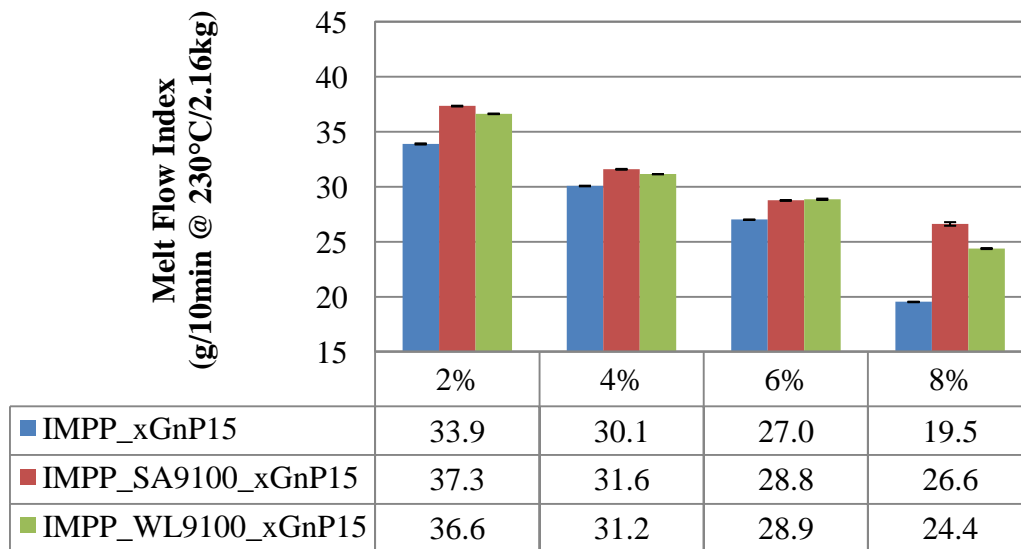


Figure 3.11 Melt flow index experimental results for xGnP<sup>15</sup> filled composites.

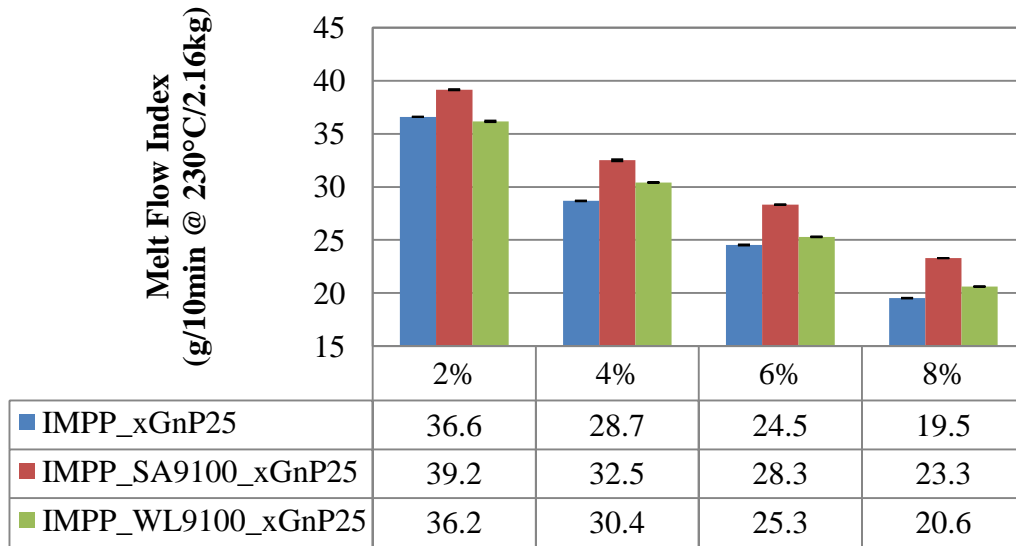


Figure 3.12 Melt flow index experimental results for xGnP<sup>25</sup> filled composites.

Teng et al. studied multi-wall carbon nanotubes-filled polypropylene composites. They reported an increase of MFI at low filler loading levels and decrease of MFI for continued addition of MWCNTs. In fact, at least a 94% decrease in MFI occurred for all grades of polypropylene investigated when filler loading was 10 parts per hundred parts (phr) of PP resin. Sources were presented justifying this behavior in similar studies for porous carbon-based fillers (Teng et al. 2008). Bera and Kale investigated polypropylene filled with rice husk, both neat and compatibilized. Decrease in MFI for increased filler loading was reported (Bera and Kale 2008). According to Ratnayake et al., the addition of maleic anhydride to polypropylene results in significant increase in MFI compared to the neat polymer. It is suggested that the maleic anhydride promotes flow of the polymer melt by inducing wall slip at the flow boundary of the polymer chains under constant applied shear stress. With the addition of 2 wt. % nano clay to the polypropylene/maleic anhydride blends, MFI was decreased 37% (Ratnayake et al. 2009).

It is well understood that MFI is dependent upon molecular properties such as molecular weight and structure of a polymer system. High MFI polymers have low molecular weight and vice versa (Balasuriya et al. 2001; Lu et al. 2006; Teng et al. 2008). Work performed by Lu et al. showed high molecular weight HDPE to result in much improved impact energy absorption capabilities when compared to lower molecular weight HDPE. Lu et al. reported that previous research has found impact strength to be proportional to the molecular weight and therefore attempted to correlate MFI with impact strength experimental results (Lu et al. 2006). The same approach was taken in this study and lead to opposite, but much more intriguing results. In Figure 3.13 experimental melt flow index results for the well dispersed IMPP\_WL9100\_xGnP<sup>5</sup> composites were plotted versus filler loading level. A logarithmic trend line resulted in the best correlation coefficient ( $R^2 = 0.972$ ) for the data.

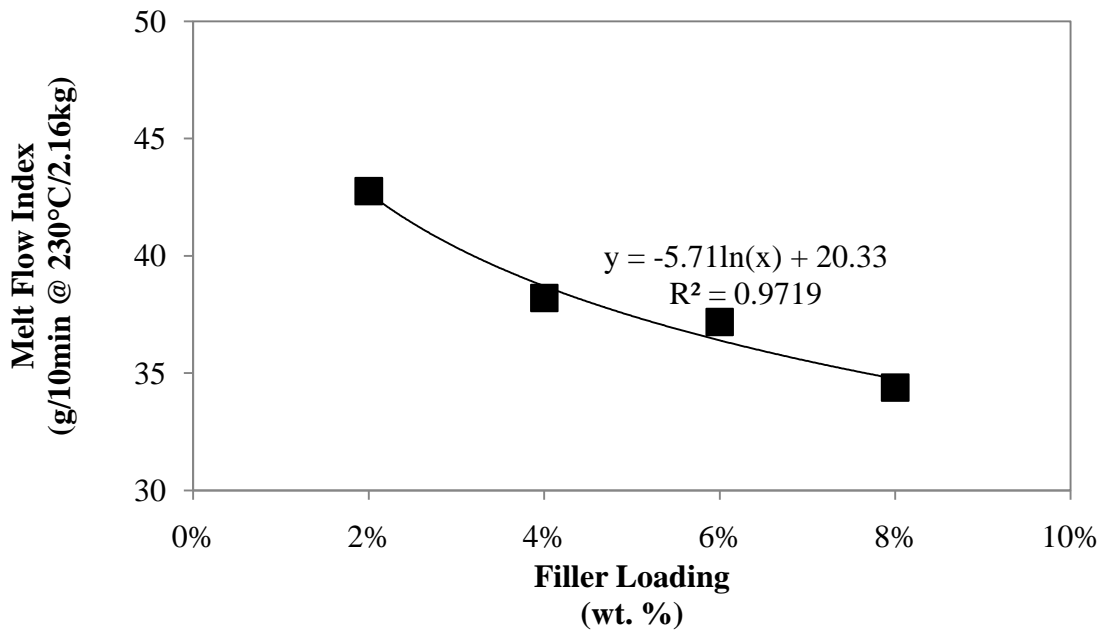


Figure 3.13 Correlation of melt flow index with filler loading for IMPP\_WL9100\_xGnP<sup>5</sup> composites.



Figure 3.14 has been provided to illustrate the correlation of experimentally determined impact properties with melt flow index for IMPP\_WL9100\_xGnP<sup>5</sup> composites. Recall in the study performed by Lu et al., impact properties increased with molecular weight of polyethylene. Dissimilarly, all impact properties from this study were shown to increase with MFI and therefore decrease with increased molecular weight. Linear trend lines resulted in the best correlation coefficients equal to 0.999, 0.998 and 0.838 for the unnotched, FIR, and notched impact strength data, respectively. This proved the correlation of impact properties with MFI was extremely linear.

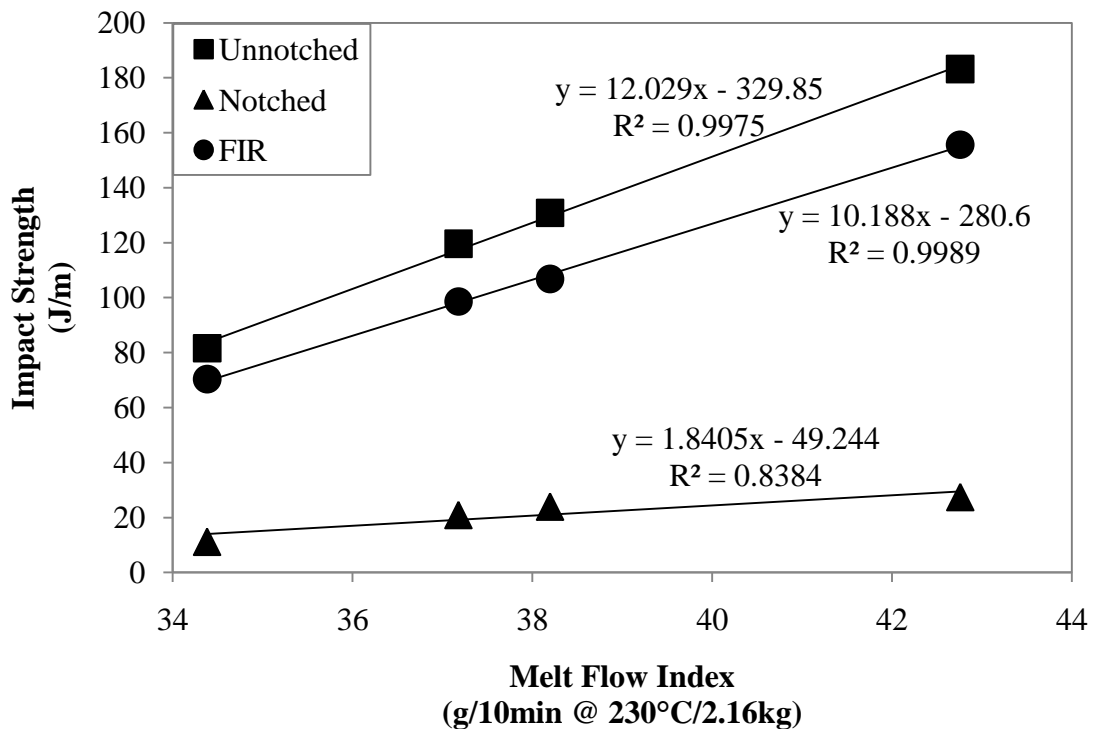


Figure 3.14 Correlation of impact properties with melt flow index for IMPP\_WL9100\_xGnP<sup>5</sup> composites.

The above discussed trends and the respective equations were then implemented to back calculate an educated starting point for filler loading levels in future xGnP-filled IMPP nanocomposite studies. Using the correlations presented above calculations indicate that it was necessary for filler content to be below 0.044% and 0.315% to improve unnotched and notched impact strengths, respectively. Michigan State researchers found large increases of notched impact strength in xGnP-filled polypropylene homopolymer composites at 3 vol. % (~1.1 wt. %) filler loading (Kalaitzidou et al. 2007d). We know that the magnitude of inherent stress concentrations decreases as the thickness at the tip of the graphite agglomerates decreases (Thostenson et al. 2005). It can be imagined that lower volumes of well dispersed filler could result in inherent stress concentrations low enough in magnitude such that the conventional toughening mechanisms presented in Figure 3.1 could still be induced. Simultaneously, energy absorbing mechanisms such as crack bridging and crack branching (redirection of crack as a result of the presence of a filler) may further enhance the impact properties of IMPP (Lesser 2009; Jiang and Drzal 2010). Table 3.6 shows a summary of melt flow behavior of all compounded composites.

Table 3.6 Summary of melt flow behavior for all compounded materials.

Study Label	Melt Flow Behavior
	MFI (g/10min @ 230°C/2.16kg )
Neat IMPP	35.4 (0.1)
IMPP_xGnP <sup>5</sup> _2%	33.2 (0.0)
IMPP_xGnP <sup>5</sup> _4%	30.2 (0.0)
IMPP_xGnP <sup>5</sup> _6%	27.9 (0.0)
IMPP_xGnP <sup>5</sup> _8%	26.1 (0.0)
IMPP_SA9100_xGnP <sup>5</sup> _2%	37.7 (0.1)
IMPP_SA9100_xGnP <sup>5</sup> _4%	42.6 (0.1)
IMPP_SA9100_xGnP <sup>5</sup> _6%	34.7 (0.0)
IMPP_SA9100_xGnP <sup>5</sup> _8%	34.2 (0.1)
IMPP_WL9100_xGnP <sup>5</sup> _2%	42.8 (0.1)
IMPP_WL9100_xGnP <sup>5</sup> _4%	38.2 (0.0)
IMPP_WL9100_xGnP <sup>5</sup> _6%	37.2 (0.1)
IMPP_WL9100_xGnP <sup>5</sup> _8%	34.4 (0.1)
IMPP_xGnP <sup>15</sup> _2%	33.9 (0.1)
IMPP_xGnP <sup>15</sup> _4%	30.1 (0.0)
IMPP_xGnP <sup>15</sup> _6%	27.0 (0.0)
IMPP_xGnP <sup>15</sup> _8%	19.5 (0.0)
IMPP_SA9100_xGnP <sup>15</sup> _2%	37.3 (0.0)
IMPP_SA9100_xGnP <sup>15</sup> _4%	31.6 (0.0)
IMPP_SA9100_xGnP <sup>15</sup> _6%	28.8 (0.0)
IMPP_SA9100_xGnP <sup>15</sup> _8%	26.6 (0.2)
IMPP_WL9100_xGnP <sup>15</sup> _2%	36.6 (0.0)
IMPP_WL9100_xGnP <sup>15</sup> _4%	31.2 (0.0)
IMPP_WL9100_xGnP <sup>15</sup> _6%	28.9 (0.1)
IMPP_WL9100_xGnP <sup>15</sup> _8%	24.4 (0.0)
IMPP_xGnP <sup>25</sup> _2%	36.6 (0.0)
IMPP_xGnP <sup>25</sup> _4%	28.7 (0.0)
IMPP_xGnP <sup>25</sup> _6%	24.5 (0.0)
IMPP_xGnP <sup>25</sup> _8%	19.5 (0.0)
IMPP_SA9100_xGnP <sup>25</sup> _2%	39.2 (0.1)
IMPP_SA9100_xGnP <sup>25</sup> _4%	32.5 (0.1)
IMPP_SA9100_xGnP <sup>25</sup> _6%	28.3 (0.0)
IMPP_SA9100_xGnP <sup>25</sup> _8%	23.3 (0.0)
IMPP_WL9100_xGnP <sup>25</sup> _2%	36.2 (0.1)
IMPP_WL9100_xGnP <sup>25</sup> _4%	30.4 (0.0)
IMPP_WL9100_xGnP <sup>25</sup> _6%	25.3 (0.0)
IMPP_WL9100_xGnP <sup>25</sup> _8%	20.6 (0.0)

Parenthesis indicates standard deviation.

### 3.5. Conclusions

Both neat and xGnP-filled IMPP composites containing coupling agents were prepared via melt compounding followed by injection molding. Mechanical, morphological and melt flow characterization yielded conclusions in understanding the influence of (1) particle diameter, (2) filler loading, and (3) coupling agent, on the impact properties of xGnP-filled IMPP composites.

The smallest diameter filler investigated in this study (5 $\mu$ m) performed the best in terms of impact properties of xGnP-filled IMPP composites. Impact properties were greatly deteriorated with as little as 2 wt. % xGnP with and without coupling agent. The addition of coupling agent amplifies the degradation of impact properties because of the improved adhesion between the filler and the matrix. A correlation study to determine a relationship between impact properties and MFI was explored. Impact properties were shown to increase with MFI linearly. Experimental MFI results for the well dispersed IMPP\_WL9100\_xGnP<sup>5</sup> composites were plotted versus filler loading level, resulting in a logarithmic trend with a high correlation coefficient. Using these relationships it was determined necessary for filler content to be below 0.044 and 0.315 wt. % to improve unnotched and notched impact strengths, respectively. Future work will need to be completed to determine the filler loading domain for which these correlated relationships remain valid.

### 3.6. References

Ahmad S.H., Rasid R., Surip S.N., Anuar H., Czigany T., Abdul Razak S.B. “Mechanical and Fracture Toughness Behavior of TPNR Nanocomposites.” *Journal of Composite Materials*, 41(17) (2007): 2147-2159.

Balasuriya P.W., Ye L., Mai Y.-W. “Mechanical properties of wood flake-polyethylene composites. Part I: effects of processing methods and matrix melt flow behaviour.” *Composites: Part A*, 32 (2001): 619-629.

Bera J. and Kale D. D. “Properties of Polypropylene Filled with Chemically Treated Rice Husk.” *Journal of Applied Polymer Science*, 82 (2001): 2506-2513.

Cantwell W.J. and Morton J. “The impact resistance of composite material - a review.” *Composites*, 22(5) (1991): 347-362.

Jiang X. & Drzal L. T. “Multifunctional High Density Polyethylene Nanocomposites Produced by Incorporation of Exfoliated Graphite nanoplatelets 1: Morphology and Mechanical Properties.” *Polymer Composites*, (2010): 1091-1098.

Kalaitzidou K., Fukushima H., Drzal L. T. “Mechanical properties and morphological characterization of exfoliated graphite-polypropylene nanocomposites.” *Composites: Part A*, 38 (2007d): 1675-1682.

Lesser A.J. “Fundamentals in Toughening.” *Proceedings of NSF Summer Institute on Nanomechanics, Nanomaterials, and Micro/Nanomanufacturing*, University of Massachusetts Lowell (2009).

Lim J.W., Hassan A., Rahmat A.R., Wahit M.U. “Phase Morphology and Mechanical Properties of Rubber-Toughened Polypropylene Nanocomposites: Effect of Elastomer Polarity.” *Polymer-Plastics Technology and Engineering*, 47 (2008): 411-419.

Lu J.Z., Wu Q., Negulescu I. I., Chen Y. “The Influences of Fiber Feature and Polymer Melt Index on Mechanical Properties of Sugarcane Fiber/Polymer Composites.” *Journal of Applied Polymer Science*, 102 (2006): 5607-5619.

Oksman K. and Clemons C. “Mechanical Properties and Morphology of Impact Modified Polypropylene-Wood Flour Composites.” *Journal of Applied Polymer Science*, 67 (1998): 1503-1513.

Park H.M., Kalaitzidou K., Fukushima H., Drzal L. T. “Exfoliated Graphite Nanoplatelet (xGnP) /Polypropylene Nanocomposites.” Composite Materials & Structures Center, Michigan State University (2007).

Ratnayake U.N., Haworth B., Hourston D.J. “Preparation of Polypropylene-Clay Nanocomposites by the Co-Intercalation of Modified Polypropylene and Short-Chain Amide Molecules.” *Journal of Applied Polymer Science*, 112 (2009): 320-334.

Teng C.-C., Ma C.-C. M., Huang Y.W., Yuen S.M., Weng C.-C., Chen C.-H, Su S.F.  
“Effect of MWCNT content on rheological and dynamic mechanical properties of  
multiwalled carbon nanotube/polypropylene composites.” *Composites: Part A*, 39 (2008):  
1869-1875.

Thostenson E. T., Li C., Chou T.W. “Nanocomposites in context.” *Composites Science  
and Technology*, 65 (2005): 491-516.

Zhang Q., Fu Q., Jiang L., Lei Y. “Preparation and properties of polypropylene  
montmorillonite layered nanocomposites.” *Polymer International*, 49 (2000): 1561-1564.

## Chapter 4

### THERMAL PROPERTIES OF xGNP-FILLED IMPP NANOCOMPOSITES

#### 4.1. Chapter Summary

The objective of this research is to investigate the effect of particle diameter, filler loading and coupling agent on the thermal behavior of impact modified polypropylene (IMPP) nanocomposites. xGnP-filled IMPP composites were manufactured via melt mixing with and without the addition of polypropylene-graft-maleic anhydride (PP-g-MA). The thermal behavior of the nanocomposites was investigated using differential scanning calorimetry (DSC) and thermogravimetric analysis (TGA). The DSC results indicated that the addition of xGnP slightly increased the melting temperature ( $T_m$ ) and increased the crystallization temperature ( $T_c$ ) of IMPP by 2 to 3 °C which is attributed to the heterogeneous nucleation of the xGnP. The TGA results indicated that the degradation temperature of IMPP shifts to a lower temperature with the addition of PP-g-MA, indicative of the poor thermal stability of PP-g-MA. However, the thermal stability of the composites increases with xGnP loading because of the high thermal stability of the xGnP and the hypothesized “tortuosity effect” that the graphite nanoplatelets was inhibiting diffusion of oxygen and volatile products throughout the composites during thermal decomposition.



## 4.2. Introduction

Over the past several decades, there has been great interest by both academia and industry in the development of new composite materials with high performance nano fillers. The goal of any new composite material development effort is to improve working properties and extend their range of applications (Giannelis 1996; Hussain et al. 2006; Paul and Robeson 2008). Incorporating nanoscale reinforcing fillers into polymer matrices is among the most promising approaches to achieve those goals. The resulting composites are known as polymer nanocomposites (PNCs). PNCs are one component of the broad field of nanotechnology research and show significantly improved mechanical and thermal properties at far lower reinforcement volume fractions when compared to conventional micro and macro composites (Giannelis 1996; Hussain et al. 2006; Pavlidou and Papaspyrides 2008).

The most frequently studied layered structural fillers for polymer resins are silicate or smectite nanoclays in platelet form because of their availability, low cost and reasonably well understood intercalation chemistry. Recently, the most commonly studied fibrous material is carbon nanotubes (CNTs) (Kim et al. 2010; Sherman 2004; Kalaitzidou 2006). Nanoclay reinforced PNCs do not possess electrical conductivity, photonic and dielectric properties. Therefore, there has been greatly increased interest in using other materials such as CNTs and graphite for multifunctional PNCs because of their superior thermal and electrical properties as well as their excellent mechanical properties (Kim et al. 2010; Kalaitzidou 2006; Chen et al. 2001; Fukushima 2003). While

CNTs have outstanding thermal, electrical and mechanical properties, they are very expensive (250-500 \$/lb), which is one of the most serious drawbacks in developing CNT-filled PNCs. The high cost can be linked to low yield and low production and purification rates commonly associated with all of the current CNT preparation processes (Sherman 2007; Kim and Drzal 2009a; Kumar et al. 2010). Similar to the structure of layered silicates, naturally abundant graphite is composed of one-atom-thick sheets of carbon. The carbon atoms are covalently bonded in a hexagonal arrangement within the individual sheet and these layers are bonded to each other by much weaker van der Waals forces (Kim et al. 2009b; Pan et al. 2000). As shown by Drzal et al., xGnP, which combines the layered structure and lower cost of clays with the superior thermal, mechanical and electrical properties of CNTs, can be an effective alternative to both CNTs and nanoclays by providing competitive functionality (Kim et al. 2010; Kim and Drzal 2009a; Kim et al. 2009b). Application of graphite in PNCs is a relatively new research field. Although there is growing publication activity in recent years, the number of reports (journal papers, patents and theses) is still modest when compared to those regarding nanoclays and CNTs.

A wide range of polymer resins, both thermoplastic and thermoset, have been investigated as matrices for PNCs (Giannelis 1996; Paul and Robeson 2008; Pavlidou and Papaspyrides 2008; Kalaitzidou 2006). Thermoplastic nanocomposites have received considerable interest in recent years due to their promise of improved performance in engineering and packaging applications (Gopakumar and Page 2004; Spoljaric et al. 2009). Polypropylene (PP) is among the most widely used thermoplastics because of its

low density, low production costs, design flexibility and recyclability (Spoljaric et al. 2009). PP is non polar and does not interact with chemically inert graphite. Therefore, producing graphite-reinforced PP nanocomposites is very difficult because of the lack of affinity between the two constituents. This issue can be overcome by adding a coupling agent such as propylene-graft-maleic anhydride (PP-g-MA) (Gopakumar and Page 2004; Spoljaric et al. 2009). According to a study by Page et al., XRD and SEM results indicate that the functionalization of PP by addition of PP-g-MA leads to an excellent dispersion of graphite, and improvement in flexural properties and impact strength of the material (Page and Gopakumar 2006). TEM images from this research previously provided in Chapter 2 directly illustrated improved dispersion using PP-g-MA. However, there is a lack of information related to the effect of coupling agents on thermal properties of graphite/PP composites in the literature.

The objective of this study was to investigate the influence of (1) particle diameter, (2) filler loading, and (3) coupling agent, on the thermal properties of xGnP-filled IMPP composites. All compounded materials were manufactured via melt mixing and were prepared over a filler loading levels ranging from 0 to 8 wt. % xGnP. The weight ratio of filler-to-coupling agent was held constant at 2:1 throughout this study. Thermal characterization was accomplished via differential scanning calorimetry (DSC) and thermogravimetric analysis (TGA).

### 4.3. Experimental Procedures

#### 4.3.1. Materials

The IMPP was supplied as polymer pellets by Polystrand Inc., USA. The IMPP had a density of  $0.900 \text{ g/cm}^3$  and melt flow index of 35 g/10 min. The xGnP fillers were supplied by XG Sciences Inc., USA. Three xGnP fillers in powder form were used as the reinforcement with different particle diameters 5, 15, and 25  $\mu\text{m}$ . Average platelet thickness ranges from about 5 to 15 nanometers. This translates into an average particle surface area ranging from about 60 to 150  $\text{m}^2/\text{g}$ . The bulk density of all three xGnP fillers is reported to be 0.18-0.25  $\text{g/cm}^3$ . Two different PP-g-MA were used as coupling agents, labeled for this study as SA9100 and WL9100, provided by Sigma-Aldrich Co., USA and West Lake Chemical Co., USA, respectively. Both coupling agents had a density of  $0.934 \text{ g/cm}^3$ , molecular weight of 9,100 by GPC, and acid number of 45-47. SA9100 and WL9100 coupling agents differed in that their maleic anhydride content was 8-10% and <0.7%, respectively. Materials used in this study are summarized in Table 4.1.

Table 4.1 Summary of materials used in current study.

Material/Supplier	Label	Density (g/cm <sup>3</sup> )	MA Content (%)	M <sub>w</sub>	Acid #
Impact Modified Polypropylene/ <i>Polystrand Inc.</i>	IMPP	0.900	---	---	---
Exfoliate Graphite Nanoplatelets 5μ/ <i>XG Sciences Inc.</i>	xGnP <sup>5</sup>	2	---	---	---
Exfoliate Graphite Nanoplatelets 15μ/ <i>XG Sciences Inc.</i>	xGnP <sup>15</sup>	2	---	---	---
Exfoliate Graphite Nanoplatelets 25μ/ <i>XG Sciences Inc.</i>	xGnP <sup>25</sup>	2	---	---	---
Polypropylene-g-Maleic Anhydride/ <i>Sigma-Aldrich Co.</i>	SA9100	0.934	8-10	9100	47
Polypropylene-g-Maleic Anhydride/ <i>West Lake Chemical Co.</i>	WL9100	0.934	< 0.7	9100	45

#### 4.3.2. Sample Preparation

The matrix polymer IMPP was mixed with the xGnP fillers. The compounding was carried out with a Brabender Prep-mixer® equipped with a mixing bowl. The basic processing parameters used in this study are summarized in Table 4.2. The temperature was set to 180 °C and mixing speed was set at 60 rpm. All composite formulations were prepared in 150 g batches and all constituents were added to the mixer simultaneously. Mixing was done for 20 minutes; this was an optimum processing time as determined from preliminary experiments.

Table 4.2 Basic operating parameters of the Brabender rheomixer.

Batch Size (g)	Temperature (°C)	RPM	Compounding Time (min)
150	180	60	20

All composite compounds were then granulated using a lab scale grinder. The designated labels and compositions of neat IMPP, neat coupling agents, IMPP/PP-g-MA blends and coupled compatibilized xGnP-filled materials are shown in Table 4.3.

Table 4.3 Designated labels and compositions of neat IMPP, neat coupling agents, IMPP/PP-g-MA blends and coupled xGnP-filled IMPP compounded materials discussed.

Study Label	Content Per Batch (g)					
	IMPP	SA9100	WL9100	xGnP <sup>5</sup>	xGnP <sup>15</sup>	xGnP <sup>25</sup>
IMPP	150	---	---	---	---	---
SA9100	---	150	---	---	---	---
WL9100	150	---	---	---	---	---
IMPP_SA9100_2%	147	3	---	---	---	---
IMPP_WL9100_2%	147	---	3	---	---	---
IMPP_xGnP5_4%	144	---	---	6	---	---
IMPP_xGnP15_4%	144	---	---	---	6	---
IMPP_xGnP25_4%	144	---	---	---	---	6
IMPP_SA9100_xGnP5_2%	145.5	1.5	---	3	---	---
IMPP_WL9100_xGnP5_2%	145.5	---	1.5	3	---	---
IMPP_WL9100_xGnP5_4%	141	---	3	6	---	---
IMPP_WL9100_xGnP5_6%	136.5	---	4.5	9	---	---
IMPP_WL9100_xGnP5_8%	132	---	6	12	---	---

### 4.3.3. Thermal Characterization

DSC analysis was carried out using a Perkin Elmer Instrument Pyris DSC with a sample weight of 8 to 10 mg. All samples were held at 25 °C for 5 min, heated at a rate of 10 °C/min to 200 °C, subsequently held for 5 min to erase thermal history, then cooled at a rate of 10 °C/min to -50 °C, subsequently held for 5 min and heated again at a rate of 10 °C/min to 200 °C under a nitrogen atmosphere. Melting temperature ( $T_m$ ) was determined from the second scan. The  $T_m$  was taken as the peak temperature of the melting endotherm. The specimens' degree of crystallinity ( $X_c$ ) was calculated according to Equation 4.1.

$$X_c (\%) = (\Delta H_m \times 100) / (\Delta H_f \times \omega) \quad \text{Equation 4.1}$$

Where  $\Delta H_m$  is the heat of fusion of the specimen,  $\Delta H_f$  is the heat of fusion for 100% crystalline PP ( $\Delta H_f = 207.1$  J/g) and  $\omega$  is the mass fraction of IMPP in the specimen (Wunderlich 1990). At least three randomly picked specimens from ground samples were tested for each composition, and the results are presented as an average for tested samples.

TGA measurements were completed using a Mettler Toledo analyzer, model TGA/SDTA851, on samples of about 10 mg. Each sample was scanned over a temperature range from room temperature to 600 °C at a heating rate of 10 °C/min under nitrogen with a flow rate equal to 20 ml/min to avoid sample oxidation. Five randomly

picked specimens from ground samples were used for the TGA measurements, and the results are presented as an average for tested samples.

## 4.4. Results and Discussion

### 4.4.1. Differential Scanning Calorimetry (DSC)

The thermal properties of chosen compounded composites were characterized via the DSC testing methods described in Section 4.3.3. Experimental values of  $T_m$ ,  $T_c$ ,  $X_c$  and corresponding  $\Delta H_m$  and  $\Delta H_c$  for all materials discussed in this section are provided in Table 4.4.

Table 4.4 DSC summary of  $T_m$ ,  $T_c$ ,  $\Delta H_m$ ,  $\Delta H_c$  and  $X_c$  for neat IMPP, neat coupling agents, IMPP/PP-g-MA blends and xGnP-filled IMPP composites.

Sample Code	$T_m$ (°C)	$T_c$ (°C)	$\Delta H_m$ (J/g)	$\Delta H_c$ (J/g)	$X_c$ (%)
IMPP	164.3 (0.7)	122.6 (0.4)	61.0 (4.0)	-91.5 (4.6)	29.5 (1.9)
SA9100	156.0 (0.9)	105.0 (1.9)	62.6 (12.1)	-99.7 (14.9)	30.2 (5.9)
WL9100	154.0 (1.2)	104.0 (1.9)	67.3 (1.2)	-109.1 (5.1)	32.5 (0.6)
IMPP_SA9100_2%	163.2 (0.6)	116.1 (1.3)	54.4 (1.6)	-84.1 (0.8)	26.3 (0.8)
IMPP_WL9100_2%	163.9 (0.6)	116.8 (1.0)	58.2 (6.0)	-88.0 (3.4)	28.1 (2.9)
IMPP_xGnP5_4%	165.5 (0.3)	126.5 (1.4)	56.3 (3.5)	-84.2 (0.6)	28.3 (1.7)
IMPP_xGnP15_4%	165.5 (1.5)	125.8 (2.3)	59.3 (2.5)	-86.0 (1.2)	29.8 (1.3)
IMPP_xGnP25_4%	165.0 (0.2)	126.1 (0.2)	57.1 (2.0)	-86.2 (0.5)	28.7 (1.0)
IMPP_SA9100_xGnP5_4%	164.8 (0.6)	124.6 (0.4)	55.0 (3.5)	-87.1 (6.2)	27.7 (1.7)
IMPP_WL9100_xGnP5_2%	165.9 (0.0)	124.3 (0.2)	61.5 (1.9)	-84.0 (2.8)	30.3 (0.9)
IMPP_WL9100_xGnP5_4%	165.2 (0.5)	124.9 (0.3)	56.7 (2.4)	-85.1 (3.3)	28.5 (1.2)
IMPP_WL9100_xGnP5_6%	165.3 (1.0)	125.1 (0.4)	59.1 (1.9)	-81.9 (2.9)	30.3 (1.0)
IMPP_WL9100_xGnP5_8%	165.2 (0.9)	125.6 (0.3)	55.7 (1.5)	-78.7 (1.2)	29.2 (0.8)

Parenthesis indicates standard deviation.



The effect of xGnP particle sizes (5, 15 and 25  $\mu\text{m}$ ) on DSC behavior of composites was investigated via a comparison of neat IMPP against three different IMPP composites with filler loading equal to 4 wt. % xGnP<sup>5</sup>, xGnP<sup>15</sup> and xGnP<sup>25</sup>, respectively. Figure 4.1 is provided to illustrate non-isothermal crystallization and melting curves of neat IMPP as well as 5, 15 and 25  $\mu\text{m}$  xGnP-filled IMPP composites. Experimental values of  $T_m$ ,  $T_c$ ,  $\Delta H_m$ ,  $\Delta H_c$  and  $X_c$  for these composites are extremely close and what little change is seen does not appear to follow any specific trend. From this study, it was evident that xGnP particle size does not have a significant effect on the  $T_m$ ,  $T_c$ ,  $X_c$ ,  $\Delta H_m$  and  $\Delta H_c$  of xGnP-filled IMPP composites.

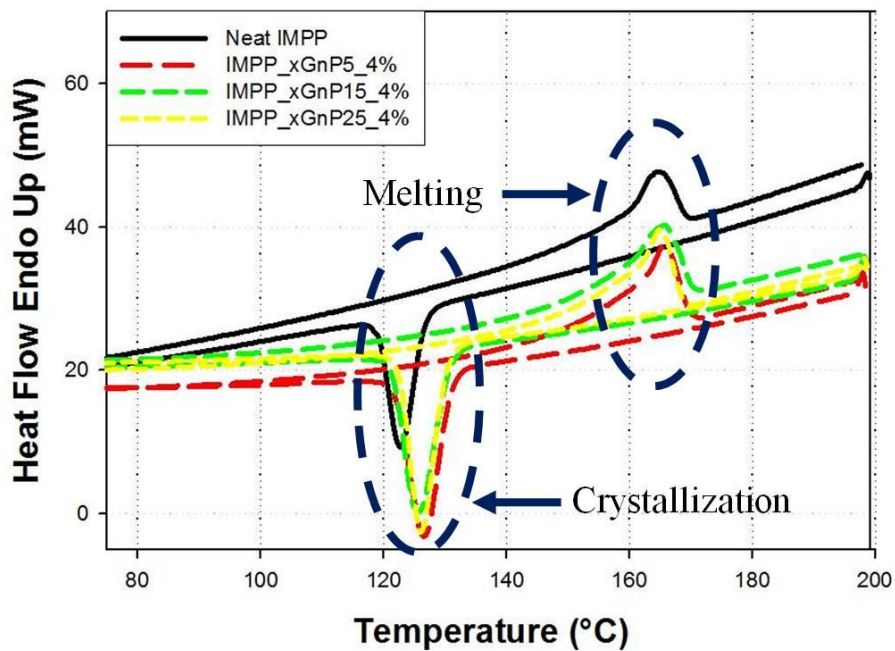


Figure 4.1 Effect of particle size on DSC behavior of 96:4 wt./wt. xGnP-filled IMPP composites.

The effect of filler loading on DSC behavior of composites was investigated via a comparison of neat IMPP against IMPP\_WL9100\_xGnP<sup>5</sup> composites with filler loading equal to 2, 4, 6 and 8 wt. % xGnP. Figure 4.2 illustrates non-isothermal crystallization and melting curves of neat IMPP and IMPP\_WL9100\_xGnP<sup>5</sup> composites. This plot shows that incorporation of xGnP increases the crystallization temperature ( $T_c$ ) of IMPP by about 2 to 3 °C attributed to the heterogeneous nucleation of xGnP. However, the  $T_c$  of IMPP changed only slightly with increasing xGnP content. Many other nanoparticles (carbon nanoparticles, nano-CaCO<sub>3</sub>) were also found to have same effect on the crystallization of PP homopolymer in the literature (Causin et al. 2007; Reyes-de Vaaben et al. 2008; Wang et al. 2010). The melting points of IMPP\_WL9100\_xGnP<sup>5</sup> composites are all between 165 °C and 166 °C. This shows that the addition of xGnP causes a slight increase in the melting temperature of IMPP, which indicates the formation of a more perfectly crystalline structure of IMPP (Wang et al. 2010). The degree of crystallinity of composites was calculated using the heat of fusion determined from DSC measurements ( $\Delta H_m$ ) and the one corresponding to a 100% crystalline PP ( $\Delta H_f$ ) reported by Wunderlich in 1990. Increasing the xGnP content does not result in a significant change in percent crystallinity. However, increasing the xGnP content in the IMPP results in smaller  $\Delta H_m$  and  $\Delta H_c$  values. Similar phenomena were also observed for the addition of other nanoparticles in PP homopolymer composites (Wang et al. 2010; Chen et al. 2007).

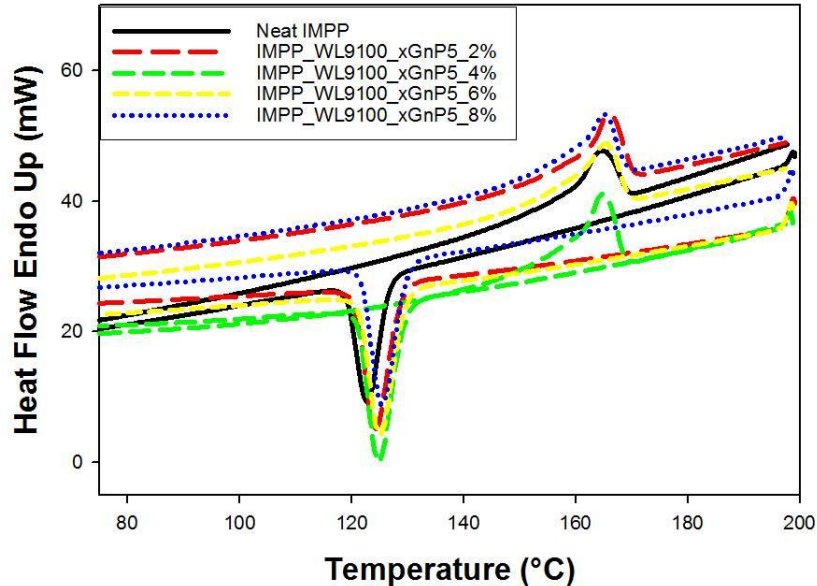


Figure 4.2 Effect of filler loading on DSC behavior of xGnP<sup>5</sup>-filled IMPP composites manufactured with the WL9100 coupling agent.

Two PP-g-MA coupling agents (SA9100 and WL9100) with the same molecular weight, similar acid number and different maleic anhydride content were used to modify the xGnP-filled IMPP composites. Figure 4.3 is provided to illustrate the non-isothermal crystallization and melting curves of neat IMPP, neat coupling agents, IMPP/PP-g-MA blends and coupled xGnP<sup>5</sup>-filled IMPP composites at 2 and 4 wt. % xGnP. It is reported that PP-g-MA acts as a nucleation agent that can increase crystallization parameters of PP homopolymer (Zhang et al. 1996; Revilla-Diaz et al. 2007). Clearly, the experimentally determined values of  $\Delta H_m$ ,  $\Delta H_c$  and  $X_c$  of the two coupling agents are higher than neat IMPP and IMPP/PP-g-MA blends. However, the  $T_m$  and  $T_c$  are much lower than neat IMPP. Interestingly,  $T_m$  and  $T_c$  are increased in xGnP-filled IMPP composites manufactured with a coupling agent. From these results, it can be concluded that the

addition of a coupling agent acts as a nucleation agent and therefore, the  $T_c$  of the coupled xGnP-filled IMPP composites is increased when compared with neat IMPP.

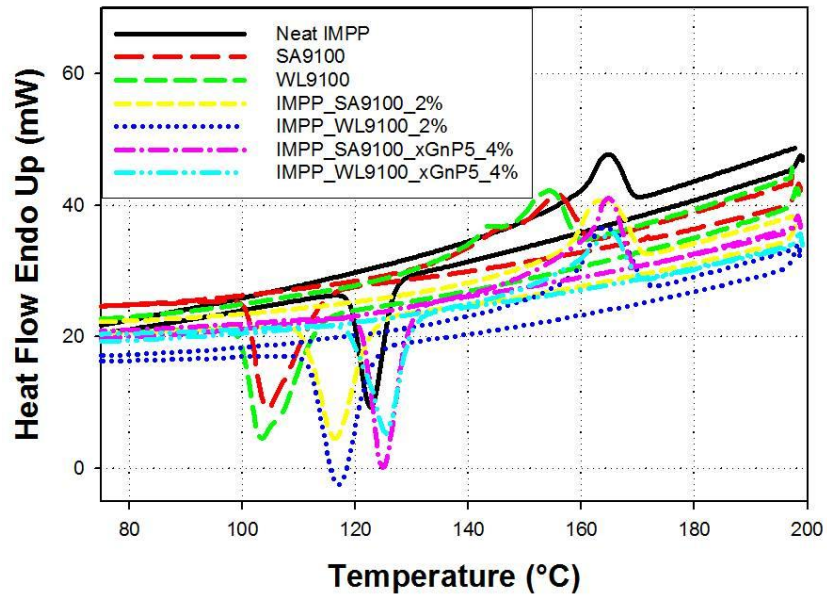


Figure 4.3 Effect of coupling agents on DSC behavior of neat IMPP and xGnP<sup>5</sup>-filled IMPP composites.

#### 4.4.2. Thermogravimetric analysis (TGA)

The degradation behaviors of chosen compounded composites were characterized via TGA testing methods described in Section 4.3.3. Experimental values of peak degradation temperature, weight loss (%) at peak degradation temperature and residual mass after 600 °C for all materials discussed in this section are given in Table 4.5.

Table 4.5 Thermogravimetric data for neat IMPP, neat coupling agents, IMPP/PP-g-MA blends and xGnP-filled IMPP composites analyzed from ambient temperature to 600 °C.

Sample Code	DTGA Temp. (°C)	Weight Loss (%)	Residual Mass (%)
IMPP	459.9 (1.3)	63.0 (3.1)	1.6 (0.1)
SA9100	458.3 (1.1)	69.8 (1.9)	4.0 (0.4)
WL9100	453.8 (1.9)	65.3 (2.7)	4.0 (0.6)
IMPP_SA9100_2%	458.9 (0.8)	74.0 (5.5)	2.3 (0.4)
IMPP_WL9100_2%	461.1 (0.9)	68.8 (2.4)	2.0 (0.1)
IMPP_xGnP5_4%	463.7 (0.3)	58.9 (0.8)	5.5 (0.1)
IMPP_xGnP15_4%	463.9 (0.7)	60.2 (1.2)	5.4 (0.3)
IMPP_xGnP25_4%	462.5 (0.6)	55.9 (1.0)	5.0 (0.3)
IMPP_SA9100_xGnP5_4%	464.8 (0.9)	63.8 (3.0)	5.1 (1.4)
IMPP_WL9100_xGnP5_2%	461.2 (1.0)	60.2 (2.5)	4.3 (0.6)
IMPP_WL9100_xGnP5_4%	462.6 (0.2)	55.4 (1.2)	6.1 (0.3)
IMPP_WL9100_xGnP5_6%	467.2 (0.4)	58.1 (1.1)	7.7 (0.3)
IMPP_WL9100_xGnP5_8%	469.1 (0.1)	58.2 (1.1)	10.0 (0.2)

The effect of xGnP particle sizes (5, 15 and 25  $\mu\text{m}$ ) on the degradation behavior of composites was investigated via comparison of neat IMPP against three different IMPP composites with filler loading equal to 4 wt. % xGnP<sup>5</sup>, xGnP<sup>15</sup> and xGnP<sup>25</sup>, respectively. Figure 4.4 is provided to illustrate the TGA and DTGA curves of neat IMPP as well as 5, 15 and 25  $\mu\text{m}$  xGnP-filled composites. All composites degraded in a similar manner (single stage), regardless of the particle size used. From this study, it was evident that xGnP particle size did not have a significant effect on the degradation behavior of xGnP-filled IMPP composites. A similar behavior was reported for wood flour/ethylene vinyl acetate composites (Dikobe and Luyt 2006).

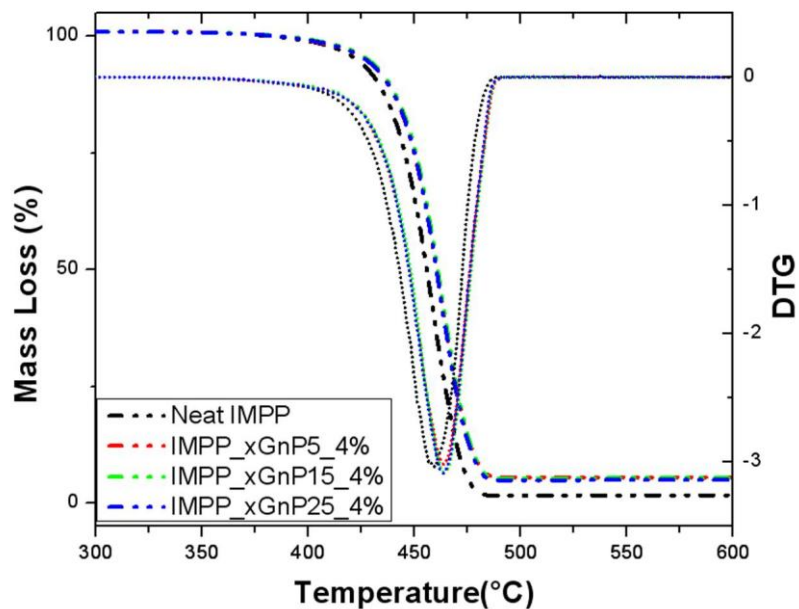


Figure 4.4 Effect of particle size on the TGA behavior of 96:4 wt./wt. xGnP-filled IMPP composites.

The temperature at 10% weight loss ( $T_{10}$ ) and the temperature at 50% weight loss ( $T_{50}$ ) for neat IMPP and 5 $\mu$ m, 15 $\mu$ m and 25 $\mu$ m xGnP-filled composites are shown in Figure 4.5. Both  $T_{10}$  and  $T_{50}$  values increased with the addition of xGnP. However, there was not any significant difference among particle sizes.

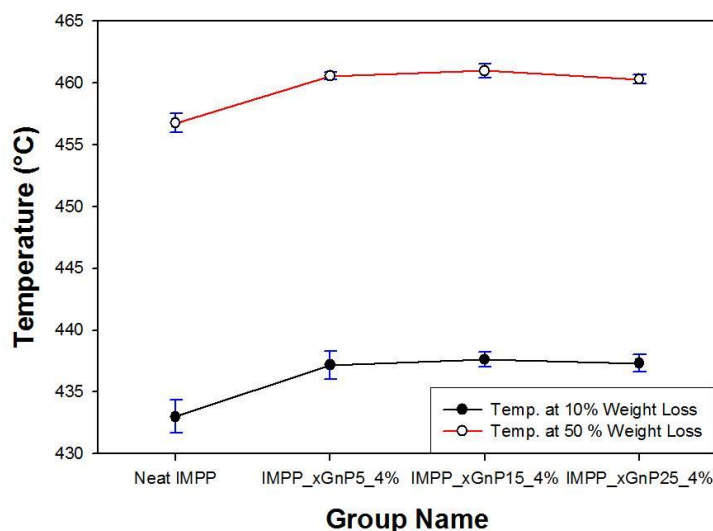


Figure 4.5 Effect of particle size on the TGA temperatures at 10% and 50% weight loss of 96:4 wt./wt. xGnP-filled IMPP composites.

The effect of filler loading on the degradation behavior of composites was investigated via a comparison of neat IMPP against IMPP\_WL9100\_xGnP<sup>5</sup> composites with filler loading equal to 2, 4, 6 and 8 wt. % xGnP. Figure 4.6 is provided to illustrate the TGA and DTGA curves for neat IMPP and IMPP\_WL9100\_xGnP<sup>5</sup> composites. The degradation temperatures of neat IMPP and composites are very similar. However, the onset temperature of rapid thermal degradation was shown to increase with xGnP loading. The IMPP exhibited single stage degradation with a peak at 460 °C. The xGnP-filled IMPP composites also show single stage degradation peak in the range of 461 to 469 °C. Furthermore, the thermal stability of the composites above 450 °C and the final ash content increased slightly as a function of xGnP loading. The final ash content consistently increased from around 1.6 % to 10% for the 8 wt. % xGnP addition. TGA results show that the thermal stability of the xGnP-filled IMPP composites is improved

compared to that of neat IMPP. It is thought that the enhanced thermal stability comes from the more thermally stable graphite as well as the tortuosity effect of the graphite nanoplatelets hampering the diffusion of oxygen and volatile products throughout the composite materials during thermal decomposition (Kim et al. 2010).

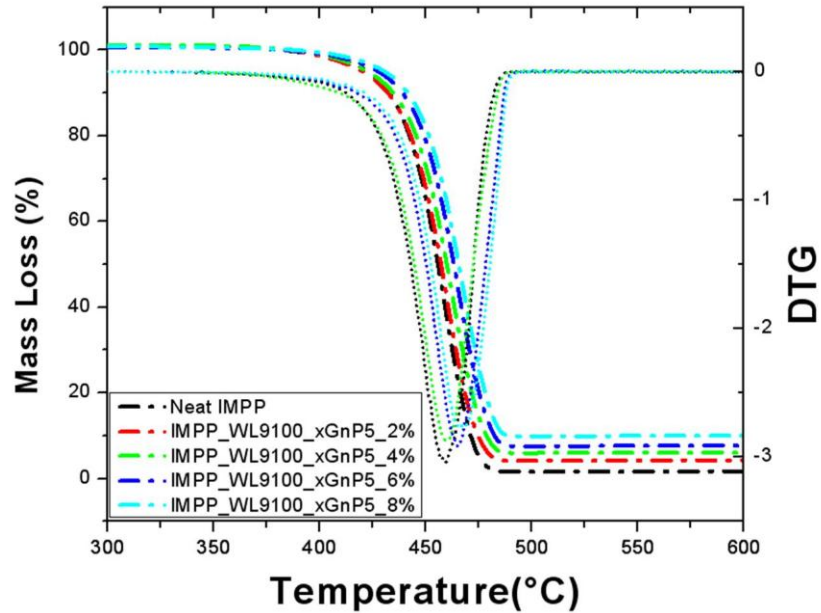


Figure 4.6 Effect of filler loading on TGA behavior of xGnP<sup>5</sup>-filled IMPP composites manufactured with the WL9100 coupling agents.

Experimental values of  $T_{10}$  and  $T_{50}$  for neat IMPP and IMPP\_WL9100\_xGnP<sup>5</sup> composites are shown in Figure 4.7. Both  $T_{10}$  and  $T_{50}$  increased monotonically from neat IMPP to the 8 wt. % xGnP addition.



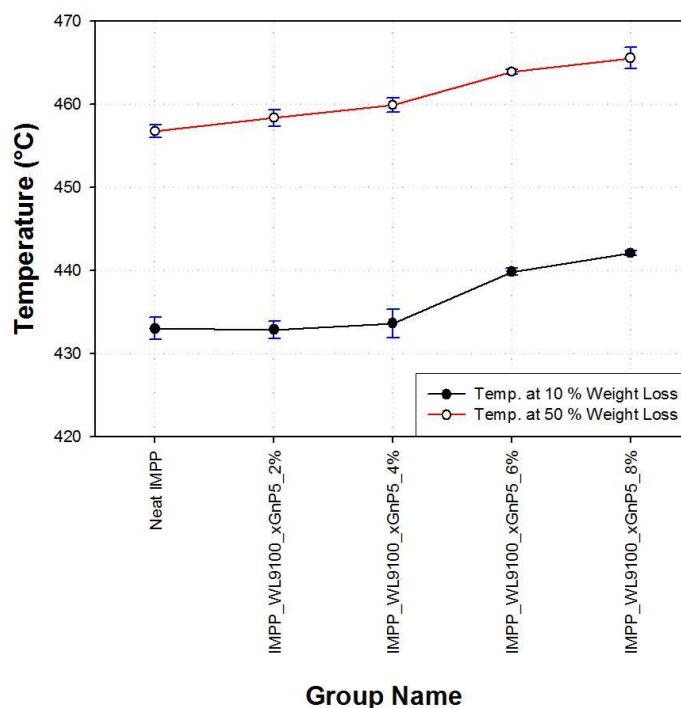


Figure 4.7 Effect of filler loading on TGA temperature at 10% and 50% weight loss of IMPP/xGnP<sup>5</sup> composites manufactured with the WL9100 coupling agent.

Figure 4.8 is provided to illustrate the TGA and DTGA curves of neat IMPP, neat coupling agents, IMPP/PP-g-MA blends and coupled xGnP<sup>5</sup>-filled IMPP composites at 4 wt. % xGnP. Both neat IMPP and IMPP/PP-g-MA blends show a single stage of degradation during the thermal degradation process. Neat IMPP begins to decompose at about 400 °C and reaches equilibrium residual mass at temperatures around 480 °C, with little residue remaining. The degradation temperature of IMPP shifts to a lower temperature in the presence of PP-g-MA, indicative of the poor thermal stability of PP-g-MA (Shen et al. 2009).

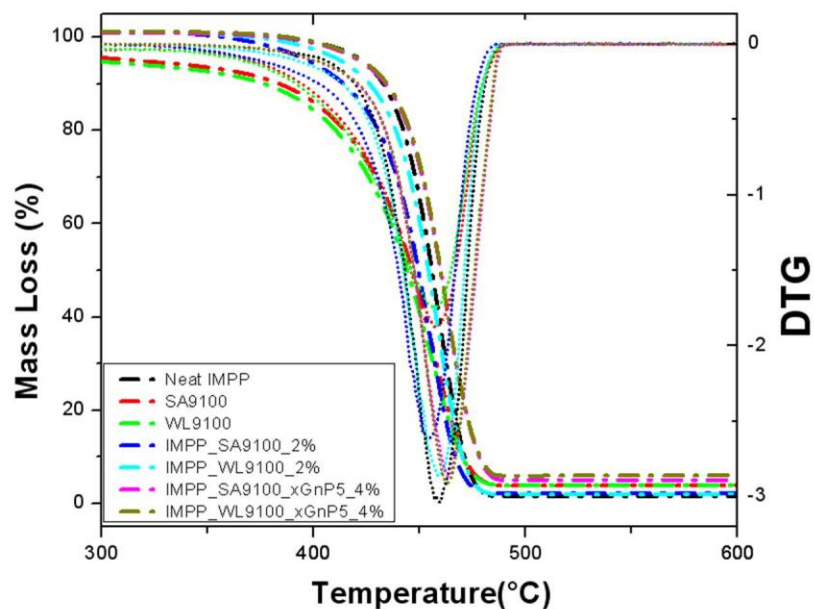


Figure 4.8 Effect of coupling agents on the TGA and DTG behavior of neat IMPP and xGnP<sup>5</sup>-filled IMPP composites.

Experimental values of  $T_{10}$  and  $T_{50}$  for IMPP, compatibilizers, IMPP/PP-g-MA blends and coupled xGnP<sup>5</sup>-filled composites at 4 wt. % xGnP are shown in Figure 4.9. Both  $T_{10}$  and  $T_{50}$  values for the PP-g-MA and IMPP/PP-g-MA blends decreased compared to neat IMPP composites. However, coupled xGnP-filled IMPP composites show improved  $T_{10}$  and  $T_{50}$  values compared to neat IMPP.

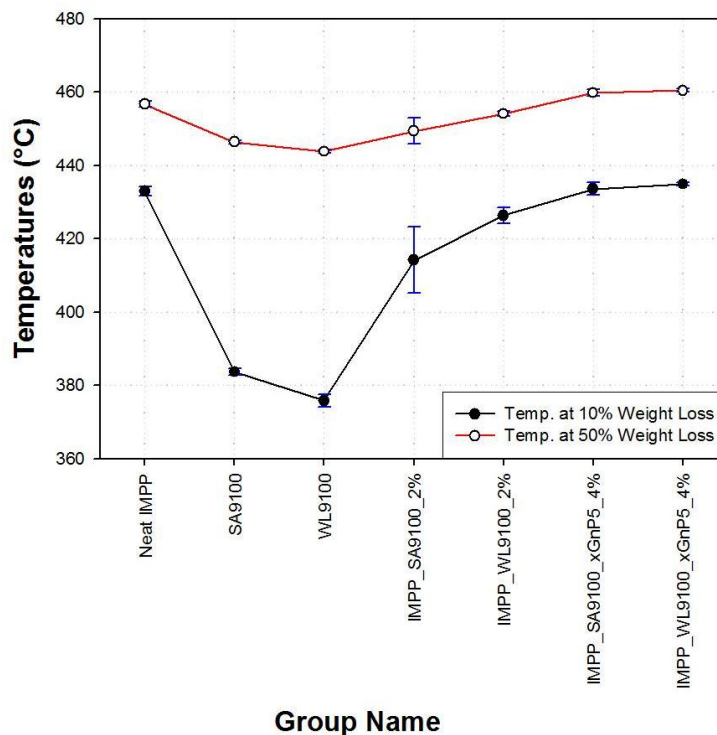


Figure 4.9 Effect of coupling agents on TGA temperature at 10% and 50% weight loss of neat IMPP and xGnP<sup>5</sup>-filled IMPP composites.

#### 4.5. Conclusions

xGnP-filled IMPP composites were prepared via melt compounding with and without the addition of a coupling agent (PP-g-MA). Thermal characterization techniques yielded conclusions in understanding the influence of (1) particle diameter, (2) filler loading, and (3) coupling agent, on the thermal behavior of xGnP-reinforced IMPP composites.

Particle diameter had no significant effect on the melting ( $T_m$ ) and crystallization ( $T_c$ ) temperatures as well as  $\Delta H_m$  and  $\Delta H_c$  of the composites. The addition of xGnP

caused the  $T_m$  to increase slightly, indicative of the formation of a more crystalline structure of IMPP, and  $T_c$  increased 2 to 3 °C, caused by heterogeneous nucleation of the xGnP. With increased filler loading  $X_c$  did not change significantly, however  $\Delta H_m$  and  $\Delta H_c$  of the composites decreased. Experimental results showed that PP-g-MA have much lower  $T_m$  and  $T_c$  and much higher  $\Delta H_m$ ,  $\Delta H_c$ , and  $X_c$  compared to neat IMPP and IMPP/PP-g-MA blends. However, the  $T_m$  and  $T_c$  increased significantly in xGnP-filled IMPP composites made with a coupling agent. Addition of a PP-g-MA was determined to act as a nucleating agent in the composites.

All materials investigated in this study resulted in similar single stage thermal degradation behavior. Particle diameter had no significant effect on degradation behavior of xGnP-filled IMPP composites and was illustrated adequately with similar  $T_{10}$  and  $T_{50}$  values for 5, 15 and 25  $\mu\text{m}$  xGnP-filled IMPP composites. The onset temperature of rapid degradation, thermal stability of the composites above 450 °C, and residual ash content increased at higher filler loading.  $T_{10}$  and  $T_{50}$  values increased monotonically from neat IMPP to coupled IMPP with 8 wt. % xGnP. The increase in thermal stability is believed to originate from the more thermally stable graphite and the “tortuosity effect” of the graphite nanoplatelets, which inhibit the diffusion of oxygen and volatile products throughout the composites during thermal decomposition. Interestingly, xGnP-filled IMPP composites made with a coupling agent exhibited improved thermal stability compared to neat IMPP, while the addition of PP-g-MA in IMPP/PP-g-MA blends caused the degradation temperature to decrease compared to neat IMPP.

#### 4.6. References

Causin V., Marega C., Saini R., Marigo A. & Ferrara G. “Crystallization behavior of isotactic polypropylene based nanocomposites.” *Journal of Thermal Analysis and Calorimetry*, 90 (3) (2007): 849-857.

Chen G.-H., Wu D.-J., Weng W.-G. & Yan W.-L. “Preparation of Polymer/Graphite Conducting Nanocomposite by Intercalation Polymerization.” *Journal of Applied Polymer Science*, 82 (10) (2001): 2506–2513.

Chen M., Wan C., Shou W., Zhang Y., Zhang Y. & Zhang J. “Effects of Interfacial Adhesion on Properties of Polypropylene/Wollastonite Composites.” *Journal of Applied Polymer Science*, 107 (3) (2007): 1718–1723.

Dikobe D.G. & Luyt A.S. “Effect of Filler Content and Size on the Properties of Ethylene Vinyl Acetate Copolymer–Wood Fiber Composites.” *Journal of Applied Polymer Science*, 103 (6) (2006): 3645-3654.

Fukushima, Hiroyuki. *Graphite Nanoreinforcements in polymer composites*. PhD Dissertation, East Lansing, MI, USA: Michigan State University (2003).

Giannelis, Emmanuel P. “Polymer Layered Silicate Nanocomposites.” *Advanced Materials*, 8 (1) (1996): 29-35.

Gopakumar T.G. & Page D.J.Y.S. "Polypropylene/Graphite Nanocomposites by Thermo-Kinetic Mixing." *Polymer Engineering & Science*, 44 (6) (2004): 1162-1169.

Hussain F., Hojjati M., Okamoto M. and Gorga R.E. "Review article: Polymer-matrix Nanocomposites, Processing, Manufacturing, and Application: An Overview." *Journal of Composite Materials*, 40 (17) (2006): 1511-1575.

Kalaitzidou, Kyriaki. Exfoliated Graphite Nanoplatelets as Nanoreinforcement for Multifunctional Polypropylene Nanocomposites. PhD Dissertation, East Lansing, MI, USA: Michigan State University (2006).

Kim S. & Drzal L. T. "High latent heat storage and high thermal conductive phase change materials using exfoliated graphite nanoplatelets." *Solar Energy Materials & Solar Cells*, 93 (2009a): 136-142.

Kim S., Do I. & Drzal L.T. "Multifunctional Exfoliated Graphite Nanoplatelets/LLDPE Nanocomposites Fabricated By Solution Compounding Method And Various Screw Rotating Systems." *Macromolecular Materials and Engineering*, 294 (3) (2009b): 196-205.

Kim S., Do I. & Drzal L.T. "Thermal Stability and Dynamic Mechanical Behavior of Exfoliated Graphite Nanoplatelets LLDPE Nanocomposites." *Polymer composites*, 31 (5) (2010): 755-761.

Kumar S., Sun L.L., Caceres S., Li B., Wood W., Pereguni A., Maguire R.G. & Zhong W.H. “Dynamic synergy of graphitic nanoplatelets and multi-walled carbon nanotubes in polyetherimide nanocomposites.” *Nanotechnology*, 21 (10) (2010): 105702 (9pp).

Page D.J.Y.S. & Gopakumar T.G. “Properties and Crystallization of Maleated Polypropylene/Graphite Flake Nanocomposites.” *Polymer Journal*, 38 (9) (2006): 920-929.

Pan Y.-X., Yu Z.-Z., Ou Y.-C. & Hu G.-H. “A New Process of Fabricating Electrically Conducting Nylon 6/Graphite Nanocomposites via Intercalation Polymerization.” *Journal of Polymer Science: Part B: Polymer Physics*, 38 (12) (2000): 1626–1633.

Paul D.R. & Robeson L.M. “Polymer nanotechnology: Nanocomposites.” *Polymer*, 49 (15) (2008): 3187-3204.

Pavlidou S. & Papispyrides C.D. “A review on polymer-layered silicate nanocomposites.” *Progress in Polymer Science*, 33 (12) (2008): 1119–1198.

Revilla-Diaz R., Sanchez-Valdes S., Lopez-Campos F., Medellin-Rodriguez F.J. & Lopez-Quintanilla M.L. “Comparative Characterization of PP Nano and Microcomposites by In-Mold Shrinkage Measurements and Structural Characteristics.” *Macromolecular Materials and Engineering*, 292 (6) (2007): 762–768.

Reyes-de Vaaben S., Aguilar A., Avalos F. & Ramos-de Valle LF. "Carbon nanoparticles as effective nucleating agents for polypropylene." *Journal of Thermal Analysis and Calorimetry*, 93 (3) (2008): 947-952.

Shen H., Wang Y. & Mai K. "Effect of compatibilizers on thermal stability and mechanical properties of magnesium hydroxide filled polypropylene composites." *Thermochimica Acta* , 483 (1-2) (2009): 36-40.

Sherman, Lilli Manolis. "Carbon nanotubes: Lots of potential-If the price is right" *Plastic Technology*, 53 (2007): 68-73.

Sherman, Lilli Manolis. "Chasing Nanocomposites." *Plastics Technology*, 50 (11) (2004): 56-61.

Spoljaric S., Genovese A. & Shank R.A. "Polypropylene–microcrystalline cellulose composites with enhanced compatibility and properties." *Composites Part A: Applied Science and Manufacturing*, 40 (6-7) (2009): 791-799.

Wang Y., Shen H., Li G. & Mai K. "Crystallization and melting behavior of PP/nano-CaCO<sub>3</sub> composites with different interfacial interaction." *Journal of thermal Analysis and Calorimetry*, 99 (2) (2010): 399-407.

Wunderlich, Bernhard. *Thermal Analysis*, 609-610. New York: Academic Press, 1990.



Zhang X., Yin Z., Li L. & Yin J. "Grafting of glycidyl methacrylate onto ethylene-propylene copolymer: Preparation and characterization." *Journal of Applied Polymer Science*, 61 (13) (1996): 2253–2257.

## Chapter 5

### CONCLUSIONS AND RECOMMENDATIONS

#### 5.1. Conclusions

The main objective of this research was to fabricate well dispersed xGnP-filled IMPP nanocomposites via melt compounding followed by injection molding. Furthermore, the aim was to characterize the effect of particle diameter, filler loading and the addition of coupling agents on the mechanical, rheological and thermal properties of xGnP-filled IMPP nanocomposites. The following results were determined over the course of this research:

- 1) The smallest diameter filler investigated in this study (5 $\mu\text{m}$ ) performed the best in terms of flexural and tensile mechanical properties of xGnP-filled IMPP composites. It is suspected that incorporation of xGnP with an average particle diameter smaller than 5  $\mu\text{m}$  would result in largely increased improvements in flexural and tensile properties.
- 2) Tensile and flexural moduli and strengths both increased with xGnP filler loading for compatibilized composites. Elongation at break was greatly deteriorated with as little as 2 wt. % xGnP with and without coupling agent.

- 3) The addition of coupling agent has been proven to dramatically enhance dispersion within xGnP filled IMPP composites. Enhanced dispersion has been proven indirectly via mechanical testing and Halpin-Tsai modeling comparisons as well as directly via TEM imaging. However, the addition of coupling agent amplifies the degradation of elongation at break because of the improved adhesion between the filler and the matrix.
- 4) The smallest diameter filler investigated in this study (5 $\mu$ m) performed the best in terms of impact properties of xGnP-filled IMPP composites.
- 5) Impact properties were greatly deteriorated with as little as 2 wt. % xGnP with and without coupling agent.
- 6) The addition of coupling agent, similarly to the elongation at break discussion, amplifies the degradation of impact properties because of the improved adhesion between the filler and the matrix.
- 7) A correlation study to determine a relationship between impact properties and MFI was explored and showed impact properties to increase with MFI linearly. Experimental MFI results for the well dispersed IMPP\_WL9100\_xGnP<sup>5</sup> nanocomposites were plotted versus filler loading level. Using these relationships it was determined necessary for filler content to be below 0.044 and 0.315 wt. % to improve unnotched and notched impact strengths, respectively.

- 8) Particle diameter had no significant effect on the melting ( $T_m$ ) and crystallization ( $T_c$ ) temperatures as well as  $\Delta H_m$  and  $\Delta H_c$  of the composites.
- 9) The addition of xGnP caused the  $T_m$  to increase slightly which indicates the formation of a more crystalline structure of IMPP, and  $T_c$  increased 2 to 3 °C, caused by heterogeneous nucleation of the xGnP. With increased filler loading  $X_c$  did not change significantly, however  $\Delta H_m$  and  $\Delta H_c$  of the composites decreased.
- 10) The coupling agent (PP-g-MA) had much lower  $T_m$  and  $T_c$  and much higher  $\Delta H_m$ ,  $\Delta H_c$ , and  $X_c$  compared to neat IMPP and IMPP/PP-g-MA blends. However, the  $T_m$  and  $T_c$  increased significantly in xGnP-filled IMPP composites made with a coupling agent. Addition of a PP-g-MA was determined to act as a nucleating agent in the composites.
- 11) All materials investigated in this study resulted in similar single stage thermal degradation behavior. Particle diameter had no significant effect on degradation behavior of xGnP-filled IMPP composites and was illustrated with similar  $T_{10}$  and  $T_{50}$  values for xGnP<sup>5</sup>, xGnP<sup>15</sup> and xGnP<sup>25</sup> reinforced composites.
- 12) The thermal stability of the composites above 450 °C, and residual ash content increased at higher filler loading.  $T_{10}$  and  $T_{50}$  values increased monotonically from neat IMPP to coupled IMPP with 8 wt. % xGnP. The increase in thermal stability is believed to originate from the more thermally stable graphite and the tortuosity

effect of the graphite nanoplatelets, which inhibit the diffusion of oxygen and volatile products throughout the composites during thermal decomposition.

- 13) Interestingly, xGnP-filled IMPP composites made with a coupling agent exhibited improved thermal stability compared to neat IMPP, while the addition of PP-g-MA in IMPP/PP-g-MA blends caused the degradation temperature to decrease compared to neat IMPP.

## 5.2. Recommendations for Future Work

The ductility and energy absorption capabilities of xGnP-filled IMPP were much lower than the neat IMPP at the filler loading levels investigated. However, through insightful analysis there remains a potential for future work in nano-reinforced IMPP:

- 1) The filler loading domain must be determined for which the MFI vs. filler loading and the impact strength vs. MFI relationships remain valid. xGnP<sup>5</sup>-filled IMPP with the addition of WL9100 coupling agent should be fabricated at low filler loading levels ranging from 0.01 to 0.5 wt. % and tested for experimental flexural and tensile behavior, MFI and impact results.
- 2) The effect of nanoparticle geometry should be investigated. Nanoscale spheres, rods, tubes or whiskers may change the stress concentrations around the filler

inclusions and result in different behavior. Perhaps different particle morphology will allow the elastomeric phase present in the IMPP to still induce the three conventional toughening mechanisms (inelastic void growth, shear yielding or crazing and cavitation of rubber particles).

- 3) Different compatibilization methods should be investigated. Potential approaches are surface modification of xGnP powder as well as modification of the matrix polymer (IMPP).
- 4) Viscoelastic properties and long-term behavior of xGnP-filled IMPP nanocomposites should be investigated using dynamic mechanical analysis (DMA).
- 5) Experiments should be conducted to determine the effect of strain rate on the performance of PNCs.
- 6) Electrical conductivity and conversely electrical resistance of xGnP-filled IMPP should be investigated. Graphene reinforced polymers are being considered throughout R&D efforts as multifunctional composites producing both superior mechanical and thermal properties as well as creating a conductive material out of what is traditionally an insulator.

7) Nano-reinforcement of engineering thermoplastics should be investigated. There is a great commercial potential for starting with the superior properties of engineering thermoplastics and working to improve these properties using nano material fillers.

## BIBLIOGRAPHY

Ahmad S.H., Rasid R., Surip S.N., Anuar H., Czigany T., Abdul Razak S.B. "Mechanical and Fracture Toughness Behavior of TPNR Nanocomposites." *Journal of Composite Materials*, 41(17) (2007): 2147-2159.

Balasuriya P.W., Ye L., Mai Y.-W. "Mechanical properties of wood flake-polyethylene composites. Part I: effects of processing methods and matrix melt flow behaviour." *Composites: Part A*, 32 (2001): 619-629.

Bera J. and Kale D. D. "Properties of Polypropylene Filled with Chemically Treated Rice Husk." *Journal of Applied Polymer Science*, 82 (2001): 2506-2513.

Brouwer, Derk. "Potential for exposure to (manufactured) nano-objects (particles) in workplaces." *Proceedings of NSF Summer Institute on Nanomechanics, Nanomaterials, and Micro/Nanomanufacturing*, University of Massachusetts Lowell (2009).

Cantwell W.J. and Morton J. "The impact resistance of composite material - a review." *Composites*, 22(5) (1991): 347-362.

Causin V., Marega C., Saini R., Marigo A. & Ferrara G. "Crystallization behavior of isotactic polypropylene based nanocomposites." *Journal of Thermal Analysis and Calorimetry*, 90 (3) (2007): 849-857.

Chen G.H., Wu D.J., Weng W.G., Yan W.L. "Preparation of Polymer/Graphite Conducting Nanocomposite by Intercalation Polymerization." *Journal of Applied Polymer Science*, 82 (2001): 2506-2513.

Chen J. & Gardner D.J. "Dynamic mechanical properties of extruded nylon-wood composites." *Polymer Composites*, 29 (4) (2008): 372-379.

Chen M., Wan C., Shou W., Zhang Y., Zhang Y. & Zhang J. "Effects of Interfacial Adhesion on Properties of Polypropylene/Wollastonite Composites." *Journal of Applied Polymer Science*, 107 (3) (2007): 1718-1723.

Dikobe D.G. & Luyt A.S. "Effect of Filler Content and Size on the Properties of Ethylene Vinyl Acetate Copolymer-Wood Fiber Composites." *Journal of Applied Polymer Science*, 103 (6) (2006): 3645-3654.

Fukushima, Hiroyuki. *Graphite Nanoreinforcements in polymer composites*. PhD Dissertation, East Lansing, MI, USA: Michigan State University (2003).

Giannelis, Emmanuel P. "Polymer Layered Silicate Nanocomposites." *Advanced Materials*, 8 (1) (1996): 29-35.

Gopakumar T.G. & Page D.J.Y.S. "Polypropylene/Graphite Nanocomposites by Thermo-Kinetic Mixing." *Polymer Engineering & Science*, 44 (6) (2004): 1162-1169.



Houphouet-Boigny, Chrystèle. Fiber Reinforced Polypropylene Nanocomposites. PhD Dissertation, Lausanne, Switzerland: Institute of Technology (EPFL) (2007).

Hussain F., Hojjati M., Okamoto M. and Gorga R.E. "Review article: Polymer-matrix Nanocomposites, Processing, Manufacturing, and Application: An Overview." *Journal of Composite Materials*, 40 (17) (2006): 1511-1575.

Jacobsen R.L., Tritt T.M., Guth J.R., Ehrlich A.C. and Gillespie D.J. "Mechanical Properties of Vapor-Grown Carbon Fiber" *Carbon*, 33 (9) (1995): 1217-1221.

Jiang X. & Drzal L. T. "Multifunctional High Density Polyethylene Nanocomposites Produced by Incorporation of Exfoliated Graphite nanoplatelets 1: Morphology and Mechanical Properties." *Polymer Composites*, (2010): 1091-1098.

Kalaitzidou K., Fukushima H., Drzal L. T. "Mechanical properties and morphological characterization of exfoliated graphite-polypropylene nanocomposites." *Composites: Part A*, 38 (2007d): 1675-1682.

Kalaitzidou K., Fukushima H., Drzal L. T. "Multifunctional polypropylene composites produced by incorporation of exfoliated graphite nanoplatelets." *Carbon*, 45 (2007b): 1446-1452.

Kalaitzidou K., Fukushima H., Drzal L.T. "A new compounding method for exfoliated graphite-polypropylene nanocomposites with enhanced flexural properties and lower percolation threshold." *Composites Science and Technology*, 67 (2007a): 2045-2051.

Kalaitzidou K., Fukushima H., Miyagawa H., Drzal L. T. "Flexural and Tensile Moduli of Polypropylene Nanocomposites and Comparison of Experimental Data to Halpin-Tsai and Tandon-Weng Models." *Polymer Engineering and Science*, 47 (2007c): 1796-1803.

Kalaitzidou, Kyriaki. Exfoliated Graphite Nanoplatelets as Nanoreinforcement for Multifunctional Polypropylene Nanocomposites. PhD Dissertation, East Lansing, MI, USA: Michigan State University (2006).

Kim H., Abdala A. A., Macosko C. W. "Graphene/Polymer Nanocomposites." *Macromolecules*, 43(16) (2010): 6515-6530.

Kim S. & Drzal L. T. "High latent heat storage and high thermal conductive phase change materials using exfoliated graphite nanoplatelets." *Solar Energy Materials & Solar Cells*, 93 (2009a): 136-142.

Kim S., Do I. & Drzal L.T. "Multifunctional Exfoliated Graphite Nanoplatelets/LLDPE Nanocomposites Fabricated By Solution Compounding Method And Various Screw Rotating Systems." *Macromolecular Materials and Engineering*, 294 (3) (2009b): 196-205.

- Kim S., Do I. & Drzal L.T. “Thermal Stability and Dynamic Mechanical Behavior of Exfoliated Graphite Nanoplatelets LLDPE Nanocomposites.” *Polymer composites*, 31 (5) (2010): 755-761.
- Kim S., Do I., Drzal L. T. “Multifunctional xGnP/LLDPE Nanocomposites Prepared by Solution Compounding Using Various Screw Rotating Systems.” *Macromolecular Materials and Engineering*, 294 (2009b): 196-205.
- Kim S., Seo J., Drzal L. T. “Improvement of electric conductivity of LLDPE based nanocomposite by paraffin coating on exfoliated graphite nanoplatelets.” *Composites: Part A*, 41 (2010b): 581-587.
- Kumar S., Sun L.L., Caceres S., Li B., Wood W., Pereguni A., Maguire R.G. & Zhong W.H. “Dynamic synergy of graphitic nanoplatelets and multi-walled carbon nanotubes in polyetherimide nanocomposites.” *Nanotechnology*, 21 (10) (2010): 105702 (9pp).
- Lesser A.J. “Fundamentals in Toughening.” *Proceedings of NSF Summer Institute on Nanomechanics, Nanomaterials, and Micro/Nanomanufacturing*, University of Massachusetts Lowell (2009).
- Lim J.W., Hassan A., Rahmat A.R., Wahit M.U. “Phase Morphology and Mechanical Properties of Rubber-Toughened Polypropylene Nanocomposites: Effect of Elastomer Polarity.” *Polymer-Plastics Technology and Engineering*, 47 (2008): 411-419.
- Lu J.Z., Wu Q., Negulescu I. I., Chen Y. “The Influences of Fiber Feature and Polymer Melt Index on Mechanical Properties of Sugarcane Fiber/Polymer Composites.” *Journal of Applied Polymer Science*, 102 (2006): 5607-5619.
- Luo J-J. & Daniel I.M. “Characterization and modeling of mechanical behavior of polymer/clay nanocomposites.” *Composites Science and Technology*, 63 (2008): 1607–1616.
- Maniar, Ketan K. “Polymeric Nanocomposites: A Review.” *Polymer-Plastics Technology and Engineering*, 43 (2) (2004): 427–443.
- Miloaga D. G., Hosein H.A. A., Misra M., Drzal L. T. “Nucleating Effect of Expanded Graphite Nanoplatelets on Poly(Hydroxybutyrate).” *Composite Materials & Structures Center, Michigan State University* 2005.
- Okamoto M., Nam H.P., Maiti P., Kotaka T., Hasegawa N. and Usuki A. “A House of Cards Structure in Polypropylene/Clay Nanocomposites under Elongational Flow” *Nano Letters*, 1 (6) (2001): 295-298.
- Oksman K. & Clemons C. “Mechanical Properties and Morphology of Impact Modified Polypropylene-Wood Flour Composites.” *Journal of Applied Polymer Science*, 67 (1998): 1503-1513.

Page D.J.Y.S. & Gopakumar T.G. "Properties and Crystallization of Maleated Polypropylene/Graphite Flake Nanocomposites." *Polymer Journal*, 38 (9) (2006): 920-929.

Pan Y.-X., Yu Z.-Z., Ou Y.-C. & Hu G.-H. "A New Process of Fabricating Electrically Conducting Nylon 6/Graphite Nanocomposites via Intercalation Polymerization." *Journal of Polymer Science: Part B: Polymer Physics*, 38 (12) (2000): 1626–1633.

Park H.M., Kalaitzidou K., Fukushima H., Drzal L. T. "Exfoliated Graphite Nanoplatelet (xGnP) /Polypropylene Nanocomposites." Composite Materials & Structures Center, Michigan State University (2007).

Patel H.A., Somani R.S., Bajaj H.C. and Jasra R.V. "Nanoclays for polymer nanocomposites, paints, inks, greases and cosmetic formulations, drug delivery vehicle and waste water treatment." *Bulletin of Material Science*, 29 (2) (2006): 133-145.

Paul D.R. & Robeson L.M. "Polymer nanotechnology: Nanocomposites." *Polymer*, 49 (15) (2008): 3187-3204.

Pavlidou S. & Papaspyrides C.D. "A review on polymer-layered silicate nanocomposites." *Progress in Polymer Science*, 33 (12) (2008): 1119–1198.

Powell M.C. & Kanarek M.S. "Nanomaterial Health Effects – Part 1: Background and Current Knowledge." *Wisconsin Medical Journal*, 105 (2) (2006a): 16-20.

Powell M.C., Kanarek M.S. "Nanomaterial Health Effects – Part 2: Uncertainties and Recommendations for the Future." *Wisconsin Medical Journal*, 105 (3) (2006b): 18-23.

Ratnayake U.N., Haworth B., Hourston D.J. "Preparation of Polypropylene-Clay Nanocomposites by the Co-Intercalation of Modified Polypropylene and Short-Chain Amide Molecules." *Journal of Applied Polymer Science*, 112 (2009): 320-334.

Revilla-Diaz R., Sanchez-Valdes S., Lopez-Campos F., Medellin-Rodriguez F.J. & Lopez-Quintanilla M.L. "Comparative Characterization of PP Nano and Microcomposites by In-Mold Shrinkage Measurements and Structural Characteristics." *Macromolecular Materials and Engineering*, 292 (6) (2007): 762–768.

Reyes-de Vaaben S., Aguilar A., Avalos F. & Ramos-de Valle LF. "Carbon nanoparticles as effective nucleating agents for polypropylene." *Journal of Thermal Analysis and Calorimetry*, 93 (3) (2008): 947-952.

Roco, M.C. "Broader societal issues of nanotechnology." *Journal of Nanoparticle Research*, (5) (2003): 181-189.

Rowell, Roger M. "Economic Opportunities in Natural Fiber-Thermoplastic Composites." In *Science and Technology of Polymers and Advanced Materials: Emerging Technologies and Business Opportunities*, 869-872. New York: Plenum Press, 1998.

Savage S.J. "Defence applications of nanocomposite materials." FOI Swedish Defence Research Agency. User Report. December 2004.

Sharma P., Ganti S., and Bhate N. "Effect of surfaces on size-dependent elastic state of nano-inhomogeneities." *Applied Physics Letters*, 82 (4) (2003): 535-537.

Shen H., Wang Y. & Mai K. "Effect of compatibilizers on thermal stability and mechanical properties of magnesium hydroxide filled polypropylene composites." *Thermochimica Acta*, 483 (1-2) (2009): 36-40.

Sherman, Lilli Manolis. "Carbon nanotubes: Lots of potential-If the price is right" *Plastic Technology*, 53 (2007): 68-73.

Sherman, Lilli Manolis. "Chasing Nanocomposites." *Plastics Technology*, 50 (11) (2004): 56-61.

Spoljaric S., Genovese A. & Shank R.A. "Polypropylene-microcrystalline cellulose composites with enhanced compatibility and properties." *Composites Part A: Applied Science and Manufacturing*, 40 (6-7) (2009): 791-799.

Stankovich S., Dikin D.A., Dommett G.H.B., Kohlhaas K.M, Zimney E.J., Stach E.A., Piner R.D., Nguyen S.T., Ruoff R.S. "Graphene-based composite materials." *Nature*, 442 (2006): 282-286.

Teng C.-C., Ma C.-C. M., Huang Y.W., Yuen S.M., Weng C.-C., Chen C.-H, Su S.F. "Effect of MWCNT content on rheological and dynamic mechanical properties of multiwalled carbon nanotube/polypropylene composites." *Composites: Part A*, 39 (2008): 1869-1875.

Thostenson E. T., Li C., Chou T.W. "Nanocomposites in context." *Composites Science and Technology*, 65 (2005): 491-516.

Vaia R., Koerner H., Lu W., Manias E. "Polymer Nanocomposites With Prescribed Morphology: Going Beyond Nanoparticle-filled Polymers." *Chemistry of Materials*, 19 (11) (2007): 2736-2751.

Wang Y., Shen H., Li G. & Mai K. "Crystallization and melting behavior of PP/nano-CaCO<sub>3</sub> composites with different interfacial interaction." *Journal of thermal Analysis and Calorimetry*, 99 (2) (2010): 399-407.

Wang Z. & Stein A. "Morphology Control of Carbon, Silica, and Carbon/Silica Nanocomposites: From 3D Ordered Macro-/Mesoporous Monoliths to Shaped Mesoporous Particles." *Chemistry of Materials*, 20 (3) (2008): 1029-1040.

Wunderlich, Bernhard. *Thermal Analysis*, 609-610. New York: Academic Press, 1990.

Zhang Q., Fu Q., Jiang L., Lei Y. "Preparation and properties of polypropylene montmorillonite layered nanocomposites." *Polymer International*, 49 (2000): 1561-1564.

Zhang X., Yin Z., Li L. & Yin J. "Grafting of glycidyl methacrylate onto ethylene-propylene copolymer: Preparation and characterization." *Journal of Applied Polymer Science*, 61 (13) (1996): 2253-2257.

## **BIOGRAPHY OF THE AUTHOR**

Alex James Duguay was born in Farmington, Maine on January 18, 1987. Until the age of five Alex resided with his family in the town of Jay, Maine. At the age of five he and his family relocated to the town of Turner, Maine where he attended K-12 education at the Maine School Administrative District (M.S.A.D.) #52.

In the fall of 2004 Alex was accepted to attend The University of Maine's College of Engineering with enrollment in the Civil Engineering program. He graduated from Leavitt Area High School in the spring of 2005 and continued on to obtain his B.S. in Civil Engineering from The University of Maine in May of 2009. He also passed the Fundamentals of Engineering (FE) exam, therefore obtaining his certification as an Engineer-in-Training (EIT). In the early spring of 2009 Alex was offered a graduate assistantship with the AEWC Advanced Structures and Composites Center to continue his education and obtain a M.S. in Civil Engineering.

In the spring of 2011 Alex accepted a position as an entry level structural engineer in the Internal Structures department at General Dynamics Electric Boat in Groton, CT. There he plans to continue to grow both personally and professionally while designing internal structures for U.S. Navy submarines. Alex is a candidate for the Master of Science degree in Civil Engineering from The University of Maine in May of 2011.